Acidity and o-xylene isomerization activity of silica-alumina catalysts
by Johnny Lealen Golden

A thesis submitted in partial fulfillment of the requirements for the degree of Doctor of Philosophy in Chemical Engineering
Montana State University

Abstract:
Surface heterogeneity of a catalyst can be described in terms of adsorption energy distribution. In the present study, acid-site adsorption energy distributions have been obtained for the amorphous silica-alumina system, with results compared to o-xylene isomerization activity.

Xerogels ranging in composition from pure silica to pure alumina were synthesized using reagents which avoid sodium contamination. Calcination at 500°C was performed prior to making physical property, chemisorption, and activity measurements.

Catalysts were tested for surface area, porosity, density, alumina content, and water loss. Results indicate that unusual materials have been synthesized in the 50-75% alumina composition range, materials with low surface areas despite having high initial water contents.

Triethylamine chemisorption isotherms were gravimetrically measured at □300°C. The minimum adsorbate injection possible with the equipment used was not low enough to measure the very low coverage portion of the isotherms. The adsorption isotherms were analyzed with a recently-developed numerical technique known as CAEDMON (Computed Adsorption Energy Distribution in the MONolayer). The calculated quantities of strong acid sites for test catalysts was in general agreement with other chemisorption studies on comparable materials.

Catalyst activity for o-xylene isomerization was measured at 300-400°C using a Berty reactor. Reaction rates were obtained avoiding equilibrium and transport limitations. Activation energies of 17 to 21 kcal/mole were observed for reactive catalysts.

Reaction rates for low alumina-content catalysts were observed to be exponentially related to the quantity of strong acid-sites. Correction of intermediate alumina content catalysts for alumina-type acidity unreactive for o-xylene isomerization yielded acidities fitting the exponential relationship.

It is postulated that two major types of strong acid sites were observed for the silica-alumina catalysts, Bronsted acid sites active for isomerization and Lewis acid sites associated with alumina which are inactive for isomerization. The exponential relationship between the quantity of Bronsted sites and catalytic activity appears to indicate a proximity effect, such that acid-site reactivity increases as the distance between acid sites decreases.

ACIDITY AND o-XYLENE ISOMERIZATION ACTIVITY OF SILICA-ALUMINA CATALYSTS

by

Johnny Lealen Golden

A thesis submitted in partial fulfillment
of the requirements for the degree

of

Doctor of Philosophy

in

Chemical Engineering

MONTANA STATE UNIVERSITY
Bozeman, Montana

August 1986

APPROVAL

of a thesis submitted by

Johnny Lealen Golden

This thesis has been read by each member of the thesis committee and has been found to be satisfactory regarding content, English usage, format, citations, bibliographic style, and consistency, and is ready for submission to the College of Graduate Studies.

June 16, 1986
Date

John T. Sears
Chairperson, Graduate Committee

Approved for the Major Department

June 16, 1986
Date

John T. Sears
Head, Major Department

Approved for the College of Graduate Studies

August 25, 1986
Date

Verney L. Sansone
Graduate Dean

STATEMENT OF PERMISSION TO USE

In presenting this thesis in partial fulfillment of the requirements for a doctoral degree at Montana State University, I agree that the Library shall make it available to borrowers under rules of the Library. I further agree that copying of this thesis is allowable only for scholarly purposes, consistent with "fair use" as prescribed in the U.S. Copyright Law. Requests for extensive copying or reproduction of this thesis should be referred to University Microfilms International, 300 North Zeeb Road, Ann Arbor, Michigan 48106, to whom I have granted "the exclusive right to reproduce and distribute copies of the dissertation in and from microfilm and the right to reproduce and distribute by abstract in any format."

Signature John L. Golden

Date 21 June 1986

ACKNOWLEDGMENTS

The opportunity to perform the work supporting this thesis was the result of efforts from many good people, and I hope that all involved know of my gratitude. However, there are some to whom I am especially indebted. The project would not have occurred without the support and guidance of Dr. John Sears. Likewise, I would like to thank Dr. Doug Smith and all members of my research committee. Essential equipment was graciously provided by the MSU Chemistry Department and Dr. Frank Williams of the University of New Mexico. Financial support was, in part, provided by the Engineering Experiment Station and the Research Creativity Committee, both of MSU. I would like to thank my fellow graduate students and the staff of the Chemical Engineering Department for maintaining such a positive, constructive working environment. But foremost, I sincerely thank my wife, Linda Jean, for her love in support of this effort.

TABLE OF CONTENTS

TABLE OF CONTENTS--Continued

LIST OF TABLES

LIST OF TABLES--Continued

LIST OF FIGURES

LIST OF FIGURES--Continued

LIST OF FIGURES--Continued

LIST OF FIGURES--Continued

LIST OF FIGURES--Continued

LIST OF FIGURES--Continued

ABSTRACT

Surface heterogeneity of a catalyst can be described in terms of adsorption energy distribution. In the present study, acid-site adsorption energy distributions have been obtained for the amorphous silica-alumina system, with results compared to o-xylene isomerization activity.

Xerogels ranging in composition from pure silica to pure alumina were synthesized using reagents which avoid sodium contamination. Calcination at 500°C was performed prior to making physical property, chemisorption, and activity measurements.

Catalysts were tested for surface area, porosity, density, alumina content, and water loss. Results indicate that unusual materials have been synthesized in the 50-75% alumina composition range, materials with low surface areas despite having high initial water contents.

Triethylamine chemisorption isotherms were gravimetrically measured at ~300°C. The minimum adsorbate injection possible with the equipment used was not low enough to measure the very low coverage portion of the isotherms. The adsorption isotherms were analyzed with a recently-developed numerical technique known as CAEDMON (Computed Adsorption Energy Distribution in the MONolayer). The calculated quantities of strong acid sites for test catalysts was in general agreement with other chemisorption studies on comparable materials.

Catalyst activity for o-xylene isomerization was measured at 300-400°C using a Berty reactor. Reaction rates were obtained avoiding equilibrium and transport limitations. Activation energies of 17 to 21 kcal/mole were observed for reactive catalysts.

Reaction rates for low alumina-content catalysts were observed to be exponentially related to the quantity of strong acid-sites. Correction of intermediate alumina content catalysts for alumina-type acidity unreactive for o-xylene isomerization yielded acidities fitting the exponential relationship.

It is postulated that two major types of strong acid sites were observed for the silica-alumina catalysts, Brønsted acid sites active for isomerization and Lewis acid sites associated with alumina which are inactive for isomerization. The exponential relationship between the quantity of Brønsted sites and catalytic activity appears to indicate a proximity effect, such that acid-site reactivity increases as the distance between acid sites decreases.

I. INTRODUCTION

Silica-alumina is one of the most extensively studied solid systems. The volumes of research are certainly due to the development of cracking catalysts for the petroleum feedstock production of gasoline. Continuous improvement of cracking catalysts over the last 40 years has lead to the development of zeolites, crystalline aluminosilicates also called molecular sieves.

Though largely replaced by zeolites for catalytic cracking, amorphous silica-alumina is still used to support the expensive zeolite to better effect heat transfer. Silica-alumina can also act as a metallic catalyst support and be used as a bifunctional catalyst. Recently, interest in the preparation and characterization of amorphous silica-alumina has been cited because of the material's newly discovered capability for converting methanol into hydrocarbons [1]. But most importantly, the extensive background concerning silica-alumina makes the system ideal for the fundamental study of an amorphous solid surface. It is the fundamental study of solid surfaces that is of interest to several Chemical Engineering researchers at Montana State University.

Despite the years of research, amorphous silica-alumina materials exhibit properties that are not well understood. What follows here is a restatement of some of the observations made by reviewers [2-7] concerning the character of cracking catalysts.

Catalytic cracking has been previously defined as the set of hydrocarbon reactions that occur on acidic solids. These reactions

include dealkylation, hydrogen transfer, isomerization, and polymerization.

In general, silica-alumina catalysts have been observed to exhibit adsorption sites suggesting Lewis and Brønsted acidity, as well as interconversion between the two types of sites. Due to observations consistent with carbonium ion chemistry, many investigators believe that the seat of catalytic cracking on silica-alumina is the Brønsted acid sites. However, some cracking reactions have been found to correlate with measurements of Lewis acidity.

Whether actual carbonium ion chemistry is occurring on cracking catalysts has been questioned. It is known that the forces bonding large cracking feedstock molecules to microporous surfaces are both physical and chemical. Such an interaction could promote a more concerted mechanism involving simultaneous bond breaking and bond formation. But at this time, it is not known if catalytic cracking reactions are being oversimplified when described as carbonium ion reactions.

Both Lewis and Brønsted acid sites on silica-alumina exhibit energetic heterogeneity, ranging from very weak acids (alcoholic) to very strong acids (superacids). The seldom-studied consequence of broad energetic heterogeneity is that the catalytic activity of these materials may be due as much to the acid-site strength distribution as to the total number of acid sites.

Measurements of some cracking reactions indicate a maximum silica-alumina catalyst activity at a bulk concentration of 15-25% alumina. However, a number of factors during synthesis, calcination, and

pretreatment affect the catalyst surface. The relationship between bulk alumina composition and the corresponding surface structures is not well understood.

Research Objectives

It is the purpose of this research to contribute to the fundamental understanding of amorphous silica-alumina catalysts. The research objectives are:

1. To synthesize and physically characterize a composition range of amorphous silica-alumina materials. These catalysts will be synthesized such that contamination is avoided. Catalyst history will be entirely under the control of this research project.
2. To determine the acid-site energy distributions for the catalysts. Adsorption isotherms for a gaseous base adsorbate will be used to numerically calculate the expected heterogeneous adsorption energy distributions.
3. To compare the calculated energy distributions to catalytic cracking activity. The measure of cracking activity will be based on a well-studied model compound reaction.

A survey of the extensive literature concerning the acidity and characterization of silica-alumina catalysts will follow in Chapter II. Chapter III contains a description of the experimental equipment and methods used in this study. The results and their discussion are contained in Chapter IV. Conclusions of research findings comprise Chapter V. Finally, observations of a more hypothetical nature and recommendations for future research are located in Chapter VI.

II. LITERATURE SURVEY

Catalytic Cracking Chemistry

Petroleum refining performed before the discovery of cracking catalysts required the thermal cracking of heavy molecular weight feedstocks via free-radical mechanisms. There are several important consequences of the free-radical reaction. Paraffin radicals will frequently undergo scission, following the empirical β rule, to form ethylene and another primary radical. Hydrogen abstraction is another common hydrocarbon radical reaction. But isomerization involving alkyl group migration or shift of the radical along a hydrocarbon chain does not occur. As a result, thermal cracking of hydrocarbons from petroleum results in the formation of large amounts of ethylene from paraffins and in the dehydrogenation of naphthenes to aromatics [6].

Catalytic cracking reactions performed on acidic surfaces are believed to proceed via carbonium ion intermediates. This theory is primarily based on the similarities in product distribution found with heterogeneous cracking and cracking performed in mineral acid solution.

Organic chemists have thoroughly studied carbonium ion, sometimes called carbocation, reactions in solution and the reactivities of these species are well understood. In general, the carbonium ion intermediate is stabilized by the availability of electrons to the

region of the ion. To a great extent, the stability of a carbonium ion determines its reaction pathway.

Carbonium ion formation reactions and mechanisms have been described in a detailed review of catalytic cracking by Gates et al. [6]. The formation of carbonium ions from hydrocarbons can occur: (1) via proton donation to olefins or aromatics by Brønsted acids, (2) via hydride abstraction from paraffins by Lewis acids, or (3) via protonation of paraffins by Brønsted acids to produce the carbonium ion and hydrogen. A secondary formation of carbonium ions, though not secondary in importance, can occur via hydride transfer (chain transfer).

Once carbonium ions are formed, they can undergo rearrangement (isomerization), polymerization (alkylation), or cracking (dealkylation). The mechanism of carbonium ion reactions is postulated as a transition through various three-centered electron deficient complexes, analogous to the electronic structures found in boranes.

The preponderance of product distribution data for catalytic cracking by acid surfaces leaves little doubt that the carbonium ion mechanism, as in solution, occurs on surfaces. However, the possibility of charge separation occurring on the catalytic surface, due to the immobility of the surface sites, has lead to speculation concerning the true degree of charge development occurring in reactant molecules. It has been suggested that carbonium ions may not actually be fully formed on the catalyst surface. Instead, the reactant molecules may become sufficiently polarized by the surface to react or

rearrange through a more concerted mechanism before a carbonium ion could be formed. There is experimental evidence of such nonionic "intermediates" for some organic elimination reactions. However, it has been stated that there is currently insufficient information to determine if catalytic cracking reactions are oversimplified by being described as carbonium ion reactions [6].

Production of Silica-Alumina Catalysts

The commercial production of silica-alumina catalysts began in the 1940's with several companies holding patents to their manufacture. It is recognized that a number of interrelated variables, such as solids concentration, pH, temperature, and time, control the physical and chemical properties of the final catalyst [3]. Generally, commercial processes involve the acidification of dilute sodium silicate with sulfuric acid to form a silica hydrogel. Aluminum is added to the silica hydrogel as aqueous aluminum sulfate and hydrolysis (incorporation) is accomplished by the addition of aqueous ammonium hydroxide. Filtration is performed with water acidified to pH 4-5.5 to aid in sodium removal. Some manufacturing processes produce loosely packed, mostly spherical particles, 0.05-3 μm in diameter, that are then pressed together into regular pellets. Other processes produce a coarse grade of catalyst with a 60 μm average particle (clump) size.

Laboratory experiments involving cracking catalysts have largely used samples of commercial catalysts as the object of study. However,

researchers wishing to vary the amount of alumina or to avoid the additional variable of sodium contamination in the catalyst have reported procedures for silica-alumina catalyst synthesis. A process described by Johnson [8] involved the interaction of a very pure silica gel, prepared at pH 3, with measured amounts of an alumina sol. The alumina sol was prepared from aluminum chloride, precipitated and thoroughly washed as the hydroxide, and then redissolved in water. The catalyst product was formed when the two components were mixed. The product was washed and then dried at 393 K.

Another laboratory process for silica-alumina synthesis was developed by Thomas [9]. A major objective of the process was to avoid sodium in the resulting product. This goal was accomplished by dissolving aluminum isopropoxide in tetraethyl orthosilicate (TEOS). The mixture was then hydrolyzed with water and ethanol.

More recently, a variety of approaches for the laboratory synthesis of silica-alumina have been reported [10-17]. One of these approaches, similar to the process by Thomas described previously, involved the formation of a silica hydrogel by reacting TEOS and hydrochloric acid at pH 2. Sufficient aluminum sulfate was dissolved in this mixture to give the chemical composition desired. Ammonia solution was then added to the mixture until it gelled at pH 6 [11].

The theory of how silicon and aluminum ions interact during the formation of active cracking catalysts has been discussed by several reviewers [2-6]. Commercial preparations generally start with the silica hydrogel, which consists of an aggregate of primary spherical particles about 30-50 Å in diameter. The primary particles consist of

an interconnected network of SiO_4 tetrahedra, with the surface silicon ions terminated by hydroxyl groups. Next, an aluminum salt solution is added to the hydrogel. When the pH of the mixture is increased, the aluminum ions react with the silica surface hydroxyls. The result is that the trivalent, six-coordinate aluminum ions isomorphously substitute into the tetrahedral silica lattice. This incorporation of aluminum produces an active cracking catalyst, generally depicted as

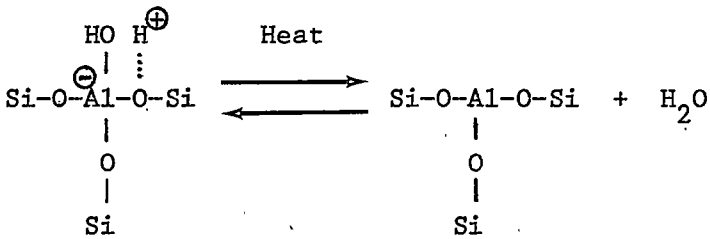

Brønsted Acid Lewis Acid

Having both Brønsted and Lewis acid character is not unique to solid cracking catalysts. An analogous class of solutions is known to exhibit high proton donor strengths (superacids).

Table 1. Superacid solutions [6].

Brønsted Acid		Lewis Acid
H_2O	+	BF_3
HF	+	BF_3
HF	+	SbF_5
FSO_3H	+	SbF_5
HCl	+	$AlCl_3$

It is important to recognize that the above considerations are all simplified concepts of the very complicated cracking catalyst surface. The groups that actually exist could have varying degrees of aluminum incorporation or aluminum ion separation. Further treatment of cracking catalysts, such as calcination, will produce different surface structures. Other methods of silica-alumina preparation, each promoting different silica-alumina interactions, will produce still other surface structures. Some of the proposed silica-alumina surface structures are reproduced in Appendix A. However, the bulk structures and the corresponding surface structures of silica-alumina are not well known [6].

Measurement of Surface Acidity

Titration Methods

The observation that both silica-alumina catalysts and mineral acid solutions produced similar reaction products caused investigators

to test silica-alumina catalysts in the aqueous phase with acid indicators. Once the catalyst surface was qualitatively observed as acidic [18], attention turned to obtaining more detailed information concerning this acidity and the chemical structure of the catalyst.

Early measurements of surface acidity continued to be performed in aqueous media. In essence, aqueous titration of surface acidity is an ion exchange process. Ion exchange measurements performed in the aqueous phase can provide some information concerning surface acidity. Good correlations of catalytic activity for acid reactions and ion exchange capacity based on the use of ammonium acetate have been reported [3]. However, titration with basic substances in aqueous solution was recognized as disadvantageous [3]. Not only will water react with the catalyst surface and alter its structure, but the acidity so determined will be limited by the acid strength of the hydronium ion.

The nonaqueous solution technique is performed using solvents such as benzene which do not react with the catalytic surface. A comparison of surface acid strengths in nonaqueous media can be based on the ability of the solid to change a neutral base into its

conjugate acid form [7]. In this manner, as previously described by Hammett and Deyrup [19], acidity is defined by the function:

$$H_o = -\log \left[a_{H^+} \frac{\gamma_B}{\gamma_{BH^+}} \right] \qquad (1)$$

where

H_o = Hammett acidity function

a_{H^+} = proton activity

γ_B = neutral base activity coefficient

γ_{BH^+} = conjugate acid activity coefficient

The nonaqueous technique, using a series of aniline bases as indicators (Hammett indicators), has been employed to determine acid strengths for a variety of solids. The data in Table 2 was obtained by a nonaqueous indicator method and reported by Tanabe [4].

The nonaqueous indicator method is the simplest way of screening solid catalysts for surface acidity. However, several disadvantages to this method have been recognized. Numerous sources [4,5,7,20-22] have discussed the necessity of water being rigorously excluded, the importance of solvent choice, the sometimes difficult recognition of end-point in the presence of colored solids, and the long time required for equilibrium. In addition, the nonaqueous indicator method cannot be used for acidity determination under cracking reactions conditions nor can it distinguish between Lewis or Brønsted acid sites on the solid surface.

Table 2. Hammett acidity of several solids [4].

Acidic Solids	Ho
Original kaolinite	-3.0 to -5.6
Hydrogen kaolinite	-5.6 to -8.2
Original montmorillonite	+1.5 to -3.0
Hydrogen montmorillonite	-5.6 to -8.2
Silica-alumina	$<$-8.2
Silica-magnesia	+1.5 to -3.0
Alumina-boria	$<$-8.2
H_3BO_3/silica gel	+3.3 to +1.5
H_3PO_4/silica gel	+1.5 to -3.0
H_2SO_4/silica gel	-5.6 to -8.2
$HClO_4$/silica gel	-5.6 to -8.2

Although the nonaqueous titration technique has several recognized drawbacks, its use has been frequently reported in the literature. Cases of strong correlation between acidity via the indicator method and catalytic activity have been published. Johnson [8] titrated the total acidity of several silica-alumina compositions dispersed in benzene using n-butylamine as titer and p-dimethylaminoazobenzene (dimethyl yellow) as indicator. The total acidity so determined was observed to vary linearly with propylene polymerization activity as shown in Figure 1. It was also found that acidity and polymerization activity increased to a maximum value and then decreased with increasing alumina content.

An improved Hammett indicator technique, avoiding several of the disadvantages previously mentioned concerning the titration method, was reported by Benesi [21]. The technique avoided the problems of water exclusion and long equilibrium time. Several mounted acids, clays, and cracking catalysts were tested. Benesi observed that 90% of the acid centers on silica-alumina catalysts were very strong ($H_o < -8.2$).

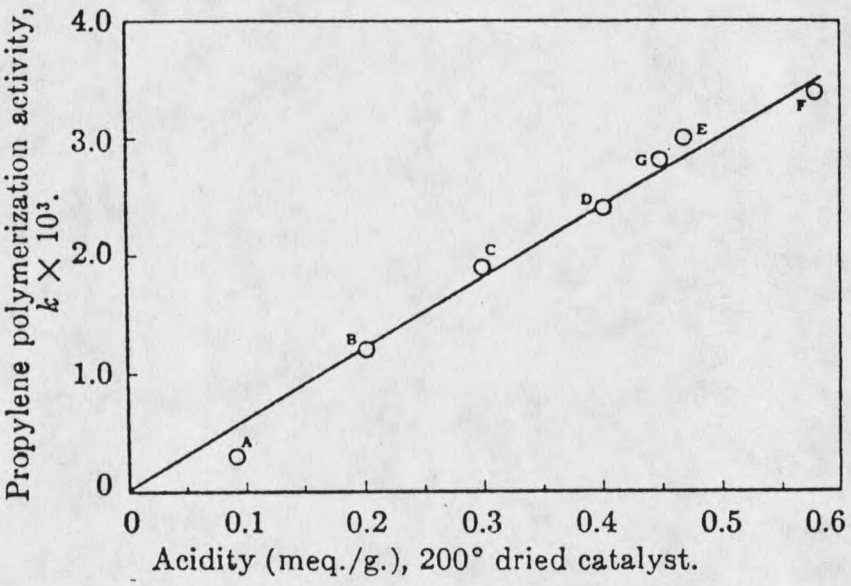

Figure 1. Propylene polymerization versus acid amount for a series of silica-alumina catalysts [8].

Catalyst:	A	B	C	D	E	F	G
Alumina:	0.12	0.32	1.04	2.05	3.56	10.3	25.1

Hammett indicators have since been obtained that extend the acid strength range of the n-butylamine titration method. These indicators are generally observed using absorption spectroscopy, which reduces the uncertainties inherent in visual observation. Using these improvements, Take et al. [23] found that the acid sites on a silica-alumina catalyst had an acid strength corresponding to an Ho between -10.5 and -12.8. A few sites had even higher acid strengths.

Another nonaqueous technique used to determine the acid amount of solids is the calorimetric titration. Temperature rise is recorded with the addition of measured amounts of a titrating base such as n-butylamine. The calorimetric titration has been used to observe both weaker acid sites than those found with indicators and energetic heterogeneity in the acid sites [4,5].

Gaseous Base Methods

The strength and number of acid sites can be more explicitly obtained by determining the amount of a gaseous base that will adsorb on an acidic solid. Gaseous bases such as ammonia, n-butylamine, pyridine, and quinoline have been adsorbed on cracking catalysts at temperatures similar to those used at reaction conditions. Of course, there is an upper limit to the adsorption temperature because gaseous bases will catalytically decompose. In addition, some gaseous bases can dissociate and consequently adsorb onto both acidic and basic sites. Since triethylamine (TEA) is very difficult to dissociate, it has been recommended to be used as an acid catalyst adsorbate [22].

Gaseous bases will also adsorb onto both Brønsted and Lewis acid sites, making it difficult to distinguish the amounts of each [5].

The classical study of cracking catalysts by Mills et al. [24] made use of the gravimetric determination of gaseous base adsorption. The study obtained a linear relationship between the amount of quinoline chemisorption and the light gas-oil cracking activity for a number of different cracking catalysts. However, the quinoline adsorption was not measured at accurately known equilibrium pressures.

Many other techniques using gaseous bases have been employed by researchers for the characterization of surface acidity. Calorimetric methods and the measurements of adsorption or desorption isotherms at several temperatures have enabled investigators to determinate the heat and entropy of adsorption for cracking catalysts as a function of surface coverage. Differential thermal analysis (DTA), thermal gravimetric analysis (TGA), and temperature programmed desorption (TPD) are similar methods that have been used to estimate the acid strengths of silica-alumina catalysts [4].

Ammonia gas TPD has been reported by Barth and Ballou [25] for several materials including silica-alumina catalysts. Total acid results were in general agreement with nonaqueous indicator measurements, but acid strength was discussed only qualitatively.

In the study by Hsieh [26], adsorption isotherms and calorimetric heats of adsorption were measured using ammonia at 273 K. Commercial cracking catalysts that were fresh, used, heat-deactivated and steam-deactivated were tested. The procedure of Adamson and Ling [27] was used to find site energy distributions. Results of this study

indicated that there were two predominant site energies (acid strengths) on the catalysts. It was also observed that the highest energy sites were those lost in the three deactivated catalysts.

The adsorption of ammonia on eleven silica-alumina gels ranging in composition from pure silica to pure alumina was studied by Clark, et al. [28]. Adsorption data was experimentally determined as isobars at several different ammonia pressures. Data plotted as isotherms was found to fit the Freundlich equation for all but the two highest silica-content catalysts. Isosteric heats of adsorption were obtained from the integrated form of the Clausius-Clapeyron equation for constant surface coverage. The isosteric heat curves (energies) dropped very rapidly with increasing coverage for the silica gel and high silica adsorbents. Curves for alumina and high alumina adsorbents dropped more slowly with coverage. The isosteric heat curves for the intermediate compositions, 55-90% silica, reached the lowest values.

Clark and his coworkers also calculated the differential molar entropy of the adsorbed ammonia. They found that the intermediate compositions provided the highest entropies. The cited authors concluded that the strongest acid sites were Lewis acid in character and the high alumina content adsorbents contained mostly this type. The intermediate compositions contained many weak acid sites which were judged to be the protonic (Brønsted) acid sites. The entropy calculations indicated that adsorption on the weak sites of intermediate compositions produced adsorbed molecules with the greatest mobility. It was also found that the trend in adsorbate

mobilities compared closely with measurements of o-xylene isomerization activity [10].

Infrared Spectroscopy Methods

Infrared spectroscopy, used in conjunction with gaseous base adsorption, has received considerable research attention in recent years due to its ability to distinguish between Lewis and Brønsted acid sites. For example, pyridine can coordinatively bond to Lewis acid sites or it can associate with Brønsted sites as the pyridinium ion. These two adsorbed species have different infrared absorption bands. The amount of either acid type can be determined from the absorption band intensities. Experimental difficulties associated with this technique are extensive sample preparation as well as complicated equipment requirements and operation.

The pioneering work utilizing infrared spectroscopy in the determination of silica-alumina surface acidity was performed by Mapes and Eischens [29] when they incorporated infrared spectroscopy with the chemisorption of ammonia. Though this work encountered significant experimental difficulties, the authors felt certain that they had observed both Brønsted and Lewis acids on the surface of a silica-alumina catalyst, and that most of the acid sites were of the Lewis type.

The use of pyridine rather than ammonia for infrared studies of chemisorbed bases was suggested by Parry [30]. The pertinent pyridine absorption bands are well separated and removed from possible interference with bands arising from water or surface hydroxyls.

Research reported by Ward and Hansford [31] has made use of the infrared spectrum of chemisorbed pyridine. A linear relationship was observed between the amount of Brønsted acid (peak height/sample mass) and the temperature required for an o-xylene isomerization conversion of 25% (See Figure 2), using a zeolite catalyst. A similar study by Schwarz [17] using silica-alumina catalysts of varying silica content measured Brønsted acid site concentrations in good agreement with previously reported activities for the isomerization of o-xylene over similar silica-alumina catalysts [10].

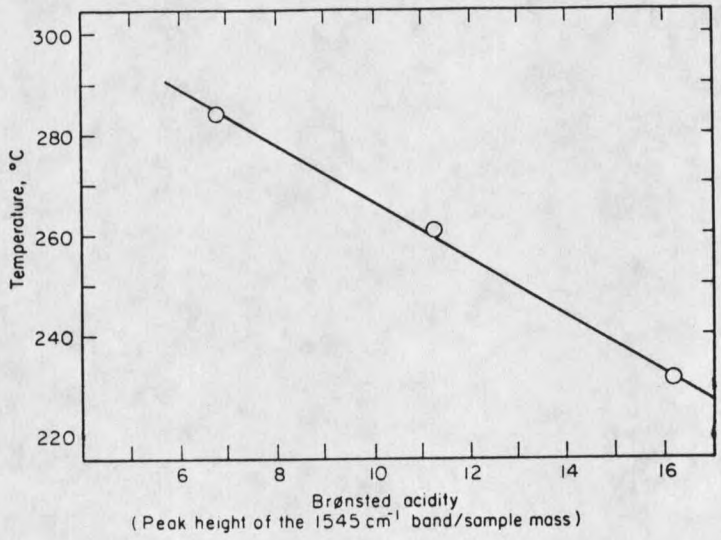

Figure 2. Correlation between catalyst activity (as measured by the temperature required for 25% conversion of o-xylene) and the Brønsted acidity of rare earth Y zeolites [31].

Infrared measurements of chemisorbed pyridine was also tried by Bourne et al. [11] as a way of identifying acid sites on two types of silica-aluminas. The two catalysts consisted of low concentrations (< 1.4 wt.%) of aluminum atoms incorporated on the surface of silica gel or within the silica framework. It was found that dehydrated alumina-on-silica contained only Lewis sites and that dehydrated alumina-in-silica contained only Brønsted acid sites. Addition of water to dehydrated alumina-on-silica converted part of the Lewis acid sites to Brønsted acid sites.

Another infrared study of the interrelationship of silica-alumina acidity and activity for olefin polymerization was performed by Mizuno et al. [32]. From the results of their experiments, the authors found that strong Lewis acid sites (25-30% of the total Lewis acid content) were active for olefin polymerization on silica-alumina.

Catalytic Activity Methods

The primary objective of the various techniques for the characterization of surface acidity thus far described was practical correlation with catalytic activity. For this reason, numerous approaches have been developed to infer surface structures from catalytic activity measurements. One technique, generally described as catalytic titration, involved monitoring a catalytic reaction while a known amount of catalyst poison was introduced into the system. Another technique made use of model compounds which required different acid types or strengths for reaction to occur. Although techniques of these types would seem to provide the most relevant information,

interpretation of data usually required the use of a supportive technique, like those previously described, for complete analysis.

When a catalyst poison is gradually introduced into an acid catalyst system, it will primarily interact with the most acidic (highest energy) sites on the surface. As a result, reactions requiring the highest acid strength will be inactivated first. If the catalyst poisoning continues, progressively weaker acid-catalyzed reactions will be inactivated. Silica-alumina gradually poisoned by pyridine has shown the following reactions have decreasing acid strength requirements [7].

1. Skeletal isomerization of isobutylene to n-butenes
2. Dealkylation of tert-butylbenzene (cracking)
3. Double bond migration and trans-cis isomerization of n-butenes
4. Depolymerization of diisobutylene to butenes
5. Dehydration of tert-butanol to butenes

Effects of partial quantitative poisoning were investigated by Mills et al. [24] by determining the catalytic cracking of cumene over silica-alumina pretreated with various amounts of nitrogenous bases. Results indicated that the amount of poison adsorbed by the catalyst was exponentially related to the weight percent benzene in the product stream. Base poisoning effectiveness was reported as being due to the basicity and thermal stability of the nitrogen bases. However, it also seems to be related to steric hindrance of the acid site,

decreasing in the order : quinaldine > quinoline > pyrrole > piperidine > decylamine > aniline (See Figure 3).

A similar catalytic titration was carried out by Parera [33]. It was found that n-butylamine was 10 times as effective a catalyst poison as sodium, again possibly indicating a steric effect.

Using a model compound for the determination of dealkylation activity on cracking catalysts was the method investigated by Johnson and Melik [34]. The dealkylation of tert-butylbenzene was reported to be catalyzed only by Brønsted acids. Therefore, the Brønsted activity of the catalyst could be determined directly from dealkylation activity. These researchers observed a loss of dealkylation activity with catalyst dehydration and found no correlation between dealkylation activity and nonaqueous titration (Hammett) method.

As previously stated, the stability of a carbonium ion determines its reaction pathway, indeed whether or not the ion will actually be formed. Studies by Andreau et al. [12] and Sugioka and Aomura [35] have made use of the known order of alkyl carbonium ion stability for the investigation of silica-alumina catalysts. Cracking activity of isomeric butylbenzenes follows the order expected when reaction occurs via carbonium ion intermediates. This is in agreement with other studies correlating catalytic activity and Brønsted acidity.

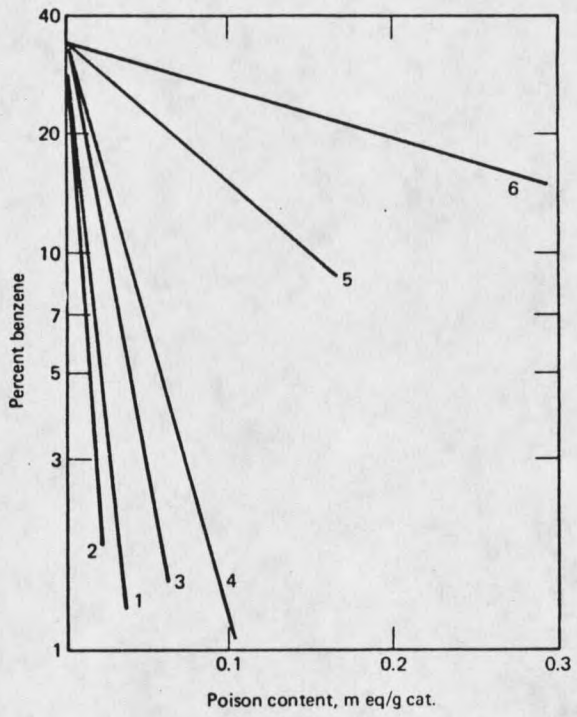

Figure 3. Poisoning effect of amines on cumene cracking over silica-alumina catalyst. 1-quinoline, 2-quinaldine, 3-pyrrole, 4-piperidine, 5-decylamine, 6-aniline [24].

Other Methods

Many more studies of the surface acidity of silica-alumina catalysts have been made, some using a combination of several techniques, some investigating unique techniques.

An extensive study of the effect of sodium poisoning was made by Bremer et al. [13] using ESR spectroscopy, infrared spectroscopy, deuterium exchange, and aqueous ion exchange. The authors concluded that silica-alumina catalysts have a variety of strong Brønsted and Lewis acid sites, with sodium poisoning the strongest Brønsted acids first.

Leonard et al. [14] have reported the use of radial electron distribution and X-ray fluorescence spectroscopies to determine surface defects in alumina and in two series of cogelled silica-aluminas. The authors concluded that Brønsted acid sites occur as aluminum ions tetrahedrally coordinated to oxide ions, found over the entire composition range of the catalysts. At alumina contents greater than 50 wt.%, silicon ions in a perturbed tetrahedral arrangement were believed to provide a new source of Lewis acidity. The researchers found this picture consistent with the patterns of cumene cracking activity observed with other silica-alumina preparations.

Gay and Liang [36] have investigated the use of ^{13}C-NMR spectra for a variety of adsorbed amines on silica-alumina surfaces. The authors have shown that this technique can be used to estimate the concentration of Brønsted acid sites.

Modern surface science is often performed with the use of "surface spectroscopies"[37], referring to methods where the solid-high vacuum interface is probed with a beam of electrons, photons, or ions and similar product species are measured. Measurements of resulting species include species number (quantity), energy, direction, mass, and charge [38].

A comparison of various surface spectroscopic methods is shown in Table 3. Detailed descriptions of the physics of these methods are described in current publications by Morrison [37] and Adamson [38].

Table 3. Surface Spectroscopies.

Technique	Energy Type	Measurement
Ultraviolet Photoemission Spectroscopy (UPS)	40 eV photons	electron energy distribution
X-ray Photoelectron Spectroscopy (XPS or ESCA)	1-1.5keV photons	electron energy distribution
Auger Electron Spectroscopy (AES)	3-10 keV electrons	derivative of electron energy distribution
Energy Loss Spectroscopy (ELS)	1-10 eV electrons	electron energy distribution
Ion Scattering Spectroscopy (ISS)	~1 kV ions	ion energy
Secondary Ion Mass Spectroscopy (SIMS)	~1 kV ions	ion mass

Recent advances in instrumentation, calibration, and analytical technique have made possible the accurate identification of different chemical states of atoms. Wagner et al. [39] have reported improving the accuracy of ESCA line energies for silicon and aluminum compounds by incorporating a modified Auger parameter which can be very accurately determined. However, there is little if any analysis in the literature of ESCA or any of the listed surface spectroscopies concerning surface acidity or catalytic cracking activity.

Adsorption Site Energy Distributions on Heterogeneous Surfaces

Heterogeneity of the solid surface must exist on a molecular level. Heterogeneity is expected to be observed from all physical adsorption and chemisorption data. One rare example of a relatively homogeneous solid surface is that of graphitized carbon. But most certainly the surface of silica-alumina is heterogeneous.

Let us describe the general situation for a gas-solid interaction as relayed by Adamson [38]. Surface coverage is controlled by the pressure (concentration) of the gas, the temperature of the system, and the energy change which occurs as a result of adsorption. As such,

$$\theta = \theta(P,T,Q) \tag{2}$$

Equation (2) assumes uniformly energetic surface adsorption sites.

The heterogeneous surface has a range of surface energies, describable as a general distribution function, f(Q)dQ. The adsorption observed experimentally is the sum over the entire range of surface energies.

$$\Theta(P,T) = \int_0^{\infty} \theta(P,T,Q) f(Q) dQ \qquad (3)$$

The change in adsorption energy with coverage will not be the same function as Θ, that is, the adsorption heat is a weighted average of adsorption occurring on all energies. The surface adsorption sites do not fill up in a distinct strongest-to-weakest energy sequence. Adsorption occurring at absolute zero (0 K) is the only condition where weighted average adsorption does not occur. Experimental data tediously extrapolated to 0 K has been used in an attempt to determine adsorption site energy distributions assuming sequential adsorption [40]. However, it would be preferable to find a way to solve equation (3) using data at more common laboratory conditions.

The first approach to the solution of the general description is to assume some function (model) for $\theta(P,T,Q)$ and f(Q) so that we can integrate equation (3). With the assumption of the Langmuir adsorption model and adsorption energy distribution logarithmically dependent on surface coverage, the Freundlich adsorption expression is obtained [41].

The entire integration problem can be bypassed by assuming linear dependence of Q on θ. A direct substitution of this sort into the Langmuir equation then yields the Tempkin equation [41].

The Freundlich and Tempkin expressions are quite different and it is thereby observed that the solution to general equation (3) is very sensitive to the choice of functions substituted. In addition, exact solutions for Θ can only be obtained by substituting relatively simple models into equation (3). It is quite possible that none of the exact solutions provide a good fit to experimental data. Of course, functions which poorly fit experimental surface coverage tend to be viewed skeptically.

In the attempt to solve equation (3), there is the option of using optimization methods with experimental data to approximate the site energy distribution. Adamson and Ling [27] developed a procedure to obtain a solution to equation (3) by successive approximation. The method begins by assuming a particular model for θ, by which coverage at a particular adsorption energy can be described. The cited authors used the Langmuir expression for θ. As a first approximation, adsorption sites are assumed to fill in a strict energy sequence and an integral adsorption energy distribution function is thereby obtained. The first approximation of the integral distribution yields a calculated adsorption isotherm. The second approximation of the integral distribution function is adjusted from the first by the ratio of experimental to calculated adsorption on a datum point-by-point basis. The second approximation of the integral distribution function yields a new calculated adsorption isotherm. Additional rounds of adjustment and approximation are continued until the graphically observed deviations between the experimental and calculated adsorption isotherms is acceptably low. As stated previously, this technique was

used by Hsieh [26] to interpret ammonia adsorption data for some silica-alumina catalysts.

The adsorption site-energy distribution from equation (3) can also be obtained numerically. The numerical approach is based on approximation of the integral in equation (3) as a summation, thereby obtaining a set of simultaneous algebraic equations. The most direct approach to solving sets of linear equations would be matrix inversion, however this approach is not workable here because the problem is 'ill conditioned'. House and Jaycock [42] developed a computer program using the set of simultaneous equations derived from the assumption that adsorption occurs on a number of surface 'patches' of different adsorptive energy with each unisorptic 'patch' described by the users choice of four model isotherm equations. The program uses the same solution technique as that described by Adamson and Ling for adjustment of the adsorption energy distribution from one iteration to the next.

Another technique for the numerical solution of equation (3) has been presented by Ross and Morrison [43] and, with some improvements, by Sacher and Morrison [44]. The model used is again that of a gas adsorbed 'patchwise' on sites of different adsorptive energy. The gas adsorption density on each patch is described by a two-dimensional virial expansion. Such a multiphase system is considered determined if the standard state chemical potentials and the areas of all patches are known. Solution of the system of simultaneous equations is performed using a sophisticated optimization algorithm. The computer program developed to perform the optimization calculation has been

designated CAEDMON (the Computed Adsorptive Energy Distribution in the MONolayer). Limited use of the computer program has suggested to some that CAEDMON qualifies as a practical technique of testing solids for the presence of surface sites that react to a probe adsorbate [45].

There are a number of comparisons to be made of the optimization methods described here for the solution of equation (3). First, consider the graphical technique of Adamson and Ling and the computer program of House and Jaycock. Both are essentially the same in their method of calculating the adsorption energy distribution. Although the computer program of House and Jaycock develops a series of simultaneous equations to describe adsorption at particular experimental pressures, the adsorption energy distribution thus calculated is smoothed by cubic splines for each iteration, yielding an analysis analogous to the graphical smoothing performed by Adamson and Ling. Both procedures use a step function (adsorption in a strongest-to-weakest energy sequence) as a first approximation for the site-energy distribution and subsequently adjust the distribution on a datum point-by-point basis.

The procedure of Ross and Morrison, like that of House and Jaycock, assumes a patchwise adsorptive energy distribution, a technique that Ross and Morrison have termed Substrate Chromatography [43]. However, Ross and Morrison derive a system of simultaneous equations based on a finite number of discrete unisorptic 'patches'. In so doing, Ross and Morrison have developed a model that permits the system of equations to be overdetermined; that is, there can be more equations (adsorption isotherm data points) than unknowns (the

adsorptive capacity of each patch). In addition, the CAEDMON program solves the system of simultaneous equations using a sophisticated optimization algorithm rather than employing the simplistic point-by-point adjustment of the integral distribution function. Finally, surface heterogeneity using the CAEDMON program is described by the adsorptive capacity or surface area of each discrete adsorption energy patch, as opposed to a smoothed distribution function versus adsorption energy.

Morrison and Ross have criticized [46] the Adamson and Ling method as being analytically unsound. These researchers point out that the Adamson and Ling method adjusts the adsorption energy distribution based on a single datum point, ignoring the effect of the adjustment on the fit of all other data points. In addition, Morrison and Ross contend that the adjustment in question has no logical justification and cannot lead to a unique and optimum solution to equation (3) using experimental data. Dormant and Adamson reply [47] that the only relevant criteria for the choice of a recursion formula is rapidity of convergence and user convenience. Dormant and Adamson also contend that unique solutions to equation (3) are mathematically impossible and that their approximate solution technique is as 'good' as any other.

Catalyst Morphology

The complete characterization of a catalyst requires the determination of the catalyst morphology. Some useful guidelines and

methods for a systematic and coherent description of catalyst morphology are found in excellent reviews by Lecloux [48] and by Lowell and Shields [49].

Some of the parameters used to describe a catalyst texture are porosity, surface area, and pore size distribution. Porosity refers to the accessible void space in a particle per unit volume of the particle. If the particle is a catalyst pellet, porosity includes the intergranular void spaces formed by agglomeration of the primary particles.

Surface area is the measure of the accessible surface per unit mass of catalyst solid. Surface area for a porous catalyst is obtained from the manipulation of physical gas adsorption data.

A technique called the BET method has been extensively investigated for determining the specific surface area of solids. The model used by Brunauer, Emmett and Teller [50] assumes that;

1. adsorption occurs on well defined surface sites of equivalent energy, one adsorbate molecule per adsorption site.
2. multilayer adsorption occurs, with interaction between adsorbed layers but no interaction laterally between molecules in the same layer.
3. ,except for the first layer, adsorbate molecules are in the liquid (condensed) state.

The resulting BET equation can be conveniently written as

$$\frac{X}{V_{ads}(1-X)} = \frac{1}{V_m C} + \frac{C-1}{V_m C} X \qquad (4)$$

where,

$X = P/P_o$, the pressure relative to saturated vapor pressure

V_{ads} = adsorbed volume of adsorbate per unit mass of adsorbent

V_m = the volume of adsorbate just sufficient to cover a unit mass of adsorbent with a single layer of adsorbate molecules

C = a constant varying with adsorbate-adsorbent interactions, related to the heat of adsorption.

The BET equation is normally able to effectively describe most physical adsorption isotherms in the relative pressure range between 0.05 and 0.35. In this relative pressure range, a plot of $X/[V_{ads}(1-X)]$ vs. X should be linear, with C and V_m calculated from the slope and intercept of the straight line.

The V_m value obtained is, by definition, proportional to the specific surface area of the adsorbent. With the use of nitrogen adsorption at liquid nitrogen temperature, the specific surface (m^2/g) obtained by the BET method is given by

$$S_{BET} = 4.35 * V_m \tag{5}$$

where V_m is expressed in cm^3 of N_2 @ STP per gram of solid. The nitrogen molecule surface area is assumed to be 16.2 $Å^2$ [49].

Pore size distribution is the distribution of pore volume versus pore radius. In the kinetic behavior of a porous catalyst, pore size distribution is an important factor.

Pore sizes in the 10-200 Å range are usually obtained from gas desorption data via the modified Kelvin equation [48]. In the 100-10,000 Å range, pore sizes are obtained by the mercury penetration technique based on the Washburn equation [49]. Highly sophisticated equipment has been recently developed to obtain mercury intrusion and gas adsorption measurements.

III. EXPERIMENTAL

Synthesis and Preparation of Silica-Alumina Catalysts

As discussed previously in Chapter II, there are a number of synthesis techniques for the formation of an amorphous silica-alumina catalyst. However, a primary consideration of this research is to minimize contamination of the synthesized catalysts. For this reason, the synthesis procedure used was that described by Bourne et al. [11]. The initial silica sol was formed by stirring a mixture of TEOS (Aldrich Chemical Co. #13,190-3) with twice its volume of deionized water adjusted to pH 2 with hydrochloric acid. It has been reported that polymerization of the TEOS hydrolysis product, silicic acid, is least rapid in this pH region [51]. The mixture was allowed to react overnight (~16 hours), during which the two liquid phases changed to a single liquid phase with a very small amount of white precipitate.

Next, a sufficient amount of aluminum nitrate solution to yield the desired aluminum content in the final catalyst was pipeted into the stirring silica sol. While continuing to stir, 2N ammonium hydroxide was added to the mixture until it gelled at pH 6, as measured with the use of pHydrion paper. The mixture at this point was a hydrogel.

The hydrogel was then transferred to a larger container and slurried with ten volumes of deionized water for about one hour. The slurry was usually centrifuged to aid in the filtration of the gel through Whatman #1 filter paper. The hydrogel was washed twice with

deionized water and then air was drawn through the hydrogel for an hour to remove as much bulk water as possible. The hydrogel was then placed in a drying oven where the material was held at 110°C overnight.

After drying, the silica-alumina material was what is termed a xerogel. The rough granular xerogel was then ground with an agate mortar and pestle, and sieved to a particle size between 140 and 325 mesh for use in all subsequent measurements. Material smaller than 325 mesh was, as a precaution, retained but was not normally used in subsequent measurements. In order to be certain that all occluded contaminant ions were removed, the xerogel between 140 and 325 mesh was slurried in one liter of deionized water. This washing step was not, however, used for the pure alumina material because of aluminum hydroxide peptization in pure water. The washed xerogel was then filtered with Whatman #42 filter paper, dried at 110°C overnight, and stored in a plastic bottle.

Pellets of each test material were made in a single pellet hand press. Approximately 0.05 grams of the washed and dried 140 to 325 mesh material was introduced to a five-mm inside diameter stainless steel cylinder. A pressure of ~10,000 psia was then applied and held for 90 seconds. The pellet thus formed was then pressed out of the cylinder, generally with little damage.

The pelleting procedure was not successful using the pure silica xerogel. For this material, the method of successive pressings described by Huizenga was used [52]. This method produced silica pellets that were more mechanically stable. Small amounts (~5 mg) of

silica xerogel were successively pressed into a single pellet, rather than pressing 50 mg of silica at once.

The final step in the preparation procedure was calcining. Calcination temperature for cracking catalysts has generally been fixed by the temperature at which the catalysts would be used (500-600°C). All of the reported calcination temperatures found in the literature fall into this temperature range. Therefore, 500°C was chosen as the calcination temperature for this study.

Both xerogel pellets and xerogel powder (between 140 and 200 mesh) were calcined in porcelain crucibles. An electric kiln was used to ramp the sample temperature to 500°C over two hours and then held at 500°C for four hours. The silica-alumina materials, now referred to as catalysts, were then removed to cool in a dessicator and finally transferred to glass sample bottles for storage.

Measurement of Water Loss

The amount of water lost by silica-alumina catalysts due to calcination was performed by measuring the weight of xerogel powders before and after calcination. Xerogel water loss measurements were also provided courtesy of Dr. Doug Smith at the University of New Mexico (UNM) Powders and Granular Materials Laboratory using TGA. TGA was performed with a DuPont 990 Thermal Analyzer. A stream of dry nitrogen removed desorbed water continuously as the sample temperature was ramped from ambient to 700°C.

Measurement of Surface Area

The surface areas of test materials used in this study were obtained by gravimetrically measuring their physical adsorption of nitrogen at liquid-nitrogen temperature. The apparatus used to make these measurements had been previously constructed by members of the Chemical Engineering Department at MSU. A diagram of the physisorption apparatus is shown in Figure 4. Sample mass was measured with the use of a Cahn/Ventron R-100 electrobalance. System pressure was determined using a mercury-filled U-tube manometer. Vacuum for the system was obtained using a Sargent-Welch Model 1400 rotary vacuum pump.

Measurements were made to test the physisorption apparatus for accuracy and blank response. Accuracy of the electrobalance was checked using calibration weights from Cahn Instrument Co. Blank response of the physisorption apparatus, primarily to check for buoyancy effects, was performed using low surface area tare weights and nitrogen pressures comparable to those used experimentally. The physisorption apparatus blank response is shown in Appendix B.

The experimental technique used to obtain physisorption isotherm data began with weighing ~0.3 grams $\pm$0.1 mg of test material onto an aluminum dish. The sample dish was hooked to the electrobalance sample hang-down wire and an appropriate tare weight was placed on the tare dish so that the 100 mg $\pm$0.01 mg electrobalance range could be operated. The system was sealed using Dow Corning High Vacuum Grease

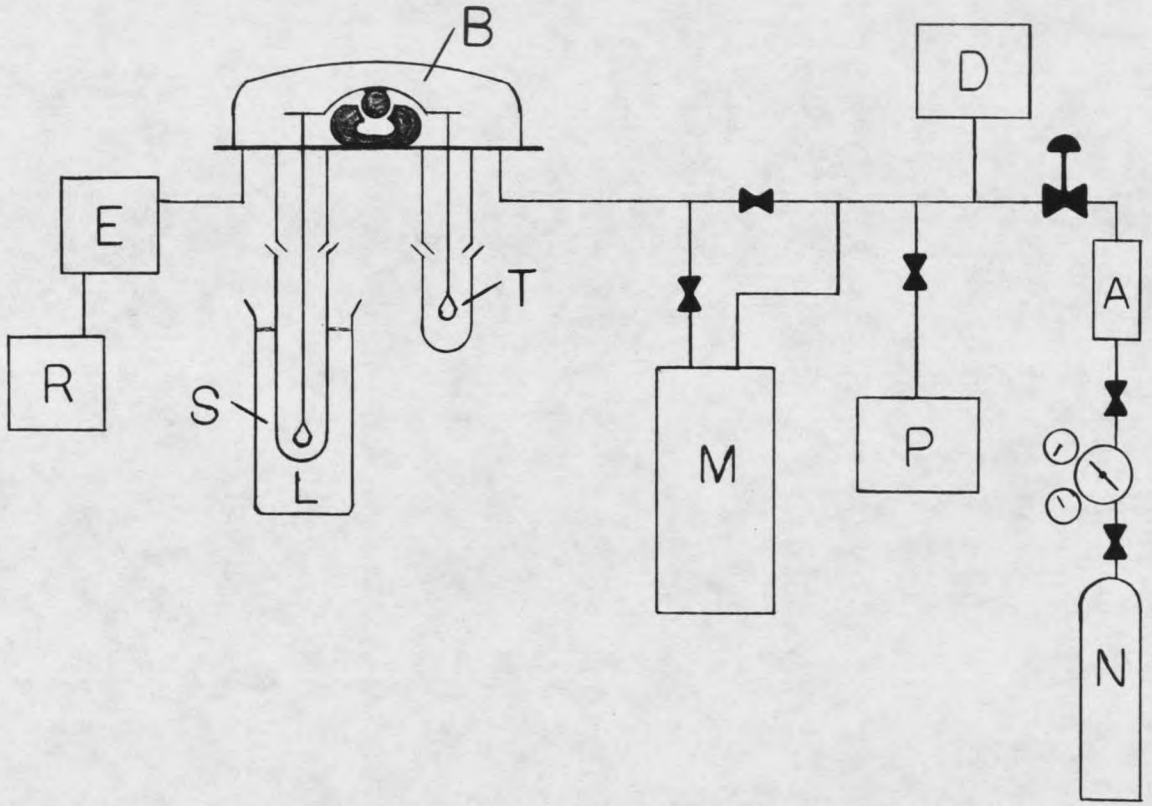

Figure 4. Schematic diagram of the physisorption apparatus for the measurement of surface area. A-water absorber, B-electrobalance, D-thermocouple vacuum gauge, E-balance electronics, L-liquid nitrogen, M-mercury U-tube manometer, N-nitrogen tank, P-rotary vacuum pump, R-chart recorder, S-sample, T-tare.

on the ground glass joints. The vacuum pump was started and the system was allowed to evacuate overnight.

Next, a Dewar flask of liquid nitrogen was raised to immerse the sample hangdown tube above the level of the test sample. Liquid nitrogen was periodically added to maintain a fairly constant level. Once the electrobalance indicated constant sample weight, the initial sample weight and atmospheric pressure were recorded. Nitrogen gas was then introduced to the system to a pressure of ~50 torr. When the electrobalance output indicated equilibrium, sample weight and system pressure were recorded. This process was continued for at least three, but generally four, equilibrium pressures up to a maximum of 225 torr.

Calculation of surface areas was performed using the BETA computer program reproduced in Appendix B. The running program asks the operator for the nitrogen saturated vapor pressure (assumed to be atmospheric pressure), the test sample weight, and the experimental equilibrium pressures with their corresponding weights of nitrogen adsorbed. The adsorbed nitrogen weights are corrected for the buoyancy effect as a function of system pressure. Program output includes the test sample monolayer capacity and surface area, the BET interaction constant (C), and a comparison between experimental data and the BET linear least squares fit of the data.

Surface areas for comparison were also measured courtesy of Dr. Smith at UNM. Measurements were made using a Quantasorb Surface Area Analyzer. Sieved and washed xerogels were pretreated at 400°C for three hours in UHP nitrogen flow prior to analysis.

Nonaqueous Titration

A quick test to verify surface acidity was required to ensure that an acidic catalyst had been synthesized. The technique described by Benesi [21] was used. The entire process was performed in a ventilation hood using protective gloves because of the highly poisonous and/or carcinogenic nature of the reagents.

Thiophene-free benzene (Aldrich #15,630-2) was first dried using dehydrated silica gel and anhydrous calcium chloride. A 0.10M n-butylamine solution was prepared by accurately pipeting one ml of n-butylamine (Union Carbide #S-627060) into a 100-ml volumetric flask and diluting to volume with dry benzene. An indicator solution was prepared by dissolving ~0.1 mg of 4-benzeneazodiphenylamine (from Aldrich #14,383-9 Hammett Indicator Set) in 100 ml of dry benzene.

A silica-alumina xerogel was first ground to <100 mesh and then calcined at 500°C. Approximately 0.5 grams of the calcined silica-alumina was weighed into each of four 50-ml conical flasks and ten ml of dry benzene was added to each. Next, enough 0.10M n-butylamine in dry benzene was added from a 10-ml buret to each of three of the flasks so as to bracket the expected titer of the silica-alumina sample, leaving one flask as a blank. The flasks were tightly sealed with cork stoppers and placed on a shaker to equilibrate overnight. After equilibration, ~3 ml of indicator was added to each flask. At one hour the indicator appeared purple in the presence of solid

acidity and yellow when more than enough n-butylamine had been added to neutralize the solid acidity.

Measurement of Pore Volume Distribution and True Density

Additional physical characterization of catalyst materials was furnished by Dr. Smith at UNM. Mercury intrusion (penetration) measurements over the pressure range of 20 to 33,000 psia were made using an Autoscan-33 Mercury Porosimeter. Catalyst pellets were outgassed at 125°C for half an hour prior to analysis. Calculations on the provided mercury intrusion curves for pore-volume distribution was performed as described by Lowell and Shields [49].

Calcined catalyst powders were tested for their true density. A helium micro-pycnometer was used to measure helium penetration into the test materials.

Measurement of Alumina Content

Alumina contents of the xerogels synthesized for this study were determined by Dr. Dennis R. Neuman at the Reclamation Research Unit of Montana State University.

Xerogel samples were dissolved using a multi-acid digestion procedure performed at atmospheric pressure and approximately 100°C [53]. The resulting solutions were diluted including an added ionization suppressant and analyzed for aluminum by flame atomic absorption spectrometry using a Varian AA-975. Results were reported

by Dr. Neuman as percent aluminum. Aluminum contents were corrected for water loss due to calcination and were adjusted stoichiometrically to be reported as percent alumina.

The aluminum analyses were done in two lots. Precision between duplicate samples for the first lot was good with 4% and 10% differences observed. Precision between the two lots was not as good with 8% and 36% differences measured. A precision between duplicates of 10% is good and acceptable for a long, complex analytical procedure like the one used here for alumina determination. Further discussion of the aluminum content results will be presented in Chapter IV.

Chemisorption of Triethylamine

The decision was made to use triethylamine (TEA) as adsorbate. TEA has been recommended [22], as stated in Chapter II, for use as a gaseous base adsorbate because of its stability against dissociation. TEA is also a large molecule when adsorbed, larger than ammonia. Apparent size effects of catalyst poisons have been reported [24,33], so comparison of acid amounts using TEA adsorption with literature values using ammonia can be made. Although TEA is a stronger base than pyridine, TEA is a sterically hindered Lewis base [54]. There is a possibility that TEA will have difficulty coordinating with surface Lewis acid sites and that the adsorption equilibrium will be distorted enough so that strong Lewis acid sites can be discriminated from strong Brønsted acid sites. In addition, TEA is more easily handled than ammonia because it is a liquid at room temperature. Finally, TEA

is not reported to form explosive compounds when in contact with mercury, as is ammonia [55].

Adsorption Apparatus

A gravimetric adsorption apparatus was constructed as part of this study to measure the chemisorption of TEA on test catalysts. Some general considerations for the design of this gravimetric adsorption apparatus were:

1. Apparatus isolation from building vibration.
2. Sensitivity to μg mass changes.
3. High vacuum production and pressure measurement.
4. Sufficiently low leak rate.
5. Corrosion resistance to TEA vapor.
6. Marginal system flexibility because of glass structural requirements.
7. Easy disassembly for sample changing.
8. Ability to inject minute quantities of adsorbate.
9. Control and measurement of test adsorbent sample temperature.

The chemisorption apparatus is shown schematically in Figure 5 and pictured in Figures 6 and 7. The apparatus, for descriptive purposes, is subdivided into four parts. The apparatus support structure is described first. Next is a description of the balance with its associated glassware and equipment. The adsorbate injection and vacuum measurement equipment is then discussed. And finally, there follows a section devoted to the vacuum pumping equipment.

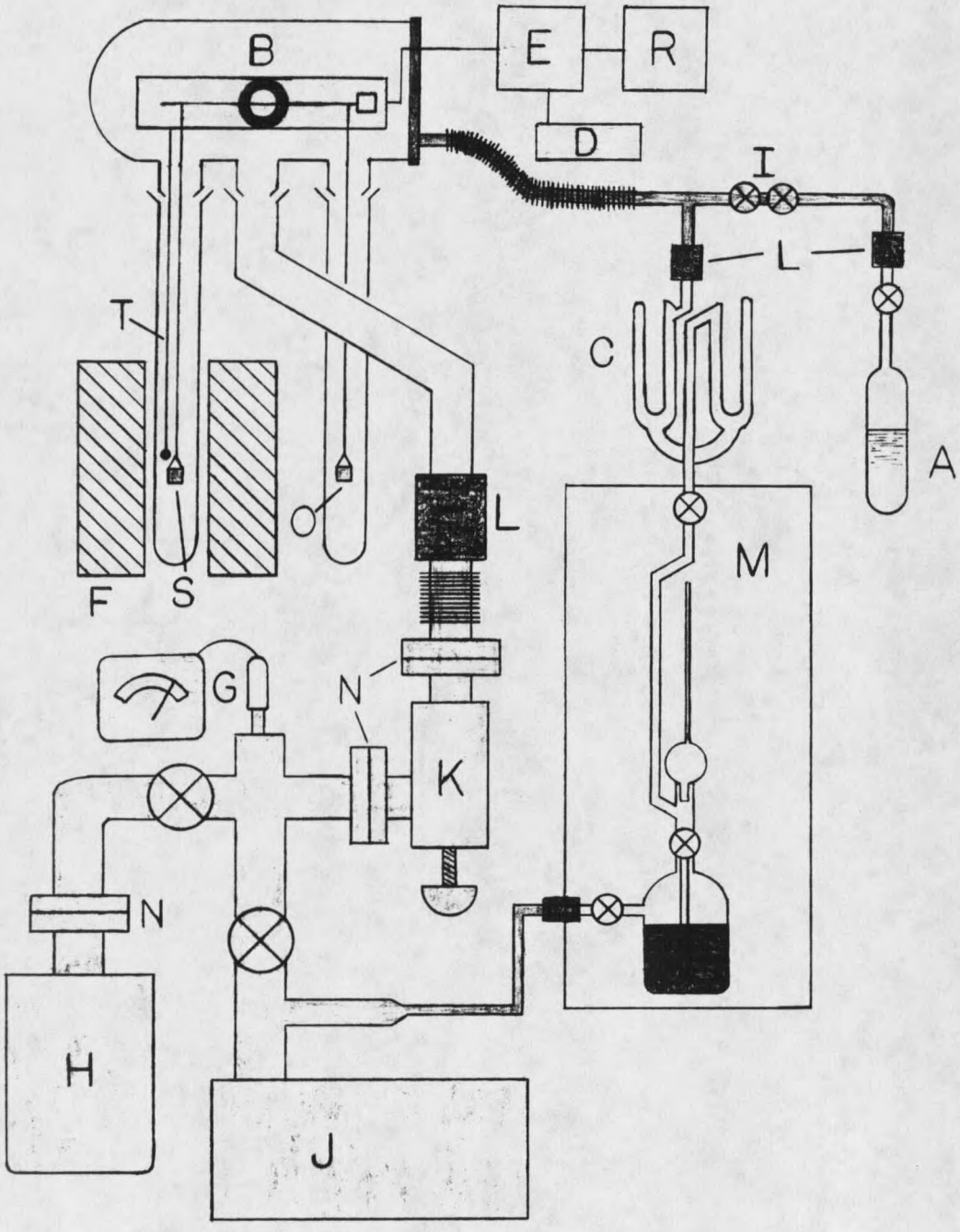

Figure 5. Schematic diagram of the chemisorption apparatus for the measurement of triethylamine adsorption isotherms. A-adsorbate reservoir, B-electrobalance, C-cold trap, D-thermocouple meter, E-balance electronics, F-furnace, G-thermocouple vacuum gauge, H-sorption pump, I-adsorbate injector, J-rotary vacuum pump, K-main vacuum valve, L-vacuum union, M-McLeod gauge, N-flange, O-tare basket, R-chart recorder, S-sample basket, T-sample thermocouple.

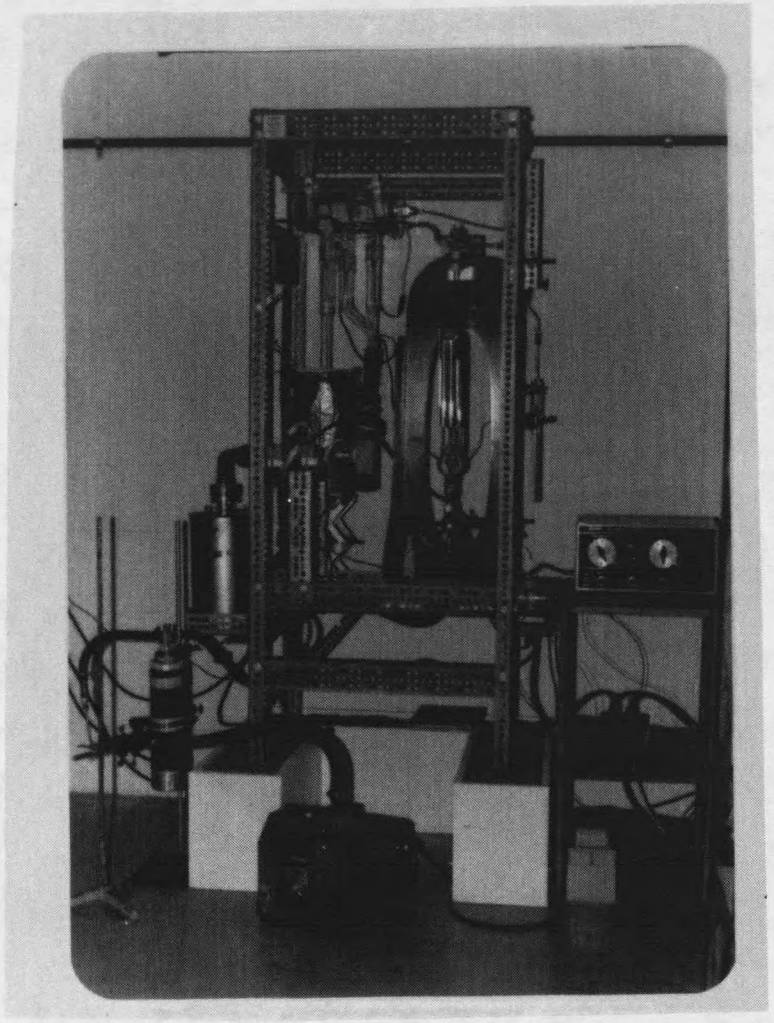

Figure 6. Front view of the chemisorption apparatus.

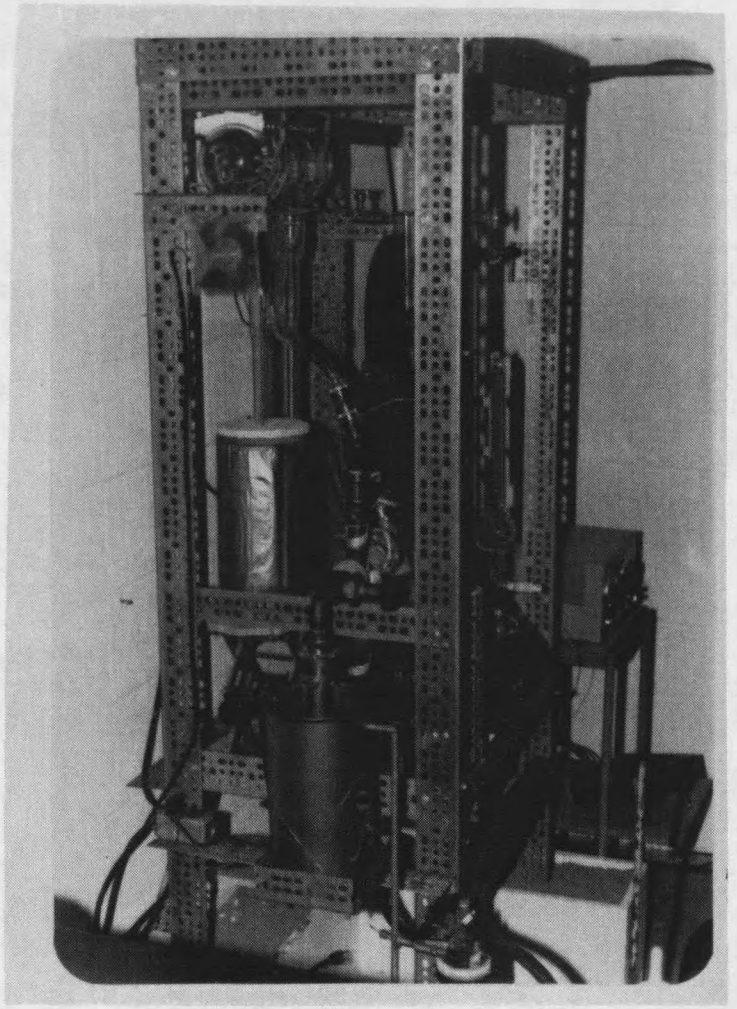

Figure 7. Left-side view of the chemisorption apparatus.

It was recognized that a gravimetric apparatus operating with the high sensitivity necessary for chemisorption measurements would be susceptible to building vibrations. However, the electrobalance installation instructions state that one should not attempt to use any kind of shock mounting and to mount the weighing mechanism as rigidly as possible. So, the angle steel support structure for the apparatus was mounted in a U-shaped sandbox. This technique holds the apparatus in a rigid fashion and yet is not actually attached directly into the building.

The balance used to measure adsorbent weight was a Cahn RG Electrobalance. This type of balance can be routinely used to measure μg quantities and can tolerate many corrosive gas environments. The electrobalance was mounted into a glass vacuum bottle supplied as a Cahn accessory. The vacuum bottle has an aluminum endplate which is o-ring sealed against the glass bottle. The endplate contains a 1/4-inch male Swagelock connector for attaching to the TEA adsorbate injector and vacuum gauge manifold, and a 15-pin electrical connector for linking the balance mechanism to the balance electronics. The vacuum bottle has three 40/35 glass joints that, during system operation, were sealed using Apiezon N grease. Symmetric hangdown tubes, 65 cm in length and 2.8 cm inside diameter, were fabricated as recommended [56-58] to enclose the sample and tare weight baskets within the vacuum system. The baskets were constructed from stainless steel (45 mesh) screen and were suspended from the balance mechanism by 0.0070 inch nickel chromium wire through the outermost glass joints. The third glass joint was used to connect the vacuum bottle

to the vacuum pumping section of the apparatus via a glass-to-metal seal, accomplished with a Cajon Ultra-torr union. Sample temperature was adjusted and controlled using a 36 cm annular resistance furnace with power supplied by a variable autotransformer. Sample temperature was obtained from a K-type thermocouple inside the vacuum system, positioned in the proximity of the sample basket. Temperature was read from a Cole-Parmer thermocouple meter. Output from the balance electronics was recorded using a Varian 9176 chart recorder.

The manifold which connects the vacuum gauge and adsorbate injector with the rest of the apparatus, constructed entirely of stainless steel tubing and Swagelock fittings, was attached to the balance vacuum bottle Swagelock connector with a 6-inch flex tube for system flexibility. A Hastings McLeod-type vacuum gauge, requiring high purity mercury, was used to measure system pressures of 10^{-5} to 20 torr. A cold trap, located between the gauge and the rest of the system, was used during measurements of pressures less than the room temperature vapor pressure of mercury (~0.002 torr). Injection of small amounts of TEA adsorbate into the apparatus was accomplished using two coupled Nupro bellows valves. A glass reservoir containing the TEA adsorbate (99+%; Aldrich #23,962-3; flammable, corrosive and toxic) was attached to the injector valves with a 1/8-inch Cajon Ultra-torr union.

The manifold for the vacuum pumps (lower-left section of Figure 5) was connected to the vacuum bottle Ultra-torr union using a 3" x 1" diameter flex tube, again for system flexibility. The manifold was constructed primarily of brazed copper fittings maintaining at least

one-inch inside diameter for pumping speed purposes. The manifold also included three 2.75 inch flanges sealed with copper gaskets. The main cut-off valve between the vacuum pumps and the vacuum system was a General Electric high-vacuum stainless steel bellows valve. In addition, two brass non-critical vacuum valves were used to switch pumping operations. Rough pressure measurement during pumping was made using a Consolidated Vacuum Products thermocouple vacuum gauge. Rough pumping of the adsorption vacuum system and the McLeod gauge mercury reservoir was performed with a Sargent-Welch rotary vacuum pump. Final vacuum pumping of the system was accomplished using a General Electric sorption pump.

The balance vacuum bottle, injector manifold, and vacuum pump manifold were wrapped with electric heating tape. Low temperature heating (~60°C) of these areas was used to bakeout the system during evacuation.

Blank Measurements

The chemisorption apparatus contained forty-three separable (not welded or brazed) connections of one type or another. Therefore, determination of the apparent leak rate of the system was an important blank measurement due to the static and expected long-term operation of the apparatus. Leak rate measurements made during initial testing of the entire chemisorption apparatus (including the vacuum pump manifold) indicated a constant leak rate of 8.7 μm Hg/hr over a two week period. Leak rate measurement of the vacuum chamber made during catalyst adsorption experiments ranged from 3.0-3.8 μm Hg/hr.

Blank measurements were made to test for changes in observed sample mass due to changes in sample temperature at constant pressure and to changes in system pressure at constant temperature. Changes in observed sample mass for both cases were highly variable. Sample temperature changes of 380°C at constant pressure caused variations in balance output as large as ±0.020 mg. The variations in observed mass with changing pressure (±0.007 mg) was comparable to the observed variability in the baseline output from the balance (±0.005 mg). Because of the random nature of these variations, no corrections of sample mass were made for changes in experimental temperature or pressure.

Experimental Method

1. Activate the sorption pump by evacuating for 4 hours using the rotary vacuum pump. During this process, the sorption pump is heated to 150°C with its internal resistance heater (power controlled by variable autotransformer). After pumping, close the sorption pump valve and allow it to cool to room temperature. The molecular sieve inside is now activated for adsorption pumping.

2. Pump out the TEA reservoir, cooled in an ice bath, through a liquid nitrogen-cooled trap using a rotary vacuum pump. This ensures that the reservoir will supply only TEA vapor to the adsorbate injector. Close the reservoir valve and install the reservoir into the chemisorption apparatus.

3. Apply Apiezon N grease to the three ground glass joints.

4. Weigh adsorbent (catalyst) sample into the sample basket to within 0.1 mg. Store the sample in a dessicator until step 6.

5. Based on the measured sample weight, adjust the tare weight for operation on the 10 mg range. Install the tare hangdown tube.

6. Hang the sample basket on the sample hangdown wire. Install the sample hangdown tube. Check for proper balance operation and for proper sample and tare basket position in the hangdown tubes. Static electricity hampering proper balance operation must be relieved using a Staticmaster ionizing unit.

7. Connect the vacuum bottle to the vacuum pump manifold.

8. With the main cut-off valve closed, start the rotary vacuum pump. When the pump has evacuated the vacuum pump manifold, slowly open the main valve. Allow the system to evacuate slowly so as not to cause stress during system adjustment to vacuum conditions.

9. A properly sealed system can be verified by observing the pressure decrease indicated by the thermocouple vacuum gauge. If all components are operating properly, the procedure is continued.

10. Pump out the system to approximately 20 μm Hg (0.02 torr). At this point, the McLeod gauge valve must be closed to prevent volatilization of mercury into the vacuum system.

11. Install the furnace around the sample hangdown tube and raise the furnace until the sample is centered in the furnace. Apply power to the furnace for a sample temperature of 150°C.

12. Switch on the power to bakeout the apparatus. Continue rotary pumping to evacuate the system overnight (~16 hours).

13. After overnight evacuation, system pressure will be about 1 μm Hg. Increase power to the annular furnace to achieve the sample temperature of interest (usually 300°C).

14. Open the sorption pump valve and continue rotary vacuum pumping of both the system and the sorption pump.

15. When the sample temperature and weight have stabilized, close the rotary pump valve and shut off the rotary pump.

16. Immediately fill the sorption pump with liquid nitrogen to commence sorption pumping.

17. Shut off power to the bakeout. Continue sorption pumping for at least four hours or until the sample weight has stabilized. The system pressure at this point will be reduced to approximately 0.01 μm Hg (10^{-5} torr).

18. Record the initial catalyst sample weight.

19. Close the main cut-off valve. Close the sorption pump valve. Close the innermost injector valve and fill the injector system with TEA vapor by opening the TEA reservoir valve.

20. Close the second injector valve and open the innermost injector valve. This process injects the small amount of TEA vapor between the valves into the system.

21. Open the McLeod gauge valve. Measure the system pressure. Allow the sample weight to equilibrate. Equilibrium was assumed to exist if the apparent sample weight changed less than 2 μg over a period of one hour. Measure the new sample weight, again measure the system pressure, and record the sample temperature.

22. Repeat the TEA adsorbate injection procedure and the measurement of weight, pressure, and temperature. This process is repeated for as many isothermal adsorption data points as are required. When injection of TEA is no longer required, close the TEA reservoir valve.

23. Isobaric adsorption data points can be obtained by varying the sample temperature at any particular system pressure.

24. Once the adsorption experiment is complete, the TEA vapor must be removed from the apparatus. Install a glass cold-finger condenser into the vacuum pump manifold between the rotary vacuum pump and the rotary vacuum pump valve (See Figure 6). Start the rotary pump and pump out the condenser with bakeout overnight.

25. Cool the condenser with liquid nitrogen. While continuing to pump, open the system main cut-off valve. TEA vapor will be trapped as a solid in the condenser, preventing contamination of the vacuum pump oil or the laboratory environment. Power is supplied to bakeout the apparatus during this process.

26. When the system pressure is reduced to that observed in the condenser and vacuum pump manifold prior to TEA removal, the main cut-off valve is closed and pumping is stopped. The condenser is removed to a ventilation hood where the TEA will melt and evaporate safely. Power to the sample furnace and to bakeout is shut off at this time.

27. Close the injector valves and separate the connection between the injector valves and the TEA reservoir. Slowly open the injector valves to allow the system to achieve atmospheric pressure. Open the main cut-off valve.

28. Remove the sample furnace. Separate the connection between the balance vacuum bottle and the vacuum pump manifold. Remove the sample and tare hangdown tubes. Remove the test catalyst from the sample basket.

29. Clean all grease from the ground glass joints. O-rings in Ultra-torr fittings are cleaned and a very small amount of grease is applied to ensure good seals. The system is now ready to repeat the entire procedure for the next test catalyst.

Calculations for TEA Adsorption Isotherms

The actual mass reading obtained from the electrobalance was the percent of the mass dial range. The relative mass for any equilibrium measurement was then obtained by multiplying the percent of the mass dial range by the mass dial range and dividing by 100. The change of mass observed for the adsorbent due to TEA adsorption at any equilibrium system pressure was obtained by subtracting the relative mass recorded at step 18 of the experimental method, when the system was completely evacuated yet prior to any adsorbate injection, from the relative mass at that equilibrium pressure.

The volume of gas adsorbed at any particular system pressure was calculated using standard temperature and pressure ideal-gas molar volume and the molecular weight of the adsorbate (for TEA = 101.19 g/mole). The volume of gas adsorbed was then divided by the mass of adsorbent as weighed into the sample basket, yielding V_{ads} in units of cm^3/g.

Adsorbent temperature was not controlled well enough to prevent as much as $\pm 2.5°C$ changes in temperature through the course of an experiment. For this reason, isobars were measured for each adsorbent at the maximum experimental pressure of each run. Most isobars were observed to be linear functions of temperature over the limited range tested. Using these isobar slopes, the V_{ads} data was corrected to an average isotherm temperature. This correction was made assuming that the isobar slope was independent of pressure over the entire experimental pressure range.

The gravimetric adsorption system pressure was measured using the McLeod gauge. In general, the pressure was determined using the calibration data supplied with the McLeod gauge instruction manual. However, system pressure could also be calculated using Boyle's Law, the volume of gas initially trapped in the gauge, and the cross-sectional area of the capillary into which the gas is compressed.

Through the course of this investigation, difficulties were observed in the use of the McLeod gauge for the measurement of system pressure. First, the gas being measured in the gauge for pressure must behave as an ideal gas. It was thought that the pressure changes occurring as a result of the McLeod gauge operation process would not compress the TEA adsorbate enough to cause condensation. However, TEA condensation was observed in the McLeod gauge on a few occasions. In addition, adsorption experiments usually required a period of 7-10 days. Even though the leak rate in the apparatus was quite low, the correction for leak rate would often become larger than the adsorbate pressure being measured.

Because of the uncertainty involved in the use of the McLeod gauge-measured pressures, equilibrium adsorbate pressures were calculated from the mass of TEA injected, the mass of TEA adsorbed and the volume of the apparatus. The injector volume was measured gravimetrically with water and with carbon tetrachloride. With the injector volume known, the apparatus volume was calculated by making injections of the atmosphere (at known pressure) and measuring the system pressure change with the McLeod gauge. Once the apparatus volume was known, the adsorbate equilibrium pressures were calculated using the ideal gas law and the amount of TEA injected less the amount of TEA adsorbed.

Calculations for the Application of the CAEDMON Program to TEA Adsorption Isotherms

Of the techniques discussed in Chapter II for describing surface heterogeneity, the CAEDMON program seemed to have the most legitimate foundation for the determination of adsorption energy distributions. This decision was in no small way influenced by the exchange of criticisms between Morrison and Ross [46] and Dormant and Adamson [47]. However, application of the CAEDMON program was not made blindly. Limitations concerning the use of CAEDMON will be detailed in this section and in Chapter IV with the discussion of TEA adsorption results.

The CAEDMON model begins with the assumption that adsorption occurs on surface sites at discrete, distinct energy levels. All adsorption occurring at a particular adsorption site energy level is

lumped together into what is termed a unisorptic 'patch'. The CAEDMON model then uses a two-dimensional virial expression to model the adsorption isotherm on each patch. Finally, the CAEDMON program optimizes the sum of the calculated adsorption on all patches to match the experimental adsorption isotherm. A more complete, mathematical description of the CAEDMON technique is shown in Appendix C.

The CAEDMON program requires a number of decisions concerning variables applied to the calculation procedure in addition to the system temperature, the equilibrium gas pressures and their corresponding amounts of gas adsorbed per unit mass of adsorbent. These variables are the number of unisorptic patches and the second and third reduced two-dimensional (2D) virial coefficients.

The CAEDMON program, as kindly supplied by Dr. Richard Sacher of Rensselaer Polytechnic Institute, included a sample data set from nitrogen adsorption on annealed Spheron at 77.0 K. Use of the sample data was made to test the program output for its sensitivity to variations in user supplied variables. Tests were made changing either the number of patches or the virial coefficients. The sample data set was observed to have several inconsistencies (increases in pressure yet decreases in volume adsorbed), perhaps incorporated by the program authors to test sensitivity to experimental error.

Observations concerning the user supplied variable tests, while shown in their entirety in Appendix C, are condensed as follows:

1. Changing the number of homotactic patches appeared to change the adsorption energy distribution shape, however the total capacity of the patches (V_m) remained fairly constant.

2. A 20% variation of the second virial coefficient (B) was observed to shift the capacities of some homotactic patches more than others. Slight energy changes were observed. The total capacity varied only 3%.
3. A 20% variation of the third virial coefficient (C) indicated a negligible effect on the energies of patches. The capacities of the patches were, in some instances, varied comparably to those variations observed due to B coefficient changes. However, the total capacity again remains relatively constant.
4. Combined variations in B and C coefficients were observed to cancel each other if the variations were set to be equal and opposite in sign. If the variations were set to be equal and same in sign, the effect was similar to that found for a variation in B alone.

Overall, variations in the virial coefficients can cause large relative changes in some patches of the adsorption energy distribution. However, this variation does not appear troublesome, especially in light of the ensuing discussion concerning the test adsorbate TEA.

In order for the CAEDMON program to be used in the analysis of TEA chemisorption, a decision must be made concerning the values of the two-dimensional virial coefficients for this adsorbate. A table of reduced second and third virial coefficients for gases in two-dimensions has been reported by Morrison and Ross [59] as a function of reduced temperature. These values were derived using the Lennard-Jones (6:12) potential to describe the interaction of gas molecules.

Although the Lennard-Jones (6:12) potential has been used to describe many gases, it is known that this simplistic description is not well founded for larger than diatomic molecules and particularly not for polar molecules. Polar molecules would be better, though not completely, described using the Stockmayer potential, which is essentially the Lennard-Jones (6:12) potential with the addition of an angle dependent term to account for the electrostatic interaction of two 'point' dipoles [60]. From the literature search, calculation of two-dimensional virial coefficients for the Stockmayer or other potential functions is formidable and publishable work. For this study, the Lennard-Jones (6:12) potential and the tables of Morrison and Ross will be used.

The Lennard-Jones (6:12) potential is a function of two parameters; ϵ -the maximum energy of attraction, and σ -the distance of closest approach of two molecules. These parameters have been calculated on a fundamental basis using quantum mechanical and spectroscopic means for, of course, only the most simple molecules. For other gases, the two parameters have been calculated from transport properties such as viscosity or diffusivity. However, these parameters are not available for TEA. The alternative was to use estimation techniques [61,62]. Calculations using four estimation techniques are included in Appendix C. There was good relative agreement between the various methods. The results from the most currently published estimation technique were used for this study (ϵ/k = 428 K, σ = 6.2 Å).

A value for ϵ is all that is required to calculate the reduced gas temperature and, subsequently, the 2D virial coefficients. However, the distance of closest approach (σ) was also estimated and its value might yield some information as to the validity of the estimation technique. The square of σ is sometimes used as a measure of molecular cross-sectional area. The value of σ^2 is 38 Å^2, which compares well with the 41-43 Å^2 found using two other molecular area estimation techniques (Appendix C) and with the 43 Å^2 reported for TEA adsorption on silica at 593 K [63].

There are some polar molecules that have Lennard-Jones (6:12) parameters reported in the literature. The closest analogy to TEA is ammonia. Unfortunately, there are two different values of ϵ and σ for ammonia in two different tables of Reid, et al. [61]. It has been recognized that this is not unusual when transport properties such as viscosity are used to calculate interaction parameters.

As is shown in Appendix C, the estimation of σ for ammonia using the method accepted by this study compares very well with one of the values found in the literature. However, this estimation technique for the ammonia energy interaction parameter yields a value that corresponds to the average of the two tabled values. With this kind of difficulty for ammonia, the energy interaction parameter for TEA is certainly suspect.

Calculations of the expected variations in the reduced 2D virial coefficients for TEA based on expected error in the energy parameter are also shown in Appendix C. Variation in the coefficients were observed to be roughly equal in magnitude but opposite in sign. As

previously discussed, this type of error seems to cancel in the CAEDMON calculation and the net effect on the adsorption energy distribution is small.

To conclude, there is doubt concerning the Lennard-Jones (6:12) interaction parameters for TEA. However, the expected errors in the implied 2D virial coefficients should not have a significant effect on the computed adsorption energy distributions. In the worst case, the adsorption energy distributions should at least be internally consistent within this study.

Catalyst Activity Using Isomerization of o-Xylene

In the 1940's and 50's, cracking catalyst testing was performed using gas-oil as the reactant and percent gasoline fraction formed as the measurement of activity. At this same time, researchers began to use less complex reactions as indicators of catalytic activity for several reasons. A less complex reaction is more easily interpreted in terms of analysis, conversion, and mechanism. In fact, it would seem that an elementary reaction would be the best choice for fundamental laboratory experiments. However, use of an elementary reaction to measure catalyst activity will always leave doubt as to the catalyst activity in an industrial process such as gas-oil cracking, where the feed material is likely to be a complex mixture.

Numerous simple reactions have been used to test silica-alumina materials in the laboratory for catalytic activity. These reactions include the cracking of octane [10], butyl benzenes [12,34,35], and

cumene [12,24,33,64], the polymerization of propylene [8,10], the transfer/exchange of hydrogen [10], and the isomerization of o-xylene [10,31,65]. As discussed in Chapter II, some reactions have been correlated with surface Brønsted acidity, some correlated with surface Lewis acidity.

The reaction that is of interest for this research study is the isomerization of o-xylene. There are several reasons for this decision. First, there is very strong correlation of silica-alumina and zeolite activity for o-xylene isomerization with infrared measurements of surface Brønsted acidity [17,31]. Next, the performance and analysis of the o-xylene isomerization reaction is comparatively and conceptually easy. For instance, the heat of reaction for o-xylene isomerization is less than ½ kcal/mole, which eliminates the potential problem of temperature gradients occurring in the catalytic reactor or in the solid catalyst itself. The reactant and products all have the same molecular weight, simplifying gas chromatography analysis. Finally, an additional reason for measuring o-xylene isomerization is because this reaction is a primary test reaction for the evaluation of acid catalysts at Union Oil Company of California [66].

Reactivity Apparatus

The apparatus constructed for the testing of o-xylene isomerization activity on silica-alumina catalysts is shown in Figure 8. For descriptive purposes, the apparatus can be subdivided into

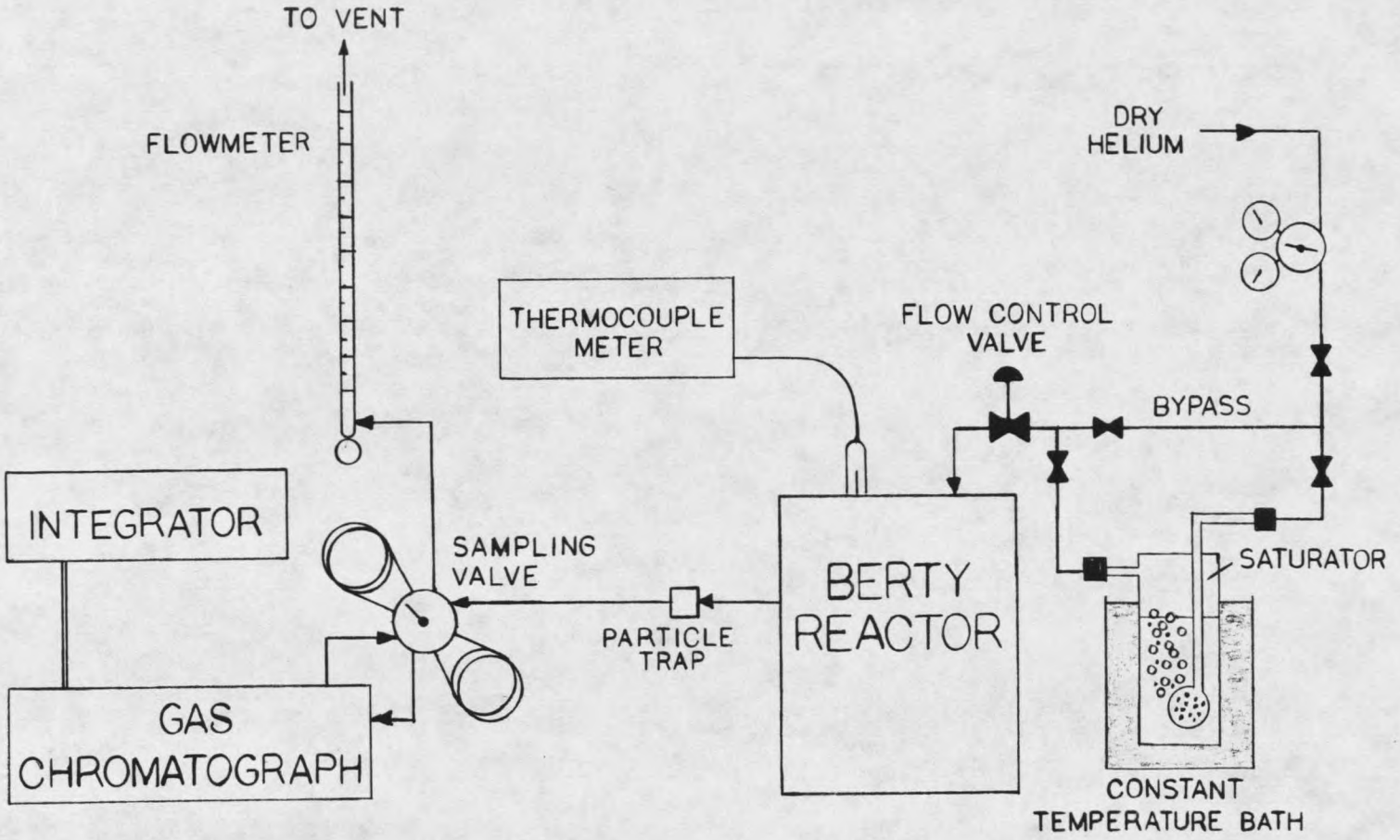

Figure 8. Schematic diagram of the reactivity apparatus.

three sections; the reactant delivery system, the reactor, and the product analysis system.

The reactant o-xylene was delivered to the reactor at its 22°C saturated vapor pressure. This process was accomplished with the use of a glass 'saturator'. Dry helium at less than 1 psig was bubbled through o-xylene (Aldrich Chemical Co. #X104-0), thermostated at 22°C ±0.1°C. Saturation of o-xylene in the helium flow stream was verified in calculations performed by Mr. Loren Luinstra [67].

The o-xylene and helium mixture flow rate was controlled using a Nupro fine metering valve. The delivery line to the reactor, constructed of stainless steel tubing and Swagelock fittings, was heated to prevent condensation of the organic vapor. A bypass line was available for purging the downstream systems with dry helium prior to activity determinations.

The reactor used to contact the gaseous reactant with the solid test catalysts was a 2-inch stainless steel Berty-type reactor from Autoclave Engineers, Inc. The Berty reactor has been described in detail by Berty et al. [68]. The reactor body is electrically heated, the reactor temperature being controlled with three variable autotransformers. The Berty reactor uses an impeller to internally circulate the reactant fluid many times faster than the overall gas-phase throughput of the reactor. Such a high internal recycle ratio yields the appearance of mixed flow reactor behavior. The high gas velocity through the catalyst bed, due to high recycle ratio, has the added benefit of greatly reducing external concentration and

temperature gradients. Such a reactor design has been termed 'gradientless'.

Two other system measurements were made from the Berty reactor. A K-type thermocouple was located in the catalyst support screen for the measurement of reaction temperature. An induction coil located on the impeller magnetic drive unit was calibrated to indicate the impeller speed in RPM.

The product analysis system (See Figure 8) includes the exit flow line from the reactor, the gas sampling valve, the gas chromatograph (GC), the recording integrator, the soap-film flowmeter, and the product gas vent.

The exit flow line from the reactor to the gas sampling valve, constructed of stainless steel tubing and Swagelock fittings, was heated to prevent organic vapor condensation. The exit line also contained a particle trap to prevent any entrained catalyst particles that may have escaped from the reactor from causing downstream damage.

The product gas was sampled using a Valco 1/8" eight-port valve. Sampling loops made of Polypenco Nylaflow pressure tubing were used to inject 8 ml of product gas into the gas chromatograph.

Gas chromatography was used to separate product gases and to quantify the conversion of o-xylene occurring in the reactor. The GC used was a Varian Aerograph Series 1400, fitted with a low-volume thermal conductivity detector. Dry helium was supplied to the GC at 30 psig for use as carrier gas.

The actual separation of o-xylene from its isomerization products was accomplished in a 12' x 1/8" stainless steel column packed with 5%

Bentone-34 + 5% diisodecylphthalate on Chromosorb P. Helium carrier gas flow rate was set at 20 ml/min through the separation column and at 10 ml/min through the reference column with a column oven temperature of 70°C. At these column conditions, complete elution of a product gas sample required one-half hour. The injector ports and the detector were heated to 160°C. The detector current was set at 150 ma. Pretreatment of the column was performed by heating the column oven to 150°C for ½ hour. This GC separation technique was patterned after that described by Spencer [69].

The analyte 'peaks' indicated by the GC detector were recorded using a Hewlett-Packard 3380A recording integrator. The 3380A integrates GC peak areas and calculates the area percent of each peak from a single injection of product gas.

After sweeping through the gas sampling loops, the product gas was directed into a 50-ml buret, used as a soap-film flowmeter. The flowmeter was connected to a vent line so that product gas could be expelled into the laboratory hood.

Blank Measurements

The apparatus for catalyst activity was operated without a catalyst charge for performing several tasks. First, the GC operating conditions were adjusted to ensure that the isomers of xylene would be adequately separated. Next, the o-xylene vapor was checked for its m-xylene contamination. From GC analysis, it was observed that the mean composition of the xylene vapor feed to the reactor was 99.05% o-xylene and 0.95% m-xylene at a saturator temperature of 22°C.

Standard deviation of the m-xylene analysis was 0.25%. Finally, the reactor system was tested for isomerization occurring either homogeneously or on the reactor's internal surface and catalyst supports. The reactor was heated to 412°C and no evidence of isomerization could be observed.

Experimental Method

Two sizes of catalyst were tested in the reactor. Cylindrical catalyst pellets, roughly 4 mm in diameter by 4 mm in length, were supported in the catalyst basket (draft tube) with a 14 mesh stainless steel screen and a glass-wool mat. Catalyst particles sized between 80 and 200 mesh (177 to 74 μm) were supported on a 200 mesh stainless steel screen.

Test catalyst was weighed into the catalyst basket to within 0.1 mg. The amounts of catalysts used varied from 0.1 to 2 grams. The reactor was then reassembled according to the procedure specified in the operation and maintenance manual supplied with the reactor.

With the reactor properly assembled, the helium supply valve to the reactor was opened and a slow flow of helium (~30 ml/min) was directed through the bypass line into the reactor. For protection from the ensuing heat of the reactor, a slow flow of water was started through the magnetic drive unit cooling jacket. Power was then supplied to the reactor heating jacket to attain the reaction temperature of interest. Because of the large thermal mass of the reactor, the heating time allowed for equilibrium reactor temperature and catalyst pretreatment was generally ~12 hours (overnight).

With the test catalyst pretreated and the reactor equilibrated at the desired temperature, the magnetic drive unit was started. The impeller speed was usually set at 1500 RPM to ensure efficient mixing. Then the helium flow was switched from the bypass through the saturator. The desired reactant flow into the reactor was adjusted using the metering valve. Reactant flow rate was ~100 ml/min.

Samples of the product gas were injected into the GC as often as analysis time would permit. At the time of each injection, the reactor temperature, the saturator temperature, the product gas flow rate, and the product gas temperature were recorded. Depending on the experiment being performed, either impeller speed, reactor temperature, or reactant flow rate could be adjusted.

Calculations

The Berty reactor design internally recycles the reactant/product fluid. Reactor operation at a high recycle ratio yields the

appearance of mixed flow reactor behavior, allowing the observed reaction rate to be calculated from the familiar relation:

$$-r_o = m \cdot \Delta X_o / W \cdot S \cdot M \qquad (6)$$

where

$-r_o$ = the rate of disappearance of o-xylene as a result of isomerization, (moles o-xylene/$m^2 \cdot s$)

m = mass flow rate of o-xylene, (g o-xylene/s)

ΔX_o = change in o-xylene conversion

W = mass of test catalyst, (g)

S = surface area of test catalyst, (m^2/g)

M = molecular weight of o-xylene (106.17 g/mole)

The feed rate of o-xylene into the reactor was calculated from the product gas flow rate, the product gas temperature, and the saturated vapor pressure of o-xylene at the saturator temperature. It was assumed that the gas phase behaved as an ideal gas at ambient atmospheric pressure.

The change in the conversion of o-xylene was determined using the integrated peak areas as calculated by the HP 3380A from GC output. Change in conversion was calculated as the sum of the area fractions of m-xylene and p-xylene in the product less the area fraction of m-xylene in the feed.

The mass of test catalyst was as weighed into the reactor catalyst basket. The surface area values used were those measured here at MSU.

The isomerization of o-xylene has been reported to be a first order reaction over several catalysts [65]. Use of the mixed flow reactor performance equation permits the calculation of the first-order reaction rate constant as:

$$k = -\frac{m}{M}\left[\frac{\Delta X_o}{1-\Delta X_o}\right] \tag{7}$$

where

k = first order rate constant (g o-xylene/g catalyst·s)

IV. RESULTS AND DISCUSSION

Preliminary Experiments

The study of silica-alumina catalysts was not a subject under active investigation in the Chemical Engineering Department at MSU until this current research project was begun. For this reason, preliminary experiments were performed to test basic experimental techniques. It was also necessary to see if test material properties were appropriate before pursuing the bulk of the research proposed.

One of the research objectives was to synthesize amorphous silica-alumina while avoiding contamination. The primary source of contamination in industrially prepared silica-alumina is sodium from sodium silicate, the silica hydrogel starting material. Because sodium has been identified as a cracking catalyst poison [3], industrial preparation procedures include a weak acid rinse to aid in sodium removal. To avoid the additional variable of sodium content in the catalysts, the xerogel synthesis procedure of Bourne et al. [11] was tested. A silica xerogel and a silica-alumina xerogel, containing approximately 10-15% alumina (based on the amount of aluminum added during synthesis), were prepared.

Both of these test materials were checked for surface area by measuring neo-pentane physisorption at 273 K. The silica xerogel indicated 660 m^2/g surface area while the silica-alumina xerogel indicated 450 m^2/g. Such surface areas indicated that microporous

materials had been synthesized. The surface areas were comparable to those reported in the literature for similar materials [3].

The silica-alumina test material was checked for solid acidity using the nonaqueous titration technique described in Chapter III. The indicator used for this determination, 4-benzeneazodiphenylamine, reflects acid sites stronger than a pKa of 1.5. Unfortunately, there is some disagreement in the literature concerning the basic-side color of this indicator. If the basic-side color of the indicator is yellow [21], then the silica-alumina material acidity was between 0.36 and 0.46 meq/g. However, if the basic-side color of the indicator is brownish-yellow [70], then the sample acidity was between 0.16 and 0.36 meq/g. Both of these results compare well with their respective references (0.43 meq/g [21], and 0.18 meq/g [70]) for industrial cracking catalysts.

Nonaqueous titration and surface area measurements both indicated that the silica and silica-alumina materials synthesized were comparable to materials described in the literature. Therefore, the synthesis procedure was considered successful.

Synthesis and Preparation of the Silica-Alumina Materials

The silica-alumina synthesis procedure, as described in Chapter III, was used to prepare xerogel materials with expected alumina concentrations of 0, 3, 7, 10, 18, 26, 44, 65, 88, and 100 percent. At this point, an abbreviated notation with which to differentiate the catalyst samples will be designated. It will be done in terms of the

catalyst alumina content as calculated from the quantities of reactants used during synthesis. For example, the catalyst that was formed using the required amounts of TEOS and aluminum nitrate solution to yield a silica-alumina material containing 10% alumina is designated as A-10.

During hydrogel precipitation, the amount of 2N NH_4OH required to bring each polymerizing hydrogel to pH 6 was qualitatively measured. A plot of the moles of hydroxide ion required to form a pH 6 hydrogel versus the moles of aluminum ion added for incorporation is shown in Figure 9.

Figure 9 suggests that a 4/1 mole ratio of hydroxide-to-aluminum is required for neutralization of the hydrogel at low aluminum concentrations in excess silica sol. Further, Figure 9 shows that the hydroxide/aluminum ratio changes to 3/1 for hydrogels formed from solutions containing mostly aluminum. This change in the hydroxide/aluminum ratio for neutralization has been observed previously [3,51]. In solutions containing mostly aluminum, aluminum ions react and polymerize with each other forming a hydrated alumina material, perhaps bayerite or pseudoboehmite [7]. However, in solutions containing mostly silica sol and low concentrations of aluminum, aluminum ions react preferentially with hydroxyl groups of the silica sol rather than polymerizing with each other. This reaction of aluminum with a silica sol has been described by Iler [51] as a metal exchange reaction. The tendency to form Al-O-Si bonds rather than Al-O-Al bonds, according to Figure 9, continues up to 0.8 moles of aluminum ion, corresponding to an alumina concentration in

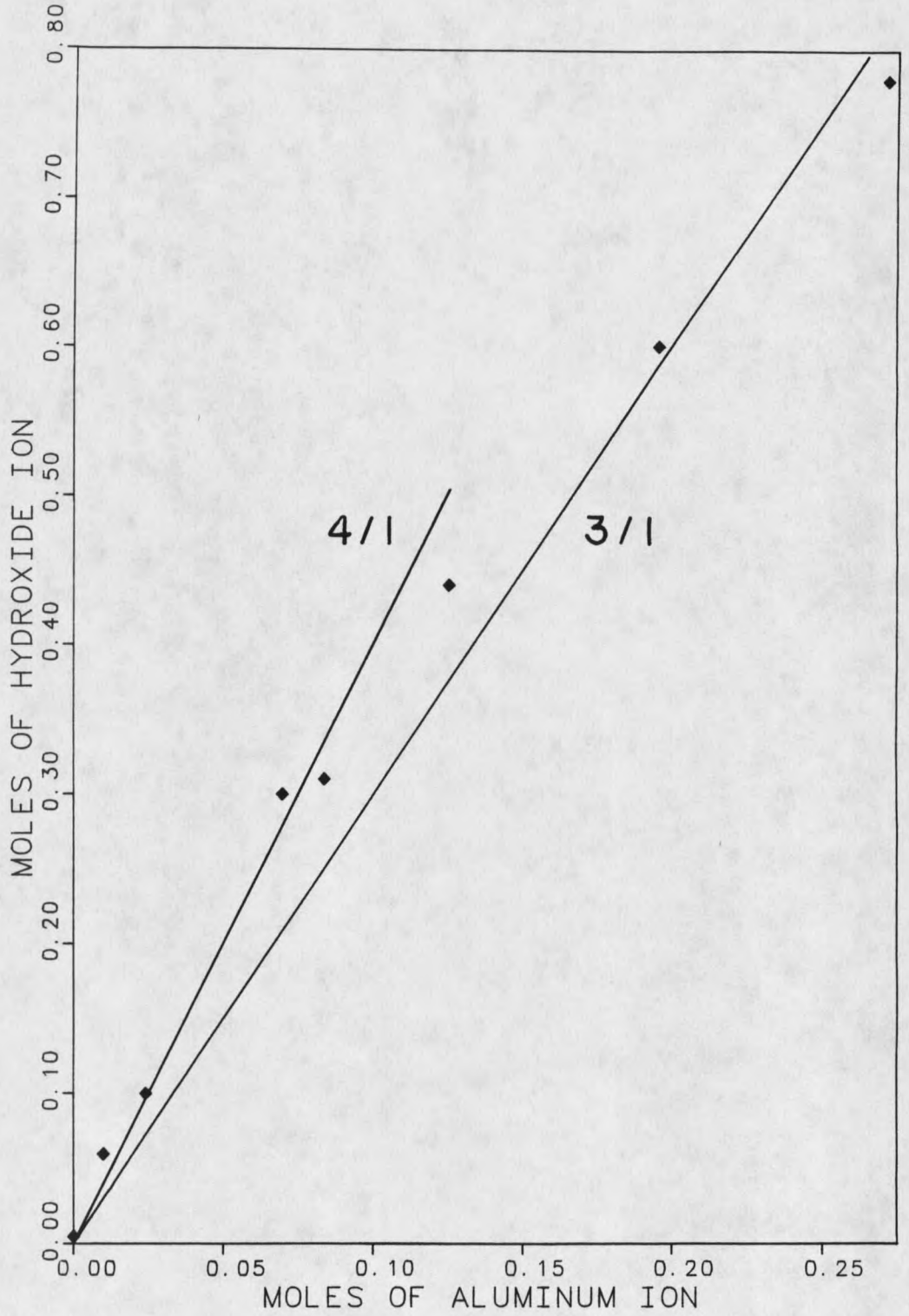

Figure 9. Qualitative relationship of the moles of hydroxide ion required to form a pH 6 hydrogel versus the moles of aluminum ion contained in the reactant solution.

silica of roughly 26%. It has been remarked that this is the concentration at which uniformly distributed aluminum cations on the surface of a silica particle would begin to be interconnected as they are in an alumina particle [6]. In addition, even the 44% alumina material appears to form a significant number of Al-O-Si bonds.

Once the hydrogel was formed, it was then slurried with ten times its volume of deionized water. This step, taken from the synthesis procedure of Bourne et al. [11], caused some peptization of aluminum hydroxide for the 44, 65, 88, and 100% alumina materials.

After grinding and sieving, the xerogels were washed with one liter of deionized water to remove contaminant ions. The washing step was not done for the 100% alumina material because of the significant peptization observed for the 88% alumina material. Peptization of colloidal size aluminum hydroxide particles from hydrogels and xerogels should have been expected due to the very low ionic strength of deionized water.

As was mentioned in Chapter III, the pure silica material was pelletted using successive pressings so that pellets with some mechanical stability could be obtained for adsorption and activity measurements. It was further observed that the catalyst pellets tended to degrade increasingly with decreasing alumina content. The increased catalyst pellet mechanical stability with increasing alumina content seems to indicate increased sintering of primary xerogel particles as the alumina/silica ratio increases.

Chemical Composition of Catalysts

Water Loss

TGA data was provided by Dr. Smith at UNM for several of the silica-alumina xerogels. The TGA curves, plotted as percent of sample weight versus temperature, are shown in Figure 10.

The most apparent observation to be made from Figure 10 is that the sample water loss increases greatly with increasing alumina content. This water loss was also observed from the calcination of pellets in which pellet shrinkage was observed, increasing with increasing alumina content. Such large losses of water, as with sample A-88, were not expected and there was some concern about the portion of this water that was reversibly adsorbed. To test for the amount of reversible water adsorption, a calcined sample of A-88 was allowed contact with the atmosphere for 3 days before heating to 400°C under vacuum. The A-88 sample gained three percent of its weight after contact with the atmosphere and subsequently lost this weight plus one percent more with heating under vacuum. Therefore, the vast majority of the weight lost during the TGA of sample A-88 was either occluded solvent or weakly adsorbed water.

Figure 10 also shows that the water loss for all samples was very slight as the temperature increased above 500°C. It appears that well over 90% of the water lost by these materials with heating to 700°C was removed by a temperature of 500°C.

Measurements of water loss were also made from weight changes due to the 500°C calcination of the silica-alumina xerogels. These

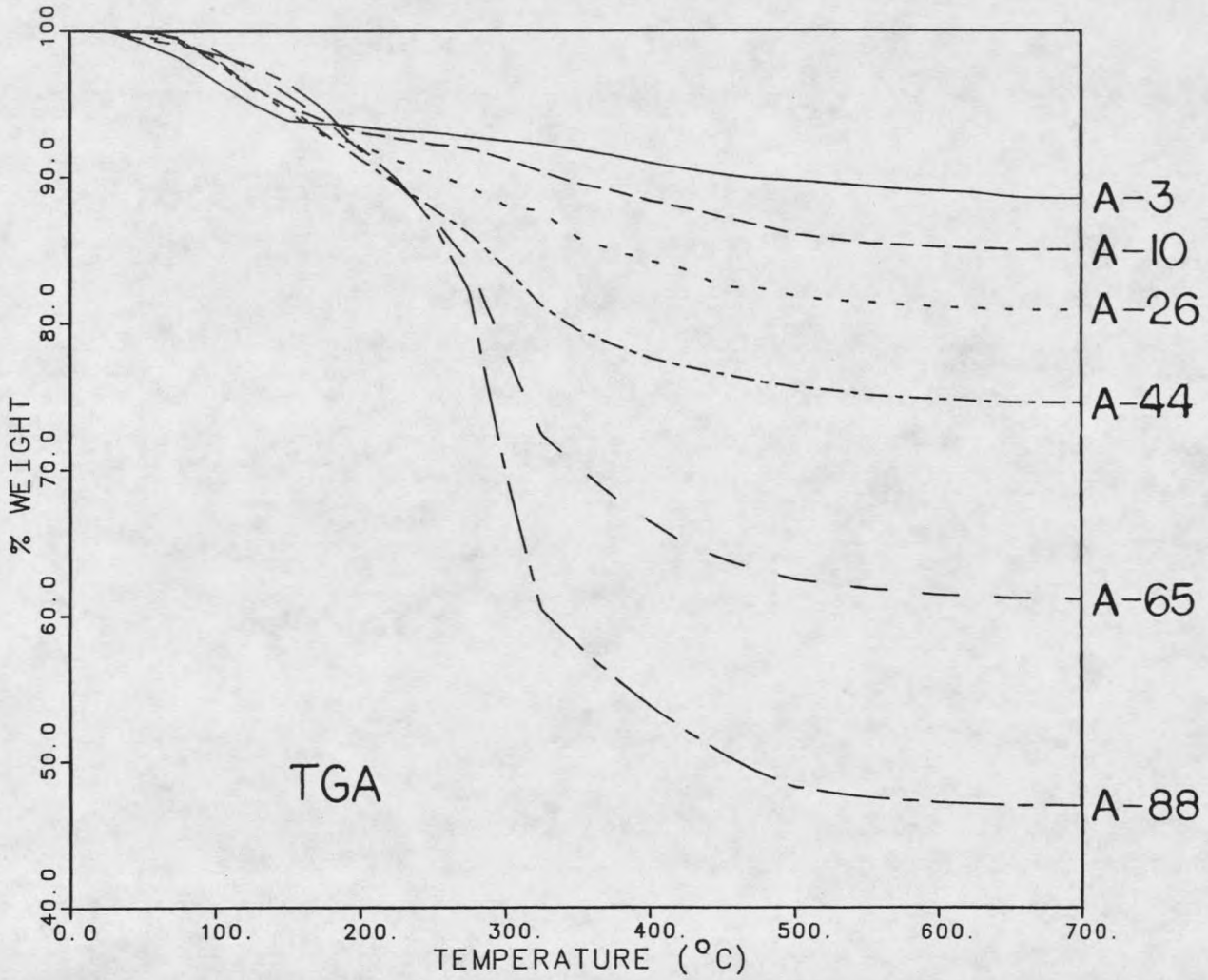

Figure 10. Thermogravimetric analysis for several of the silica-alumina xerogels, depicted as the percent of the original sample weight versus temperature.

measurements, in addition to those obtained at 700°C by TGA, are exhibited in Figure 11. It is observed that the 500°C calcination water loss deviates from that observed at 700°C by TGA for the high alumina content materials, with the exception of the pure alumina sample. Since the TGA environment is one of a dry flowing gas purge, it seems reasonable that a high water-content material would not lose as much of that water in the stagnant-air environment of calcination.

Alumina Content

Analysis of xerogel samples for their aluminum concentrations was made by Dr. Neuman of the MSU Reclamation Research Unit. The aluminum percentages measured for the xerogels are listed in Table 4. Also included in Table 4 are the xerogel water losses from heating to 700°C, taken from Figure 11.

The aluminum concentrations were corrected for water loss and converted to percent alumina. Table 4 also compares the expected and measured alumina contents of the catalysts. As observed from Table 4, precision between duplicate analyses was generally good (less than 10%). Only the duplicate analysis for A-7 indicated a poor precision of 36% difference. In addition, the pure alumina material was measured to within 4% of its expected and logical concentration.

The expected and measured alumina contents of the catalysts are graphically compared in Figure 12. The measured percent alumina of the catalysts increasingly deviates from the expected composition line with increasing alumina content. This deviation is smooth, gradual, and was expected due to the observed peptization of alumina during

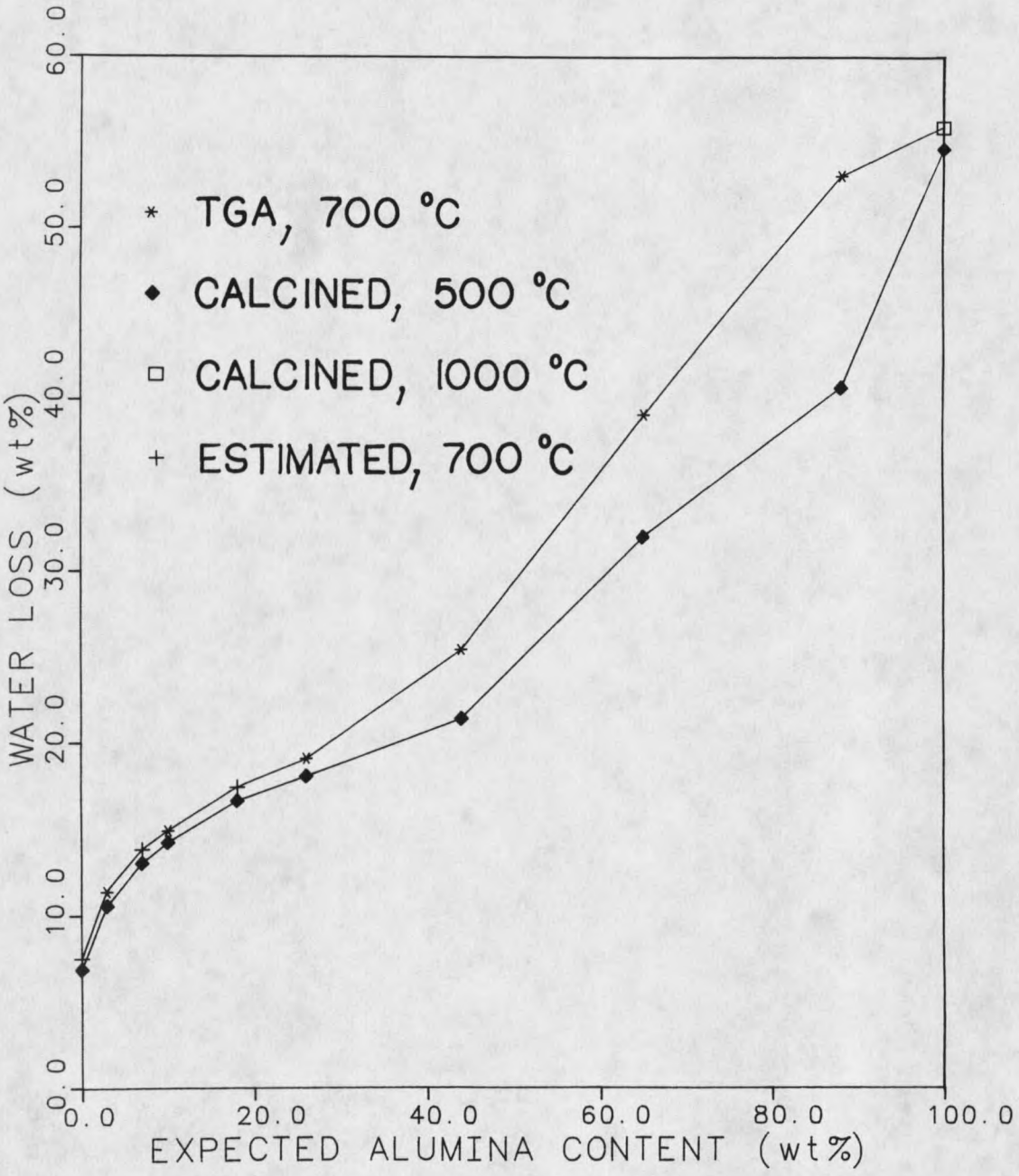

Figure 11. Weight percent water loss as a function of expected alumina content for the xerogels.

Table 4. Catalyst Alumina Compositions

Sample	Measured %Al	$\%H_2O$ Loss @ 700°C	Corrected %Al	Measured $\%Al_2O_3$	Expected $\%Al_2O_3$
A-0	-	-	-	-	0.0
A-3	1.34	11.5	1.51	2.86	3.17
A-3	1.22	11.5	1.38	2.60	3.17
A-7	2.78	13.9 †	3.23	6.10	7.12
A-7	4.02	13.9 †	4.67	8.82	7.12
A-10	3.83	15.0	4.50	8.51	9.87
A-10	3.69	15.0	4.34	8.20	9.87
A-18	6.57	17.5 †	7.96	15.0	18.0
A-26	10.51	19.1	13.0	24.5	25.9
A-44	14.14	25.4	19.0	35.8	44.0
A-44	15.27	25.4	20.5	38.7	44.0
A-65	17.50	38.9	28.6	54.1	64.7
A-88	17.50	53.0	37.2	70.4	88.0
A-100	22.54	55.9	51.1	96.6	100.

† designates estimated values

washing steps of the synthesis procedure. A small portion of the deviation could also be due to additional water loss had the catalysts been heated to temperatures above 700°C.

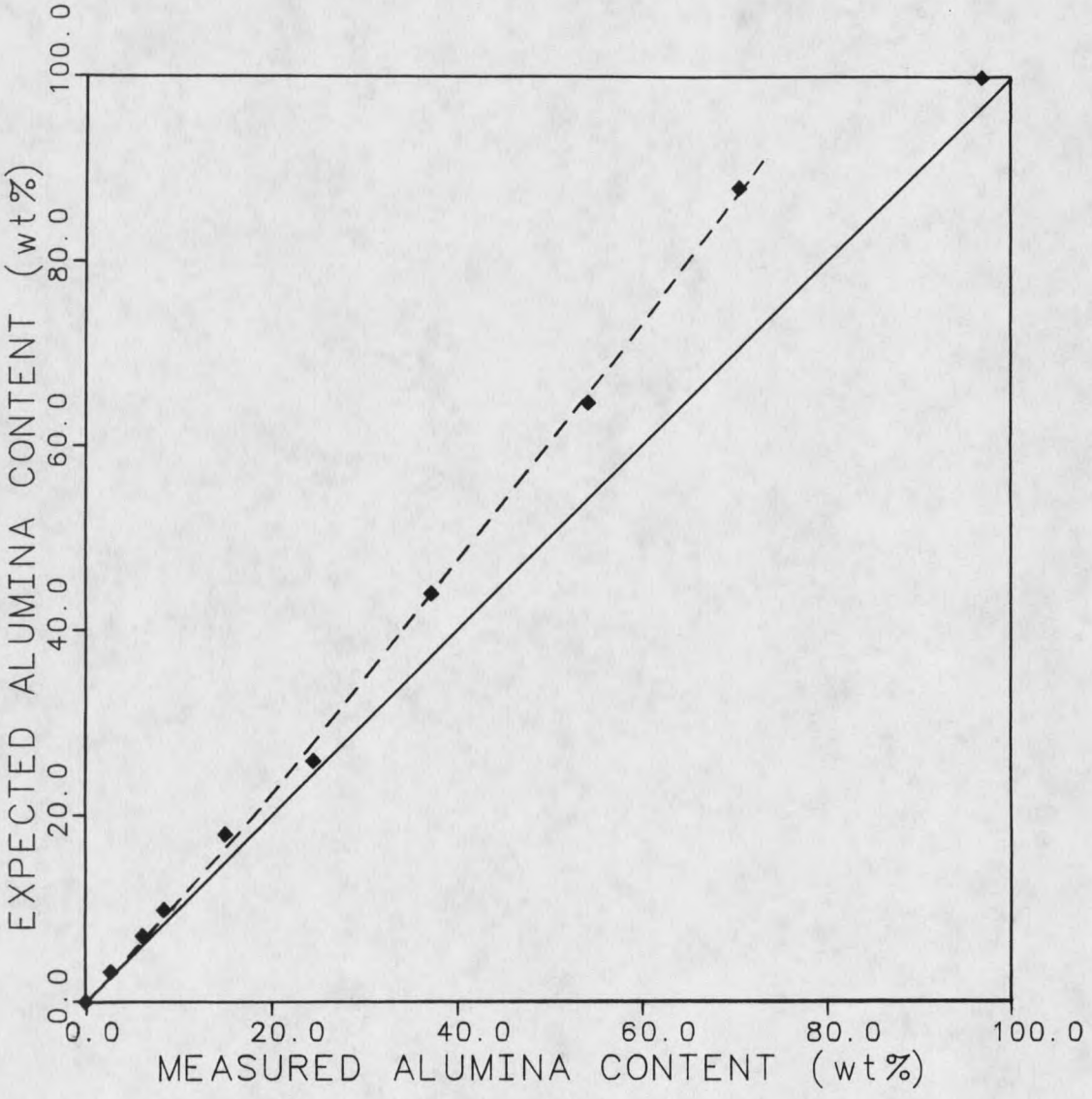

Figure 12. Comparison of the expected and measured alumina contents of the catalysts. The solid line indicates the ideal case. The dashed line is the actual trend observed.

From this evidence, it is concluded that the alumina analyses are good and within 10% of the actual bulk alumina concentrations in the catalysts. All subsequent comparisons made to catalyst composition will use the measured percent alumina values of Table 4 (average values from duplicate analyses).

Catalyst Morphology

Catalyst Surface Area

Measurements made of catalyst surface areas are reported versus catalyst composition in Figure 13. Samples A-10, A-44, and A-65 are the result of duplicate analyses. The dashed line indicates surface area information obtained courtesy of Dr. Smith at UNM.

The surface areas obtained for the pure silica and pure alumina are within the ranges of values reported in the literature for commercial grades of these materials [71]. However, the surface area behavior for the silica-alumina materials is quite unusual. There are two areas of Figure 13 where the surface area trend unexpectedly goes through a minimum. The unusual surface area changes with composition are reproduced in trend, but not always in exact amounts, by the data obtained from UNM. The data obtained from UNM was measured using uncalcined, xerogel powders pretreated at 400°C in a UHP nitrogen flow for 3 hours just prior to analysis. The surface area measurements made here at MSU were performed using calcined catalyst pellets. In addition, the catalyst pellets were not heat-treated just prior to analysis, as was the case with the UNM measurements. It is reasonable

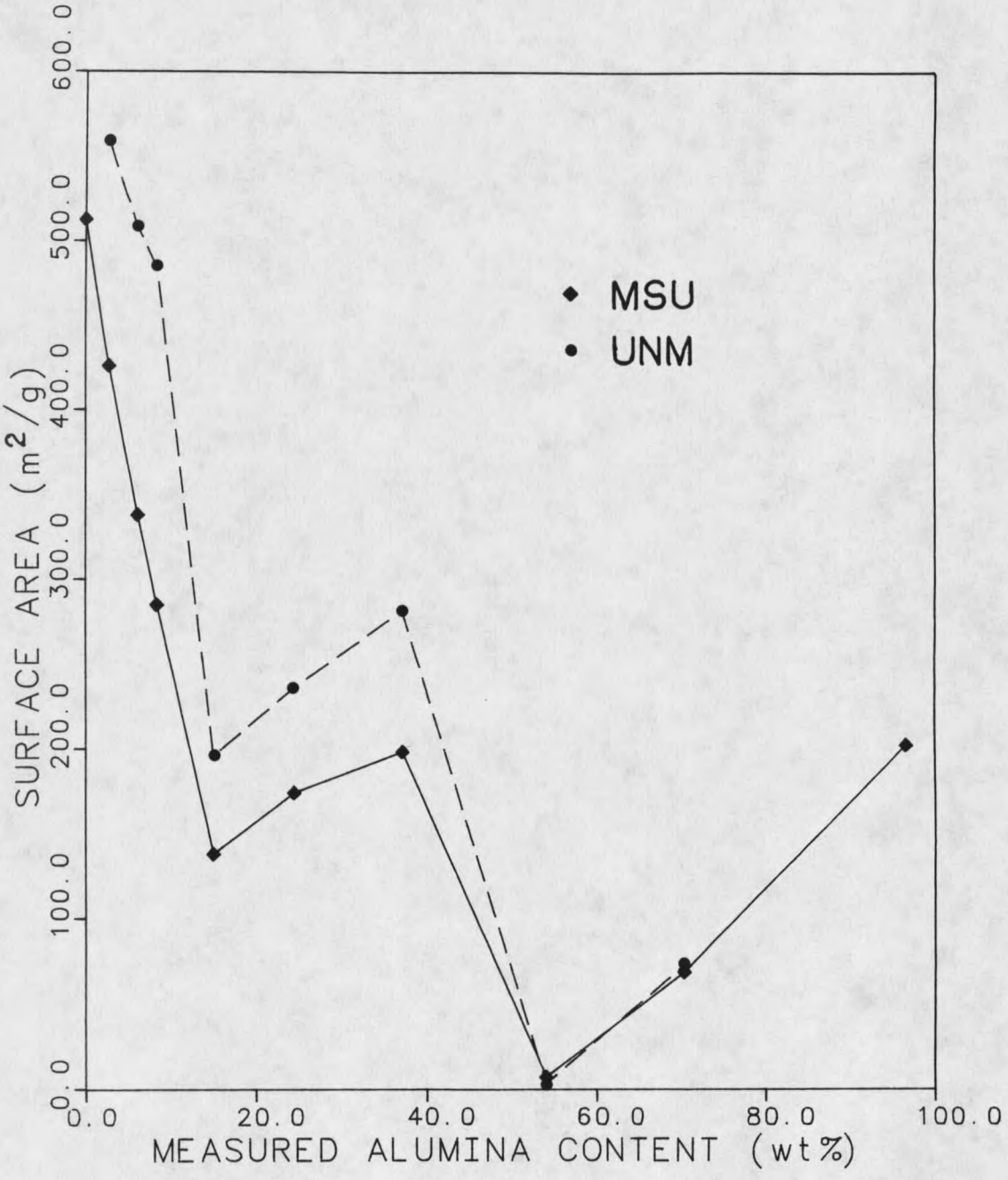

Figure 13. Surface area versus measured alumina content. Comparison of surface areas obtained at UNM to those obtained as part of this study.

that the differences observed between the two sets of surface area data be entirely due to the pretreatment differences. Therefore, the significance of the UNM surface area measurements is that they substantiate the unexpected changes of surface area with varying silica-alumina composition.

The actual surface area values for most of the individual silica-alumina materials are not unusual when compared to surface areas reported for silica-alumina catalysts in the literature. However, this type of discontinuous surface area trend with changing composition has not been previously reported [28].

The very low surface area of sample A-65 (54.1% Al_2O_3) suggests that a crystal phase has formed at this composition. On this premise, sample A-65 was tested once for crystallinity by x-ray diffraction. The x-ray test seemed to indicate that A-65 was an amorphous material, however confidence in this single determination is low due to my inexperience in the operation of the x-ray diffraction equipment. From the measured alumina composition for sample A-65, it is not known what mineral this potential crystal phase of silica-alumina might be.

Catalyst Density

Measurements of the 'true' densities of catalyst materials synthesized in this study were provided by Dr. Smith. The calcined catalyst densities are indicated in Figure 14, plotted against their alumina contents.

The pure silica density of 2.23 g/cm^3 is in excellent agreement with the value reported by Iler [51]. The pure alumina density of

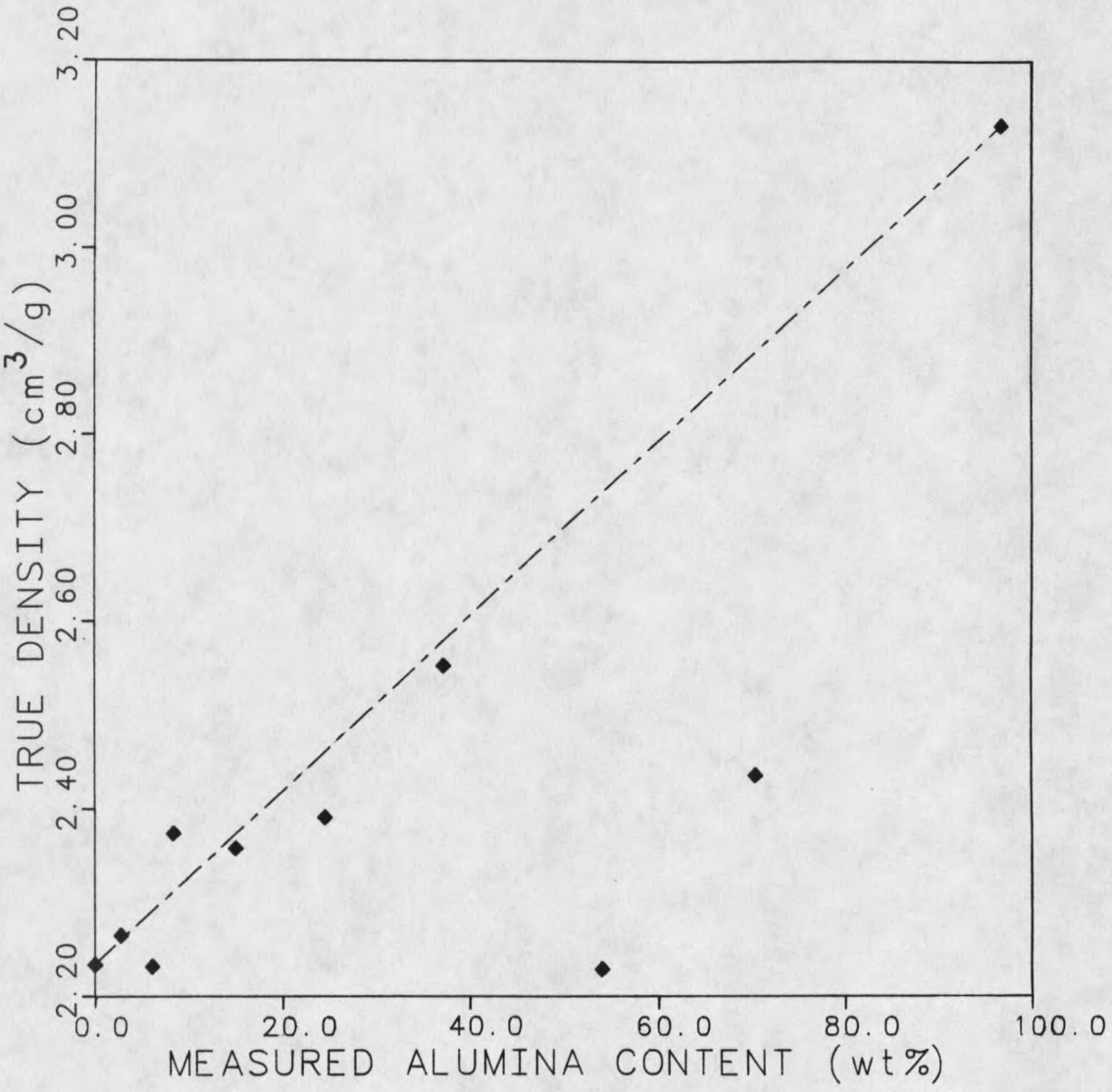

Figure 14. True density versus measured alumina content of the catalysts. The dashed line indicates the density expected from mixing bulk alumina and silica at the corresponding weight fractions.

3.13 g/cm^3 is a reasonable value. The density of sample A-100 is slightly greater than the 3.01 g/cm^3 density of aluminum monohydrate [72]. However, the A-100 sample was not calcined at a high enough temperature to form a completely anhydrous, crystalline form of alumina and thus has a density less than the 3.5-3.9 g/cm^3 reported for γ-alumina [72].

The silica-alumina catalysts would be expected to have densities between that of pure silica and pure alumina. If one were to assume that solid density could be estimated by additive volumes, then the dotted line of Figure 14 would be obtained. The density data for the silica-alumina catalysts generally follows the additive volume assumption with increasing alumina content up to sample A-44. However, discontinuance of the density trend occurs with sample A-65. Recall that sample A-65 was also observed to have an unexpectedly low surface area. In general, minerals of silica-alumina have densities greater than 2.6 g/cm^3 [72]. If indeed sample A-65 is a crystal phase of silica-alumina, it cannot at present be identified by its density.

Catalyst Pore Volume

Measurements of mercury penetration volume per gram of solid as a function of mercury pressure were obtained for calcined catalyst pellets, courtesy of Dr. Smith. An example of the surface area and pore-volume distribution calculations using the sample A-0 mercury penetration data can be viewed in Appendix D. Mercury penetration curves and pore volume distribution curves for all materials are also located in Appendix D.

In general, the mercury penetration curves were still significantly increasing when the maximum experimental pressure of 30,000 psig was achieved. The continued increase in mercury penetration indicates that there is still substantial pore volume in the catalyst materials from pores with radii smaller than 35 Å. As a result, surface area calculations using the porosimetry data fall far short of the surface areas determined from the nitrogen adsorption BET method. Pore volume distribution curves essentially indicate a minimum between the micropores and the macropores in the catalyst materials.

Once again however, the exception to the general observations is sample A-65. Calculations from the porosimetry data indicate that sample A-65 has 5 m^2/g of surface area, good agreement with the 7 m^2/g measured from gas adsorption. The pore volume distribution curve for sample A-65 shows a maximum in the volume of pores with a radius of around 65 Å.

Chemisorption of Triethylamine

With the initiation of chemisorption experiments, it was not known what equilibrium pressures of TEA would be required in order to quantify the strong acid sites on the catalysts' surfaces. In addition, it was not known what maximum experimental temperature could be used before TEA catalytically decomposed on the test sample surface. Sample A-3 was used at ~200°C to observe that the initial injection volume of TEA used for the apparatus was too large. The

equilibrium TEA pressure was above that necessary to detect the expected 'knee' in the adsorption isotherm due to strong adsorption sites. After significantly reducing the TEA injection volume, sample A-3 was again used to see if chemisorption could be measured at a temperature of ~400°C. At this temperature, the sample weight recorded by the electrobalance indicated the expected TEA uptake curve followed by sudden and rapid losses of weight, losses accounting for most of the initial weight gain. The observed weight loss after modest surface coverage is consistent with catalytic decomposition of the adsorbate.

Sample A-3 was then used to measure TEA adsorption isotherms, again at 197°C, and at 302°C. These isotherms are shown in Figure 15. At 302°C, there is enough low pressure information measured to discern a 'knee' in the adsorption isotherm, where the strong acid sites are eliciting their greatest influence. Since chemisorption is defined as the result of chemical bonding between adsorbate molecules and the adsorbent surface, it is generally observed free of physisorption interference at temperatures above the adsorbate critical temperature. The critical temperature of TEA is 262°C. Based on the TEA critical temperature and the appearance of the sample A-3 302°C adsorption isotherm, it was concluded that a temperature of ~300°C would be used to measure the TEA adsorption isotherms for all of the catalyst samples.

Determination of a single adsorption isotherm often required continuous operation for over a week. The reason for such long experiments is the requirement of equilibrium measurements. The TEA

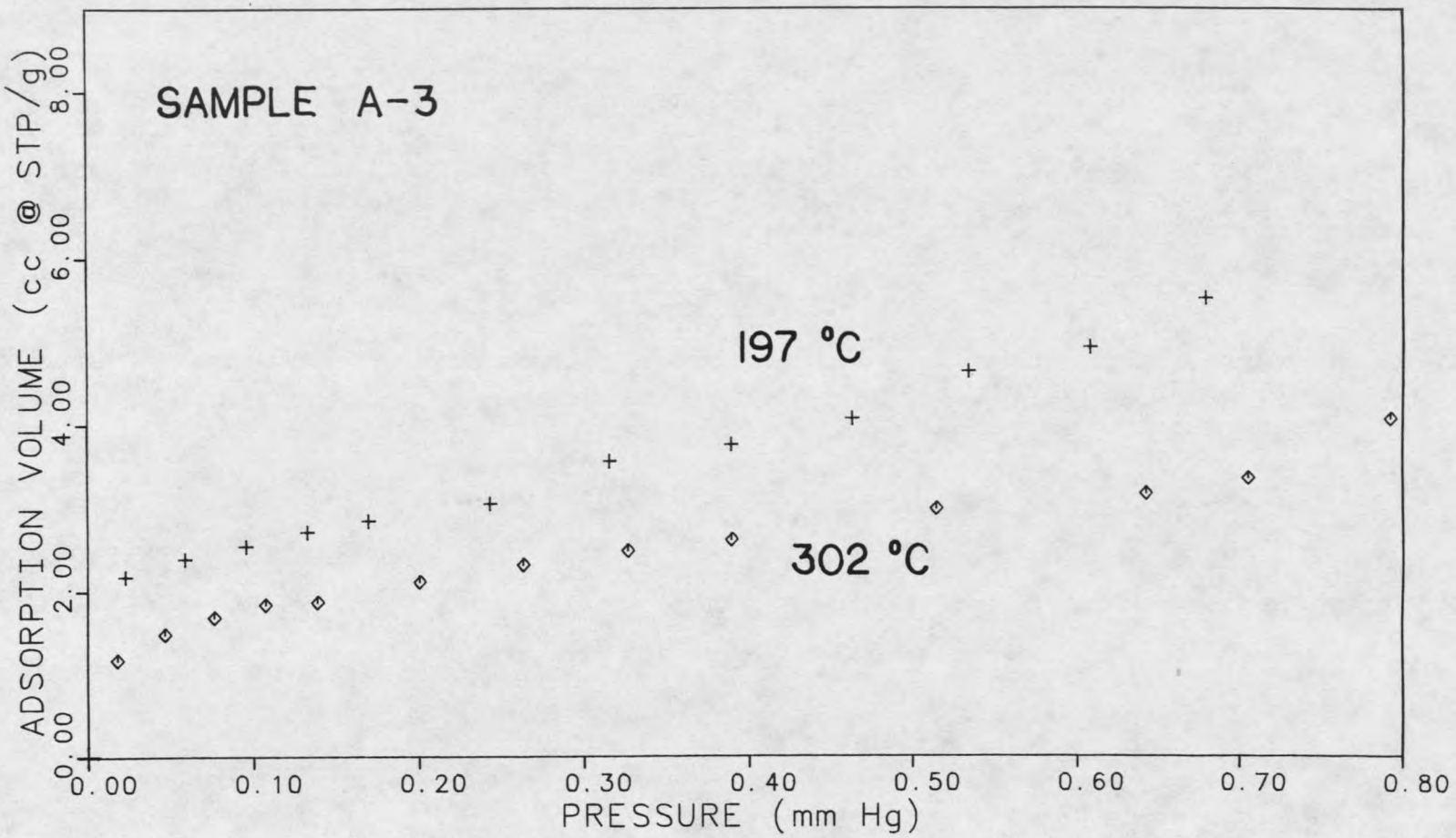

Figure 15. Adsorption isotherms for catalyst A-3, measured at two temperatures.

uptake curves for the initial adsorbate injections generally reached equilibrium in less than four hours. After enough TEA had been admitted to the system to presumably cover most of the strong adsorption sites, uptake curves indicated a very slow adsorption process occurring. The slow adsorption process generally required longer than twelve hours to eventually reach equilibrium. The slow adsorption process was also observed to account for more than half of the adsorbate uptake for a single adsorbate injection.

A calculation, shown in Appendix E, was performed in an attempt to determine the diffusivity of TEA in the chemisorption system using the observed length of time required for equilibrium. The adsorbed phase was sufficiently large to warrant its inclusion in the mass balance for the system. With the assumption of a spherical geometry, constant diffusivity, and instantaneous adsorption equilibrium, the system was solved for diffusivity as a function of the time required for a 90% approach to equilibrium. Typical experimental values substituted into the expression yield a diffusivity in the Knudsen regime, which is as expected due to the catalyst pore size indicated by mercury porosimetry.

The data and calculations yielding the adsorption isotherms are located in Appendix F. The information in Appendix F also includes isobars measured to correct adsorption isotherms for experimental variations in adsorbent temperature.

The adsorption isotherms obtained for the ten catalyst samples are presented in Figures 16-19. As anticipated [30], the sample A-0 (see Figure 16) does not evince solid phase acidity. Likewise, sample A-65

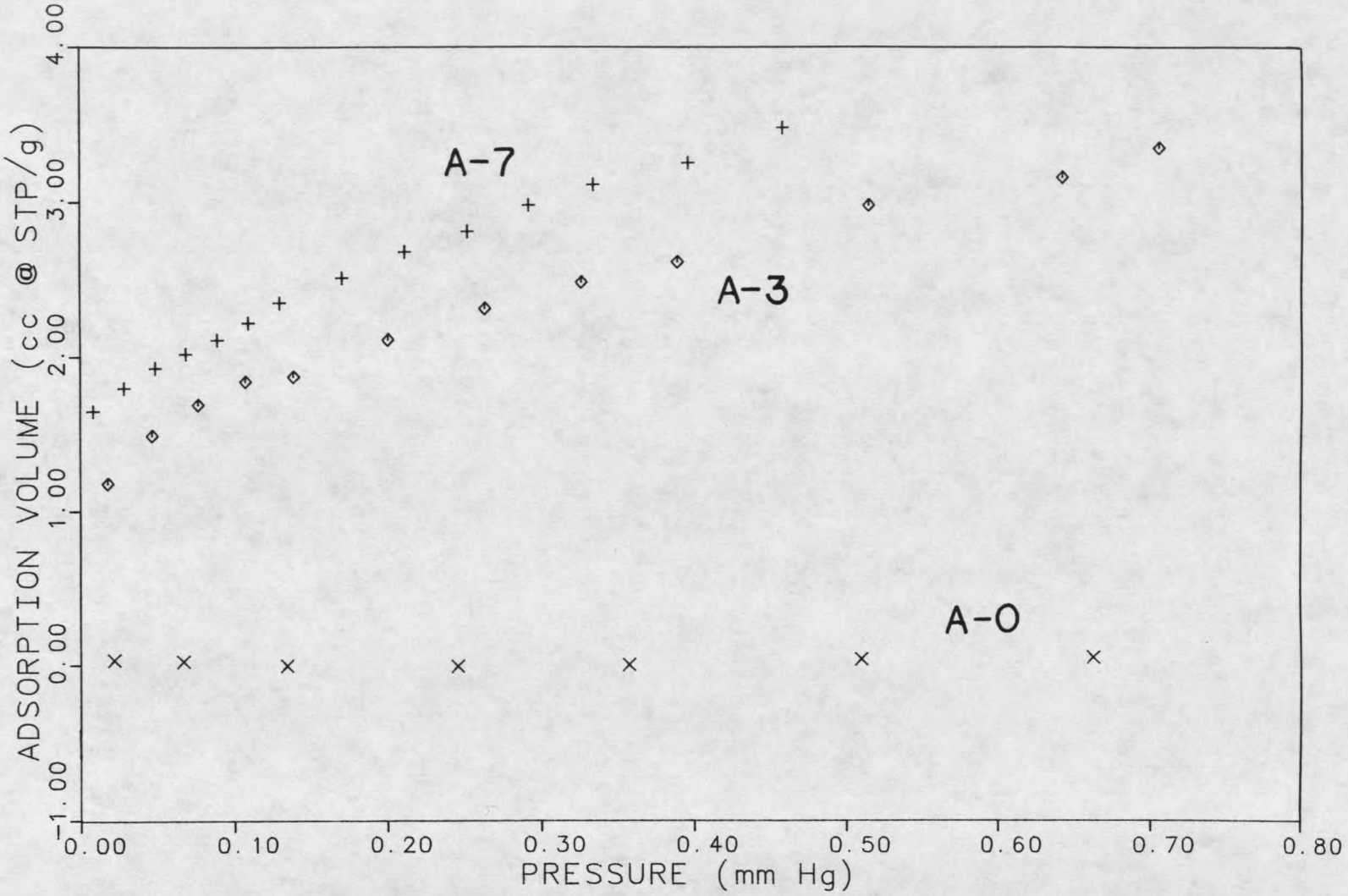

Figure 16. Adsorption isotherms for catalysts A-0, A-3, and A-7 at ~ 300°C.

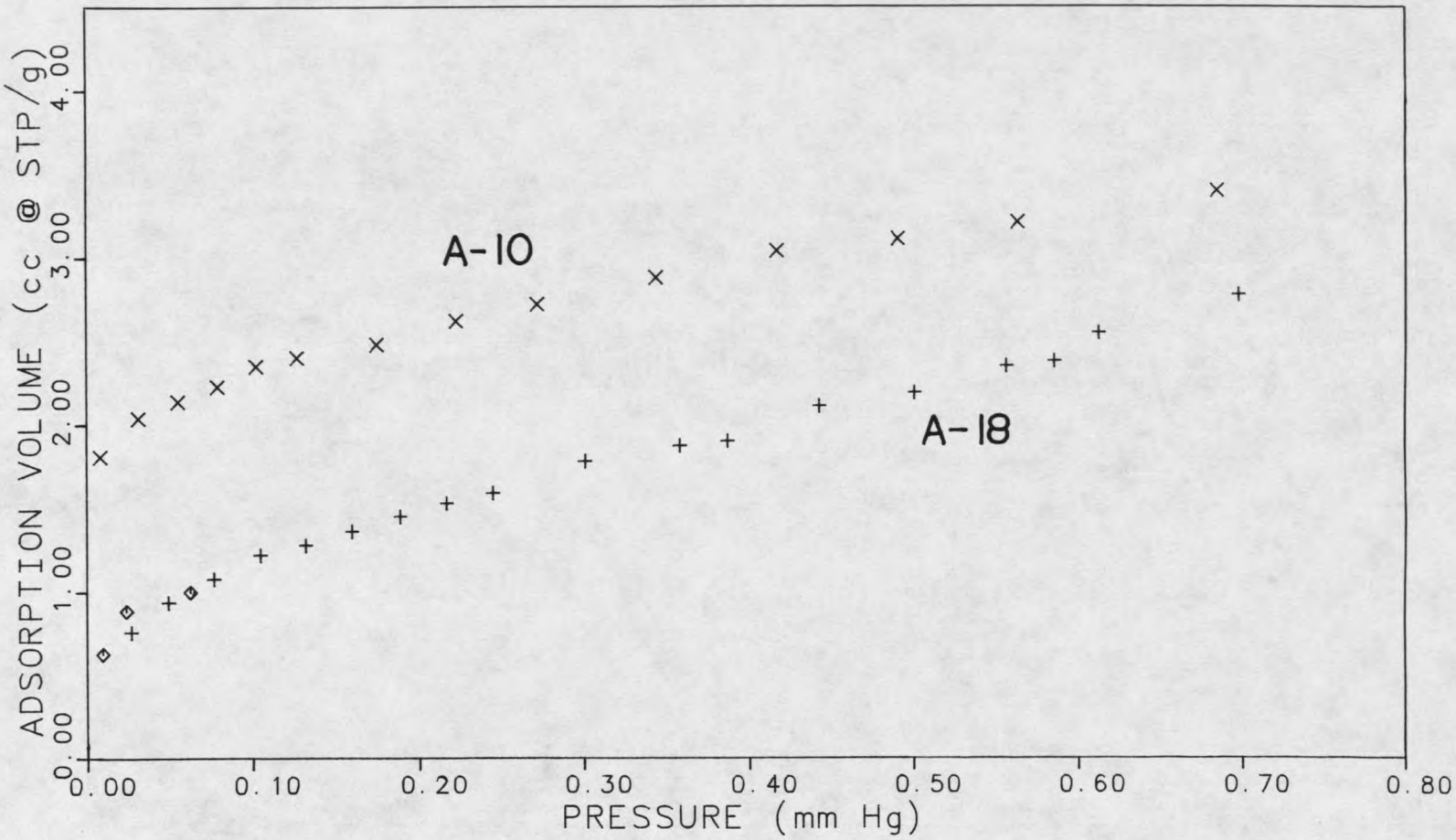

Figure 17. Adsorption isotherms for catalysts A-10 and A-18 at ~300°C.

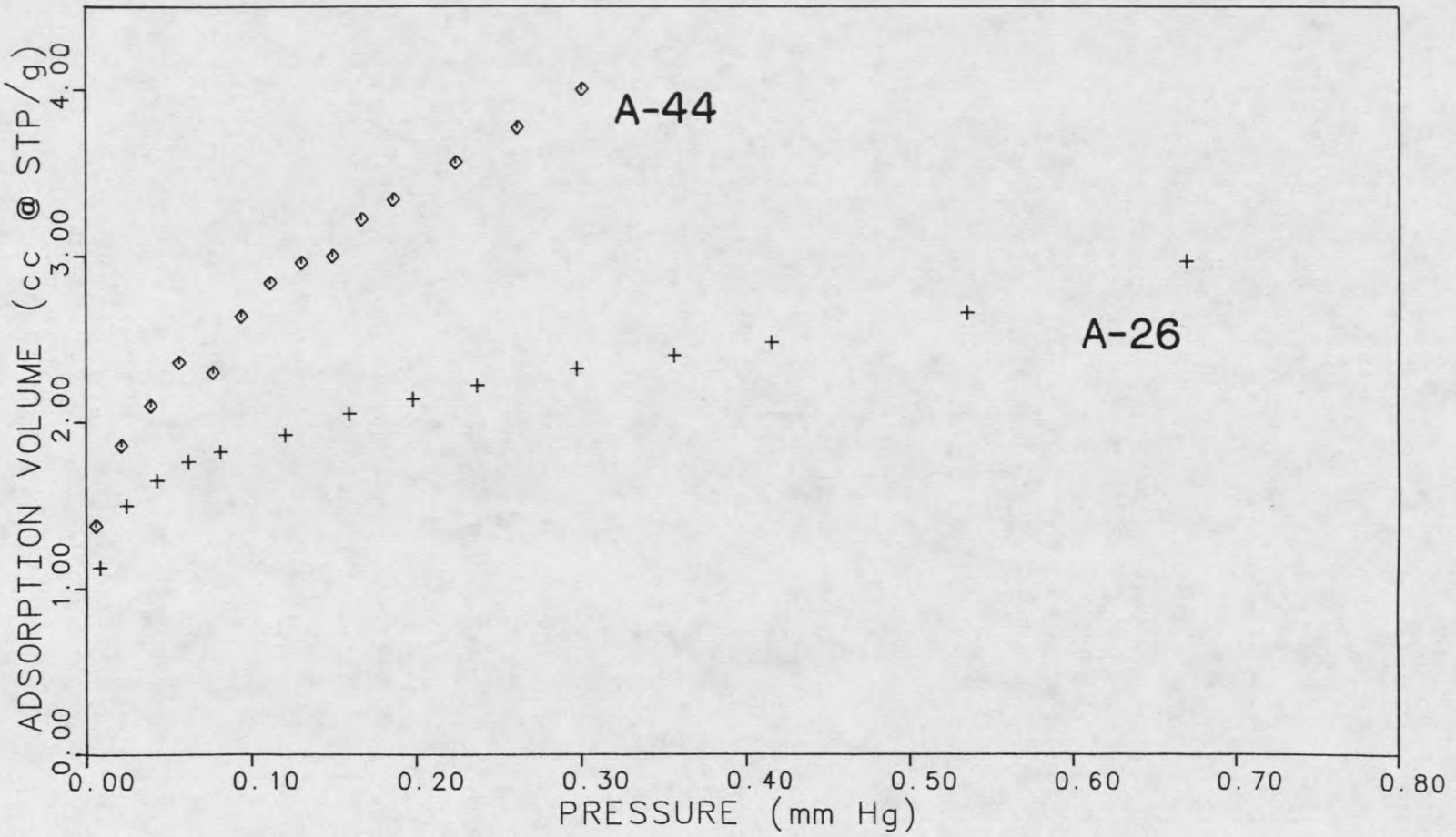

Figure 18. Adsorption isotherms for catalysts A-26 and A-44 at ~300°C.

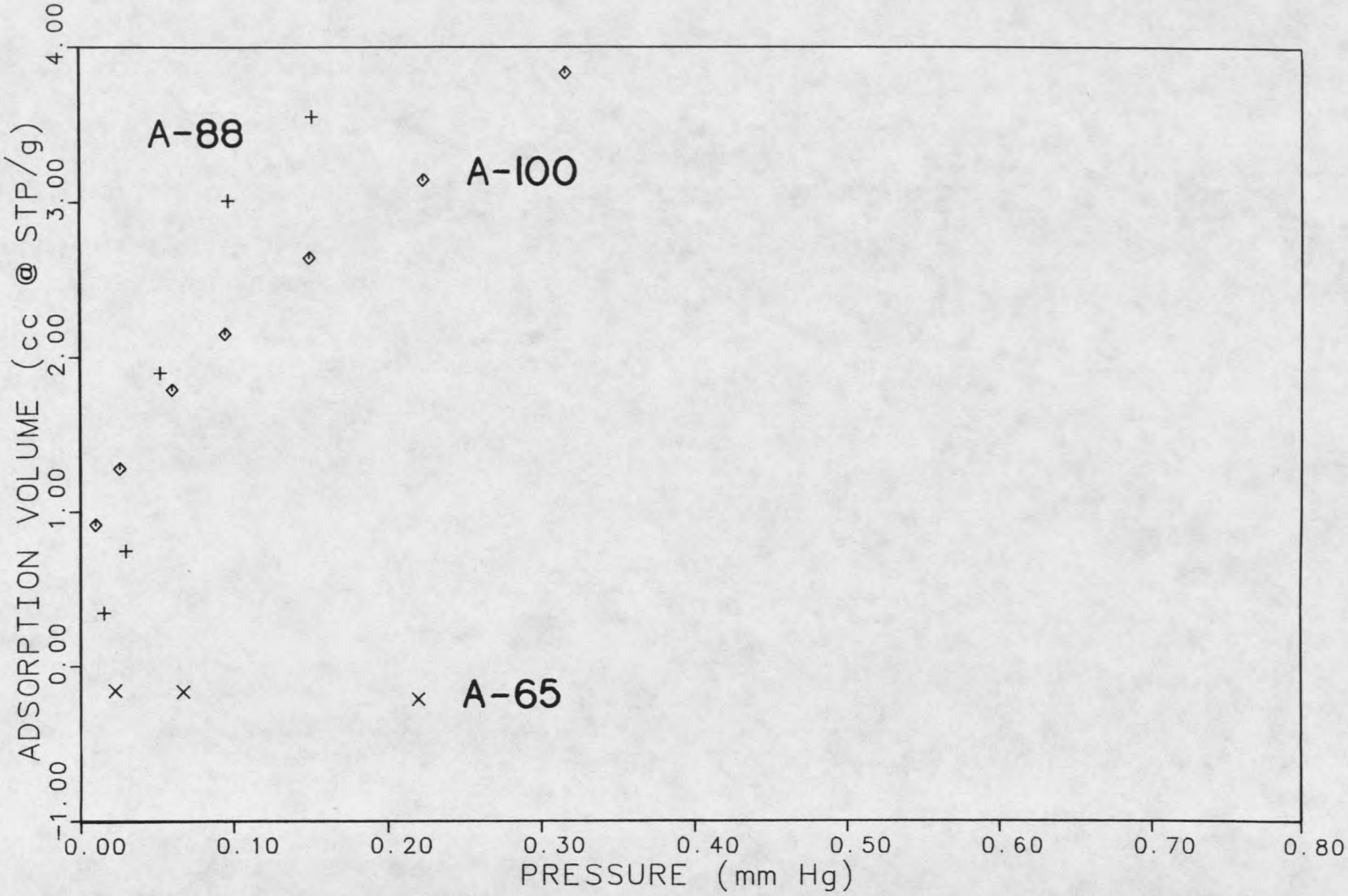

Figure 19. Adsorption isotherms for catalysts A-65, A-88, and A-100 at ~300°C.

(see Figure 19) shows no adsorption of the gaseous base vapor. Unlike sample A-0 though, the absence of chemisorption for sample A-65 is not due to a lack of acidic surface structures but due to a lack of surface area. Much larger samples of A-65 would be required to experimentally observe TEA chemisorption. In addition, sample A-65 appears to have continuously lost weight throughout the course of the 10 hour experiment despite its contact with TEA vapor. The 0.1% weight loss of A-65 is postulated as due to a very slow desorption of water. This hypothesis is based on the significant water content observed for this material, reported previously in Figures 10 and 11. However, the nature of the desorption process and attendant structure of the A-65 material are, as stated before, puzzling and not as yet identified.

As shown in Figure 19, sample A-100 was found to chemisorb a significant amount of TEA in the pressure range studied. This observation is in general agreement with other studies that have measured the chemisorption of a gaseous base on pure alumina [25,28,30]. However, this result is unfortunate when viewed from the expectation, described in Chapter III, that TEA might react weakly with the Lewis acidity associated with alumina.

Figure 16 shows that increasing the alumina content, at low alumina concentrations in silica, increases the number of adsorption sites per gram of catalyst. However, this trend is reversed in Figure 17 with sample A-18 due to the overriding effect of surface area. The increasing total TEA adsorption with increasing alumina trend returns briefly with sample A-26 and A-44 (see Figure 18), but is again lost

due to surface area effects for sample A-65. No significant differences in total adsorption for samples A-88 and A-100 can be discerned because of the limited TEA pressure range studied in this investigation.

Also shown in Figure 17 is the duplicate analysis made at low pressure for sample A-18. Agreement between the two experiments is good; their deviation is within the limits of experimental error as defined by blank measurements. Examples of experimental deviation are apparent in most of the isotherms. The extreme example of experimental deviation can be seen in the A-44 isotherm shown in Figure 18.

In general, the adsorption isotherms indicate that much of the high energy adsorption information could not be measured. The problem is a combination of two effects. First, TEA is too strong of a base, even at 300°C, and its adsorption on Lewis acid sites is not hindered. Second, much smaller injections of adsorbate should be made. The smallest injection volume possible, employing a double valve arrangement, was used in this study. Even though this arrangement would yield an initial injection pressure of only 0.020 mm Hg, the injection amount would have to be reduced by an order of magnitude to obtain the low pressure information required for a detailed analysis of the strong acid-site strength distributions.

Acid-Site Strength Distributions

The CAEDMON program was used to calculate adsorption energy distributions for all of the test materials except samples A-0 and A-65, which showed no TEA adsorption. Output from the CAEDMON program for each test sample is located in Appendix G.

Results of the adsorption energy calculation were not as detailed as had been hoped. The energy distributions essentially indicate that there are two site energies on the test material surfaces. The site energies are at the limits of the adsorption energy range defined by the experimental pressures used. Therefore, the energy distributions appear saddle-shaped, with adsorption calculated as 'zero' between the limits of adsorption energy. The actual adsorption energy of the high energy sites is probably higher than the maximum experimental adsorption energy, likewise, the low energy sites apparently have a lower adsorption energy than the minimum experimental adsorption energy.

It was also observed that deletion of high pressure data points greatly reduced the calculated capacity of the low energy adsorption sites. The difficulty is that all of the adsorption isotherms were still continuing to increase significantly at the conclusion of the adsorption experiments. According to literature reports [26,73], the adsorption isotherms would have continued to climb with increasing adsorbate pressure. In fact, neither of the previous reports observed an approach to an asymptotic limit in their adsorption isotherms, though they increased experimental adsorbate pressures to many times

that used in this investigation. The lack of any observable features in these adsorption isotherms suggesting the completion of chemisorption monolayer coverage implies the occurrence of multilayer coverage. Physisorption has not occurred, as is shown by the total lack of adsorption on sample A-0 (See Figure 16). Since the gaseous base molecules are polar hydrocarbons, coulombic interaction of the adsorbate molecules with each other forming multilayers seems reasonable. The point is that it appears impossible to separate the amount of adsorption on weakly acidic surface sites from the adsorption occurring due to multilayer formation. Thus the lack of sufficient high pressure data and the dependence of the weak adsorption site capacity on the maximum experimental adsorbate pressure constrains the results of the CAEDMON routine to the measurement of strong adsorption sites only.

The CAEDMON procedure was used to analyze the ammonia adsorption isotherm of an industrial silica-alumina catalyst included in the report by Hsieh [26]. The results, included in Appendix G, were compared to the adsorption energy distribution reported by Hsieh using the method of Adamson and Ling. The shapes of the distributions are quite similar; both techniques indicate very strong adsorption sites, an intermediate site energy range of no adsorption, and a large amount of adsorption on weak adsorption sites. However, the adsorption energy of the strong acid sites using the Adamson and Ling method is three times the free energy of adsorption calculated using CAEDMON. Although the expressions of adsorption energy are different between the two methods, their actual values should be similar. It is

possible that the energy differences between the two methods is because of an error in the CAEDMON technique, due to the use of Lennard-Jones (6:12) potential parameters in describing a polar molecule like ammonia. However, it is also possible that the method employed by Hsieh may have overestimated the adsorption energies. The adsorption energy distributions reported by Hsieh indicate weak adsorption sites with adsorption energies between 7 and 10 kcal/mole. If these weak adsorption sites include multilayer adsorption, as Hsieh himself suggests, it would seem unlikely that a multilayer adsorption energy should be as high as that calculated using the Adamson and Ling method. Therefore, there is a substantial difference in the adsorption energy of ammonia on strong acid sites in silica-alumina depending on the technique employed. However, both techniques, CAEDMON and the Adamson and Ling method, provide essentially the same distribution shape for the same data set.

The results from the CAEDMON program for the test catalysts are given in Table 5. Surface coverage and the strong adsorption site capacity on the basis of surface area are presented. Also reported in Table 5 are values of acidity in units commonly used in the literature.

The results of Table 5 indicate a strong acidity maximum of 7.09×10^{-4} meq/m^2 on sample A-26. The bulk alumina composition of the test material with the maximum acidity is in good agreement with two literature reports [12,28] but is higher than the 10% alumina composition of maximum acidity from another report [8].

The value of the maximum acidity measured by this study is in excellent agreement with that reported by Barth and Ballou [25] for industrial silica-alumina catalysts (4.7×10^{-4} to 8.6×10^{-4} meq/m^2). Barth and Ballou measured temperature programmed desorption of ammonia from silica-alumina catalysts and considered the amount of ammonia

Table 5. Strong Acid Sites Calculated by CAEDMON

Sample	Capacity (cm^3 @ STP/m^2)	Acidity (meq/m^2)	Coverage (m^2/m^2)
A-0	0	0	0
A-3	0.00638	2.85×10^{-4}	0.065
A-7	0.00964	4.30×10^{-4}	0.098
A-10	0.0133	5.93×10^{-4}	0.14
A-18	0.0122	5.44×10^{-4}	0.12
A-26	0.0159	7.09×10^{-4}	0.16
A-44	0.0156	6.96×10^{-4}	0.16
A-65	-	-	-
A-88	0	0	0
A-100	0.00990	4.42×10^{-4}	0.10

retained at 515°C as the quantity of the strong acid sites. However, there is poor agreement with other literature reports concerning the maximum acidity. The value obtained in this study is slightly less than half that reported by researchers that have used nonaqueous and aqueous titration methods [8,12,21,28,33]. But as stated previously

in this Chapter, there is some disagreement as to the endpoint color of some Hammett indicators [70] and this alone could account for the acidity discrepancy with titration methods.

In the study by Hsieh [26], the maximum acid content reported was twice that obtained in this investigation. Hsieh considered the minimum point on his ammonia heat of adsorption curves to be the point at which the strong acid sites were neutralized and used this value of coverage to estimate the strong acid site concentrations of the industrial catalysts being tested. However, Hsieh's procedure assumes sequential adsorption and is certain to yield acidities higher than that actually existing on the test surface.

The results of the CAEDMON routine indicate that pure alumina (sample A-100) has acidic surface sites of comparable strength and concentration to those of the silica-alumina materials. That most forms of alumina exhibit substantial surface acidity is not contested in the literature. There are, however, differences of opinion expressed in the literature as to the strength of the alumina acid sites. Some sources claim that alumina acid sites are weaker than the acid sites on silica-alumina [6,7]. However, the study by Barth and Ballou [25] found strong alumina acid sites of a concentration comparable to the present investigation. Strong alumina acid sites were also found in the study by Clark, et al. [28]. These researchers measured the adsorption of ammonia in the 100°C to 400°C temperature range and thermodynamically interpreted the pure alumina acid sites (presumed as being of the Lewis type) as being stronger than the Brønsted acid sites on silica-alumina materials. It is a shortcoming

of the present investigation that no difference between the strong adsorption (acid) sites associated with alumina could be discerned from those strong adsorption sites associated with silica-alumina. Further discussion of this problem will be made in the following section concerning catalyst activity.

Sample A-88 was calculated to have no strong acidity. This result is contradictory to the trend of acidity results in Table 5 and to the results of Clark et al. [28] for materials of similar alumina content. The only evidence that might be used to explain the lack of acidity on sample A-88 is the unusual surface area and density behavior observed for this region of catalyst composition. It is postulated that the lack of surface acidity for sample A-88 is related to the puzzling morphological properties of sample A-65.

Measurements of the surface coverage of strong acid sites by TEA are also listed in Table 5. These values are higher than coverages reported in the literature, but this is mostly due to differences in the assumed areas of adsorbates (here taken to be 38 $Å^2$ for TEA). The primary indication of coverages values is that the strong acid sites comprise a small fraction of the catalyst surface.

The surface densities of strong acid sites have been calculated for Table 6. Table 6 also includes values of the maximum average distance between strong acid sites and the efficiency of aluminum usage in the formation of strong acid sites. These values indicate that the average point-to-point distance between strong acid sites decreases from 24 Å to 15 Å with increasing alumina content before increasing to 19 Å for A-100, excepting samples A-65 and A-88. Table

6 also shows that the number of strong acid sites created as a fraction of the aluminum incorporated into the catalyst decreases with increasing alumina content, again excepting samples A-65 and A-88. The low efficiency of aluminum in creating strong acid sites seems to indicate substantial burial of aluminum in the catalyst framework or, perhaps, in the aggregation of alumina to create strong acid sites.

Table 6. Properties of Strong Acid Sites

Sample	Density (sites/m^2)	Average Distance Between Sites (Å)	Aluminum Efficiency (sites/100 Al molecules)
A-0	0	-	-
A-3	1.71×10^{17}	24	23
A-7	2.59×10^{17}	20	12
A-10	3.57×10^{17}	17	10
A-18	3.28×10^{17}	17	2.6
A-26	4.27×10^{17}	15	2.6
A-44	4.19×10^{17}	15	1.9
A-65	-	-	-
A-88	0	-	-
A-100	2.66×10^{17}	19	0.45

To conclude, the quantity of strong acid sites on the surfaces of test catalysts synthesized in this study were obtained via the CAEDMON program. The results from CAEDMON were disappointing because the strong acid sites associated with pure alumina could not be discriminated from those acid sites typical of silica-alumina

catalysts, formed by the isomorphous substitution of aluminum into a tetrahedral framework. However, the amounts of strong acidity obtained from the CAEDMON program were in excellent agreement with a literature report for commercial silica-alumina catalysts and were within acceptable limits to other studies due to differences in the methods of analysis. In fact, the agreement between this investigation and that of Barth and Ballou [25] is so good that it appears there is no adsorbate size effect between the use of TEA and ammonia. This investigation also found strong acidity on pure alumina, at variance with some authors [6,7]. Sample A-88 was inexplicably observed to exhibit no strong acid sites. The strong acid sites were found to cover a small fraction of the test catalysts' surfaces. Finally, the efficiency of aluminum usage in producing strong acid sites is quite low and decreases rapidly with increasing alumina content.

Catalyst Activity for o-Xylene Isomerization

Several tests were performed with a typical catalyst charge in the Berty reactor to ensure proper interpretation of the information obtained from the reactor system. One of those tests was a pulse tracer test, performed to verify that the reactor conditions were indeed that of a mixed flow reactor. Analysis of the pulse tracer experiment is detailed in Appendix H.

Results of the tracer experiment confirm that the Berty reactor, under typical operating conditions, behaves essentially as a mixed

flow reactor. However, the pulse tracer data does not yield a perfect mixed flow model. Deviation from the ideal model was observed after five times the mean residence time. This deviation could be due to the tracer (methane) not being entirely inert with respect to silica-alumina at room temperature. The deviation could also be due to mixing in and out of the drive shaft space below the reactor. In any event, the calculations in Appendix H show that 99% of the injected tracer moved through the reactor as if it were a mixed flow reactor model.

A test was made to check for the existence of external transport limitation in the reaction rate data. This test was made by varying the reactor impeller speed at otherwise constant, normal conditions. Variation of the impeller speed will vary the local reactant flow rate through the catalyst bed. If external transport limitations are important, the reaction rate will increase with increasing impeller speed. As is seen in Figure 20, there is no effect of impeller speed on the reaction rate constant.

Two sizes of catalyst were tested in the reactor, as mentioned in Chapter III. It was not expected that this would be necessary; catalyst was pelletted for use in the reactor as well as for use in chemisorption studies. Once enough chemical activity data was obtained, however, substitution into the Weisz-Prater criterion [41] indicated that pore diffusion limitations might be present when using catalyst pellets (see Appendix I). To ensure the measurement of true kinetic data, a powdered silica-alumina sample, sieved to between 80 and 200 mesh (177 to 74 μm), was used in the reactor. The Arrhenius

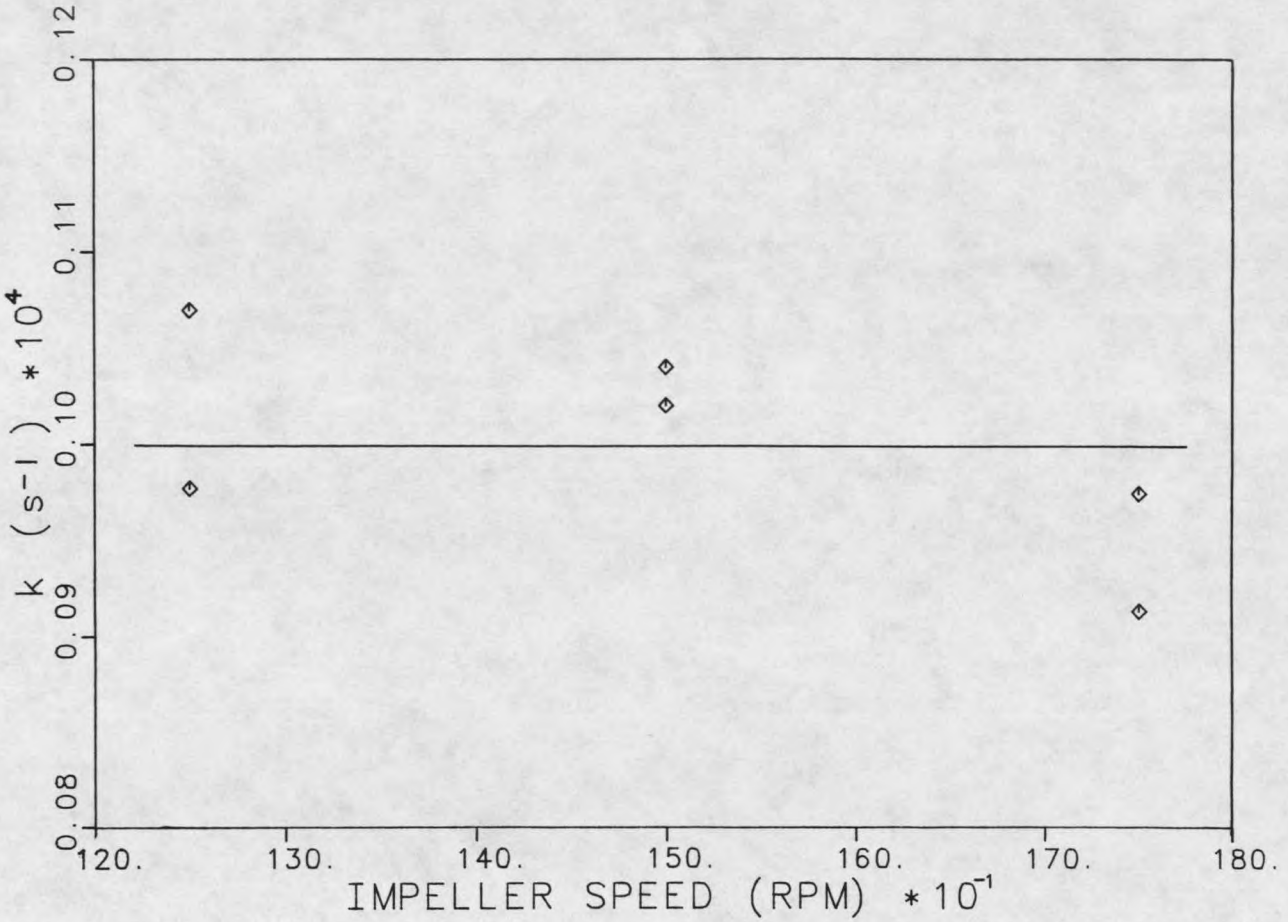

Figure 20. Test for the significance of external mass-transfer on reactivity measurements. The Berty reactor impeller speed is plotted versus the first-order reaction rate constant.

plot of the reaction rate data for both sizes of catalyst A-18, shown in Figure 21, indicates no effect of particle size on the observed reaction rate. Nevertheless, the powdered form of the catalysts was used for all of the isomerization activity experiments to ensure that diffusion-free reaction rates were measured.

Calculations were performed in order to determine to what extent the isomerization reaction could proceed before equilibrium limitations would manifest themselves. These calculations are located in Appendix J. From the equilibrium calculations, it is conservatively estimated that the conversion of o-xylene should not be allowed to exceed 40%. This conversion limit is the same as that imposed in a previous study [65]. The conversion limit was also experimentally verified when a conversion of 50% was observed to yield a dramatic reduction in the apparent activation energy.

With the myriad of limitations on reaction rate measurements either calculated or experimentally verified, tests for isomerization activity were performed using all of the catalysts synthesized for this investigation. Basic calculations and data for the isomerization activity tests are located in Appendix K.

Arrhenius plots have been used to represent the isomerization activity of the catalysts. Arrhenius plots based on the first-order rate constants are shown in Figures 22 and 23, while plots based on the surface area specific reaction rates are shown in Figures 24 and 25.

Sample A-0, A-65, A-88, and A-100 are not found in Figures 22 - 25 because no isomerization could be measured on these materials below a

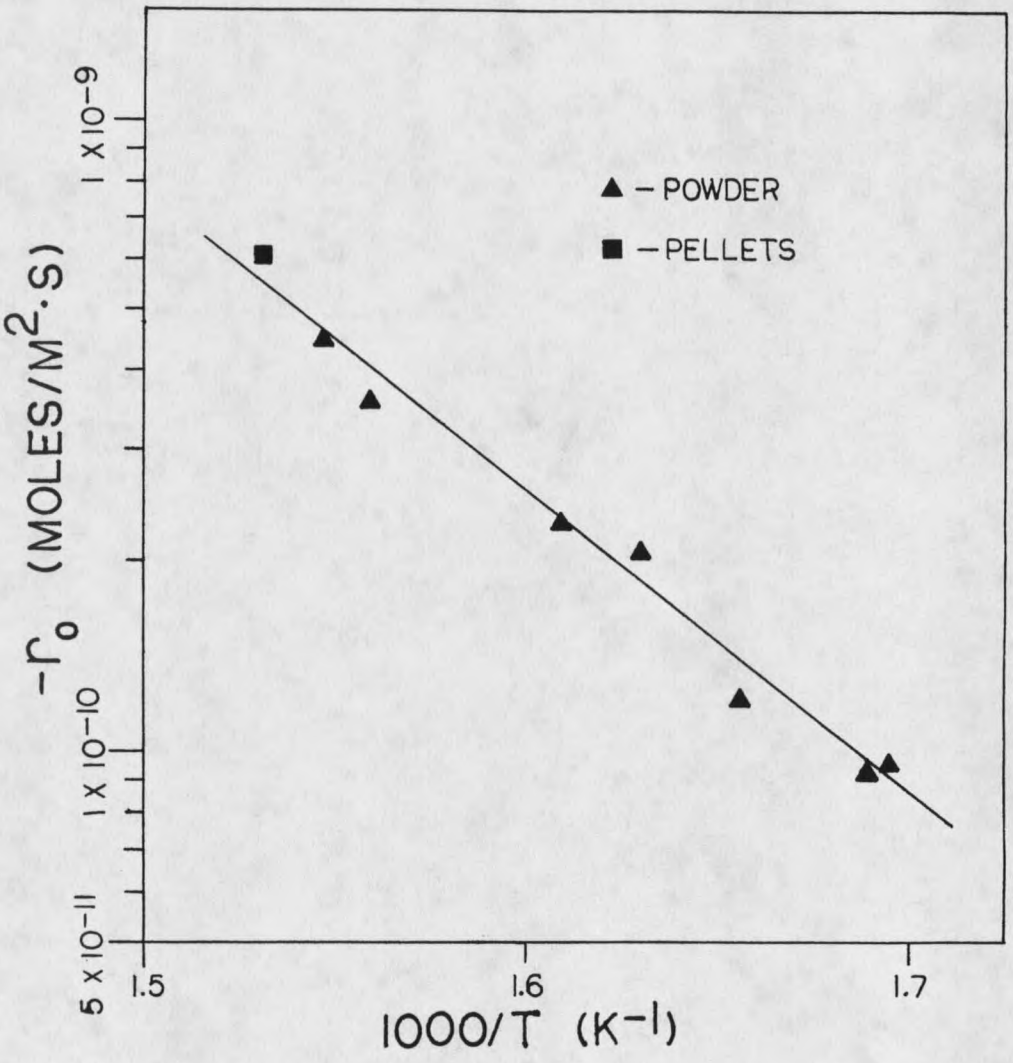

Figure 21. Test for the significance of internal mass-transfer on reactivity measurements. An isomerization rate Arrhenius plot is shown for two different sizes of catalyst A-18.

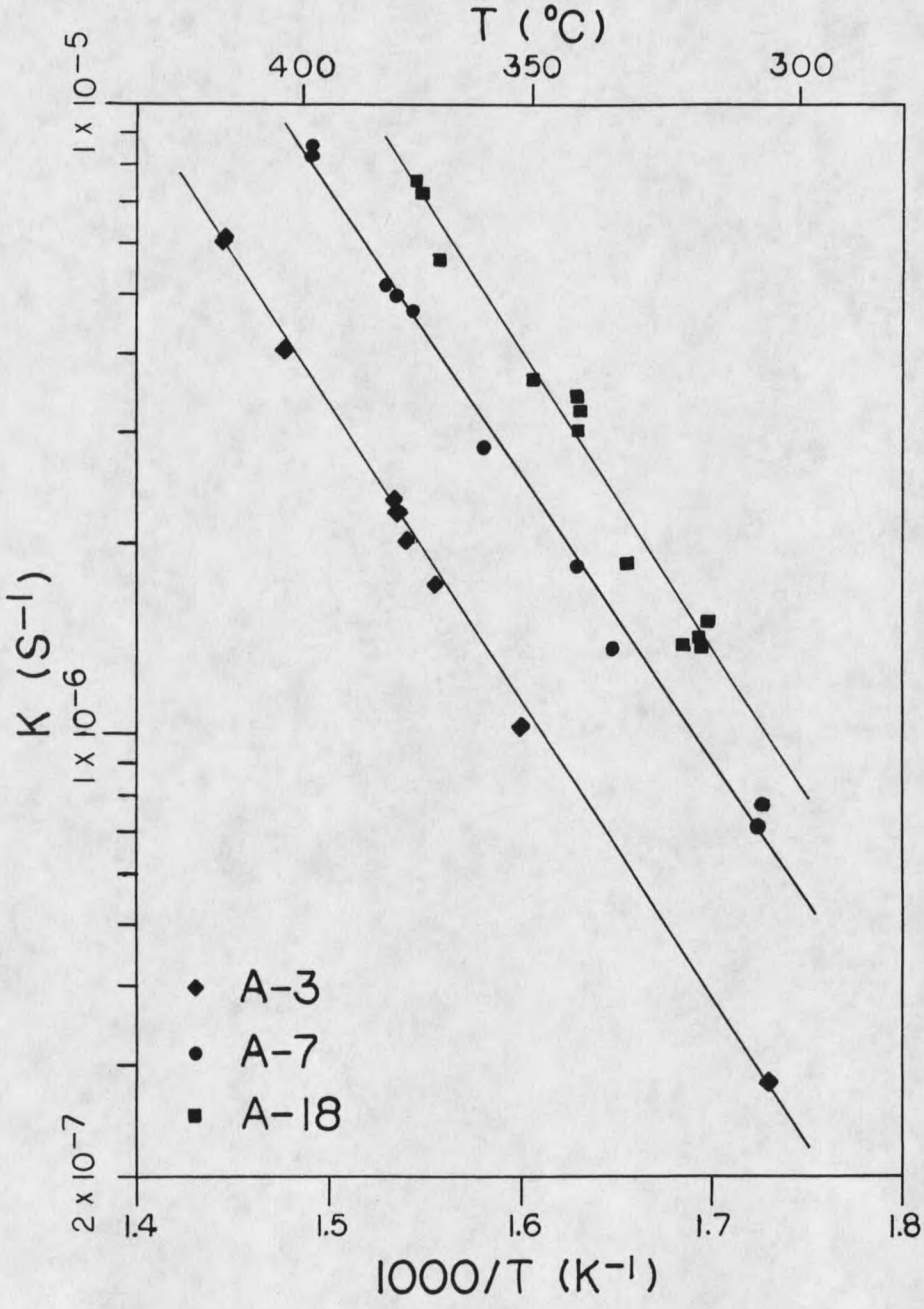

Figure 22. First-order rate constant Arrhenius plot for catalysts A-3, A-7, and A-18.

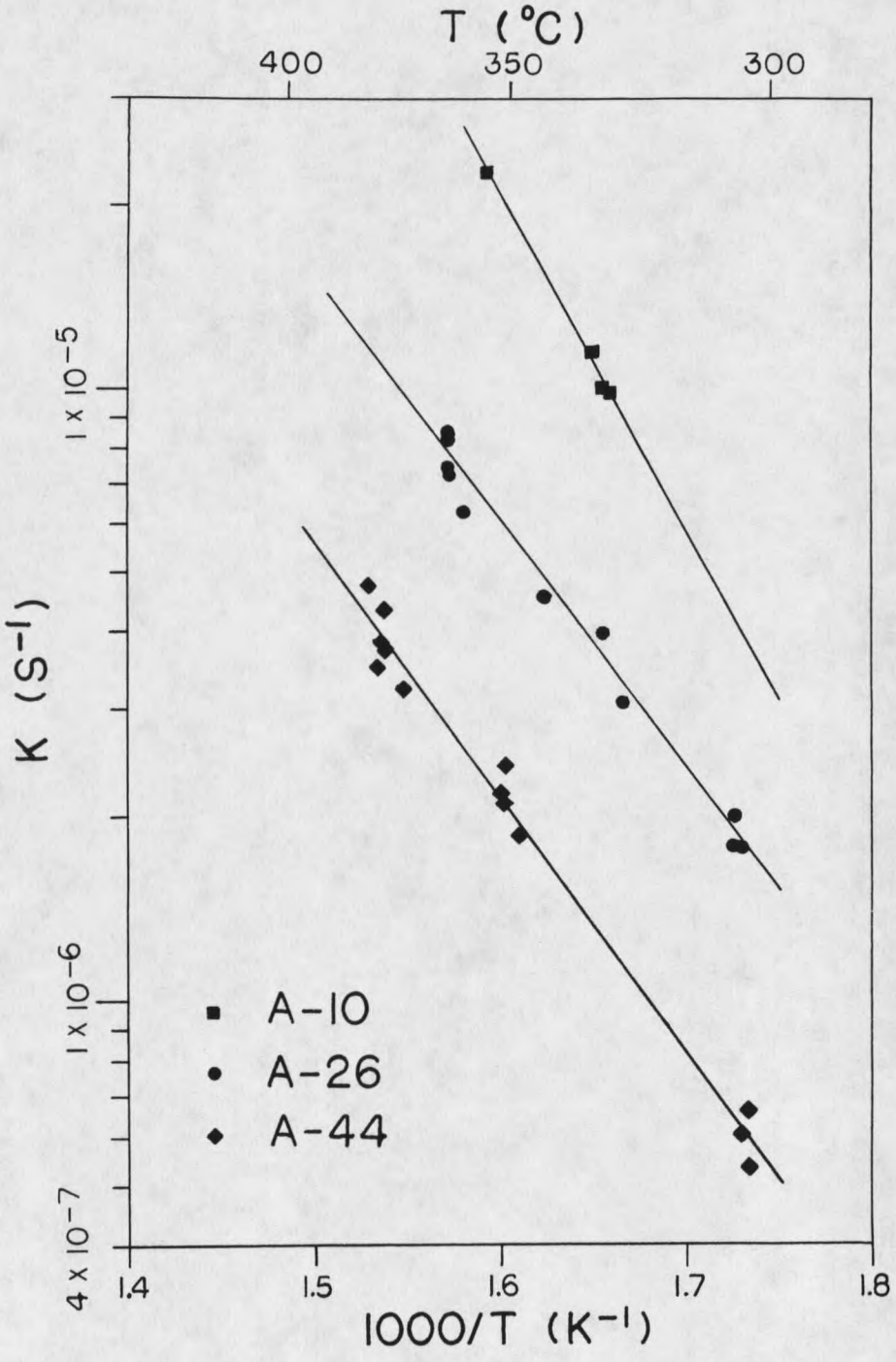

Figure 23. First-order rate constant Arrhenius plot for catalysts A-10, A-26, and A-44.

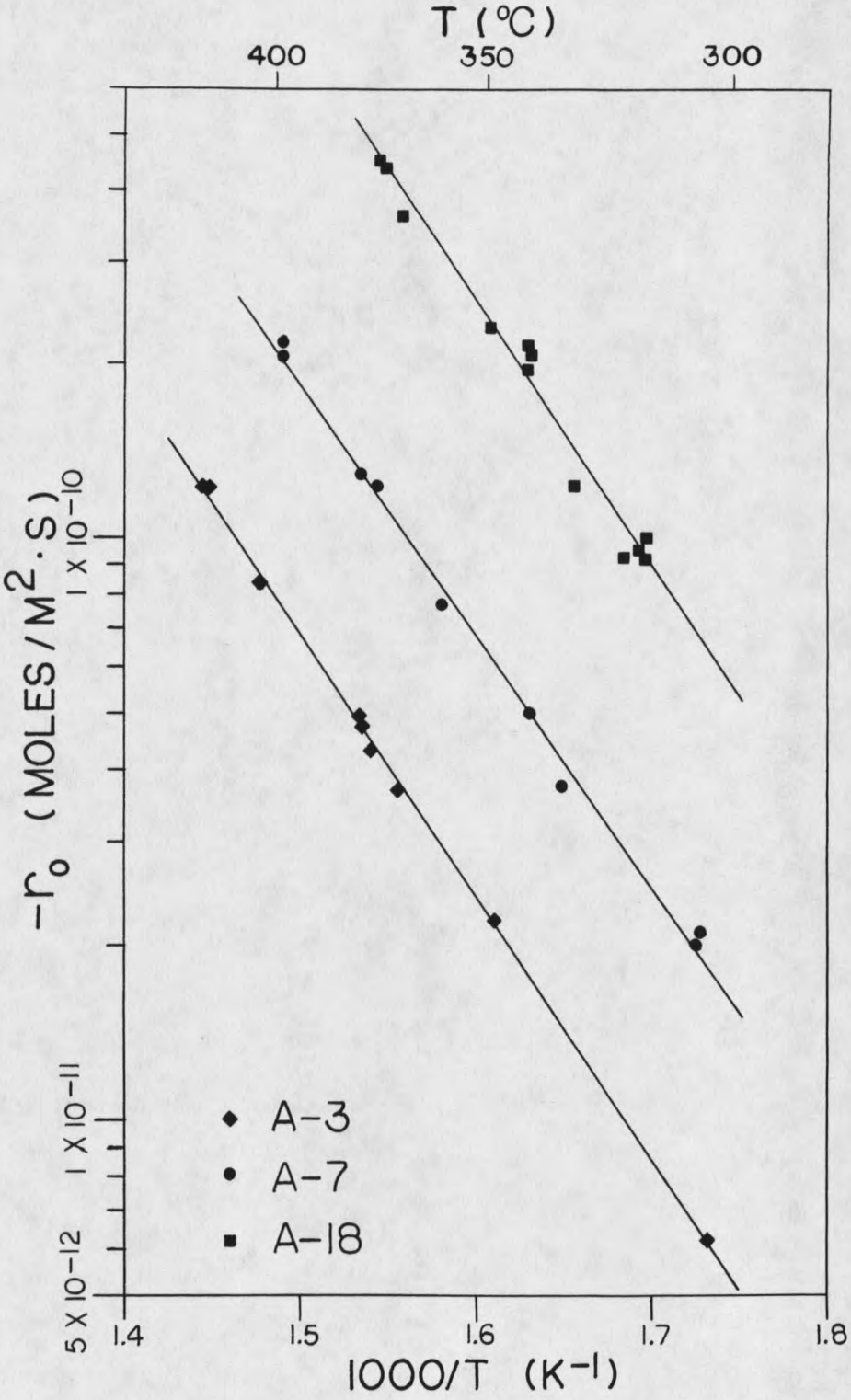

Figure 24. Isomerization rate Arrhenius plot for catalysts A-3, A-7, and A-18.

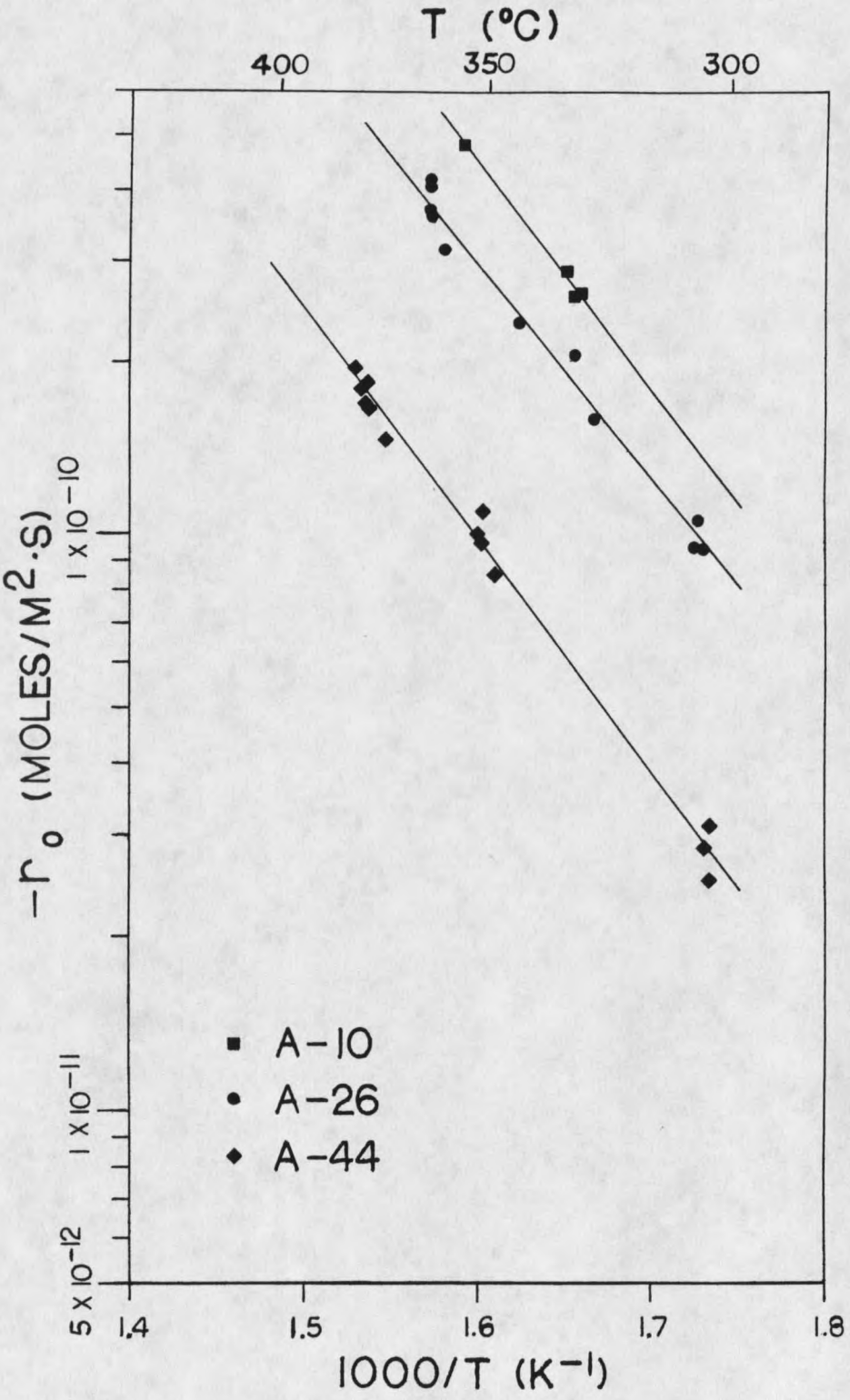

Figure 25. Isomerization rate Arrhenius plot for catalysts A-10, A-26, and A-44.

temperature of 430°C. The lower limit of a detectable o-xylene isomerization rate using the methods and equipment of this study appears to be about 5×10^{-12} moles o-xylene/$m^2 \cdot s$ (See Figure 24). The fact that A-0 and A-100 show no isomerization activity was expected from the report by Holm & Clark [10]. It was also unlikely that A-65 would have significant isomerization activity due to extremely low surface area. However the report by Holm & Clark indicated that a silica-alumina catalyst with a composition comparable to sample A-88 (70% alumina) should show some o-xylene isomerization activity.

The Arrhenius plots of Figures 22 - 25 indicate that all of the active silica-alumina catalysts have essentially the same activation energy for the o-xylene isomerization reaction. The activation energies observed range from 17 to 21 kcal/mole as reported in Table 7, in excellent agreement with the 20 $\pm$ 3 kcal/mole reported by Hansford & Ward for both crystalline (X, Y, and mordenite zeolites) and amorphous silica-alumina [65]. In addition, the magnitude of the reaction rate constant at 260°C measured by Hansford & Ward for an amorphous, commercial silica-alumina cracking catalyst is identical to that observed for sample A-10. Such comparisons give substantial support to the activity measurements made by this study.

Table 7. o-Xylene Isomerization Activity

Sample	Activation Energy (kcal/mole)	Isomerization Rate @ 300°C ($moles/m^2 \cdot s$)
A-0	-	ND
A-3	20.7	5.25×10^{-12}
A-7	19.8	1.59×10^{-11}
A-10	18.4	1.17×10^{-10}
A-18	20.8	5.57×10^{-11}
A-26	17.2	8.47×10^{-11}
A-44	18.5	2.54×10^{-11}
A-65	-	ND
A-88	-	ND
A-100	-	ND

ND-not detected

Sample A-18 was tested for its nitrogen BET surface area after having been used for the isomerization reaction. The surface area was calculated as 154 m^2/g, 12% greater than the surface area calculated for the original material. The primary reason for performing this test was to ensure that the catalyst surface area had not drastically decreased as a result of activity measurement. The increase in surface area is significant when compared to other duplicate surface area analyses. The additional surface area found for sample A-18 is probably due to the high surface area of carbon, deposited on the catalyst through the coking process.

Coking was observed on all test catalysts as a result of the activity test, with the exceptions of samples A-0 and A-65. However, the appearance of the coking was quite different depending on the composition of the catalyst. The low alumina content catalysts, samples A-3, A-7, and A-10, were observed to have a purple color as a result of coking. The intermediate alumina content catalysts, samples A-18, A-26, and A-44, reflected more of a brown color due to coking, with just a hint of the purple seen on the low alumina catalysts. Sample A-88 was discolored light brown. Sample A-100 was completely black as a result of activity testing. Heavy coke formation is generally attributed to high acid strength and high acid-site density on a catalyst [6]. No references as to the appearance of coking on silica-alumina catalysts have been found to help explain the purple discoloration of the low alumina catalysts.

Another visual observation was made concerning the appearance of active test catalyst powders after testing for isomerization activity. The catalysts, with the exception of sample A-100, were not coked homogeneously. The used catalysts had a salt-and-peppery appearance. Distinct white particles, apparently silica, are mixed in with the coked fraction of the catalyst samples. It is estimated that the uncoked fraction is less than 10% of the catalyst particles. The bulk heterogeneity observed due to coking certainly invalidates any notion of using bulk alumina content as an indication of activity in these silica-alumina catalysts.

Comparison of Acidity and Activity

The final objective of the present investigation is the comparison of calculated adsorption energy distributions to the observed catalytic activity for the silica-alumina materials synthesized. As discussed previously, the CAEDMON energy distribution calculations yield the quantity of strong acid sites on the test catalysts. This information has been plotted in Figure 26, with strong acid content per surface area as a function of bulk alumina content. For comparison, surface area specific reaction rates for the isomerization of o-xylene at 300°C (taken from Table 7) are shown as a function of bulk alumina content in Figure 27.

The similarity between Figures 26 and 27 is certainly not exact. Figure 26 shows that sample A-100 (pure alumina) has significant strong acidity. However, Figure 27 indicates no o-xylene isomerization activity for pure alumina. Although sample A-100 has strong acid sites, these sites are apparently of the Lewis type and will not catalyze the isomerization reaction. It is not obvious if the heavy coke formation on the A-100 material as a result of activity testing is due to these Lewis acid sites being stronger than Brønsted sites or to a high acid-site density as reported in Table 6.

Comparison of Figures 26 and 27 at other compositions is much better, at least in trend. Both Figures 26 and 27 indicate a minimum with sample A-18 and, of course, with samples A-65 and A-88. However, the magnitude of the acidity increase at low alumina content does not

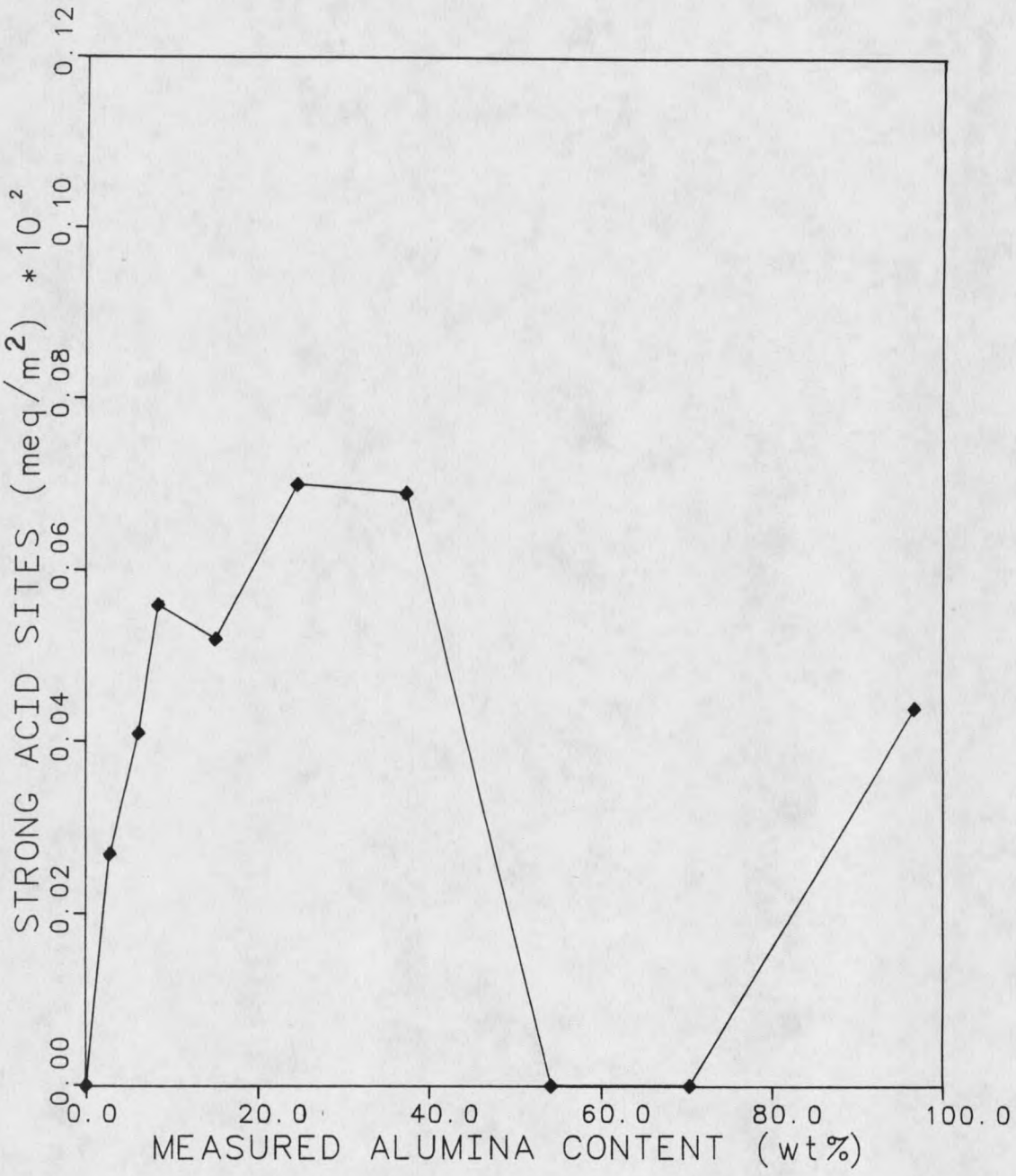

Figure 26. Relationship of the strong acidity measured from chemisorption isotherms to the measured alumina contents of the catalysts.

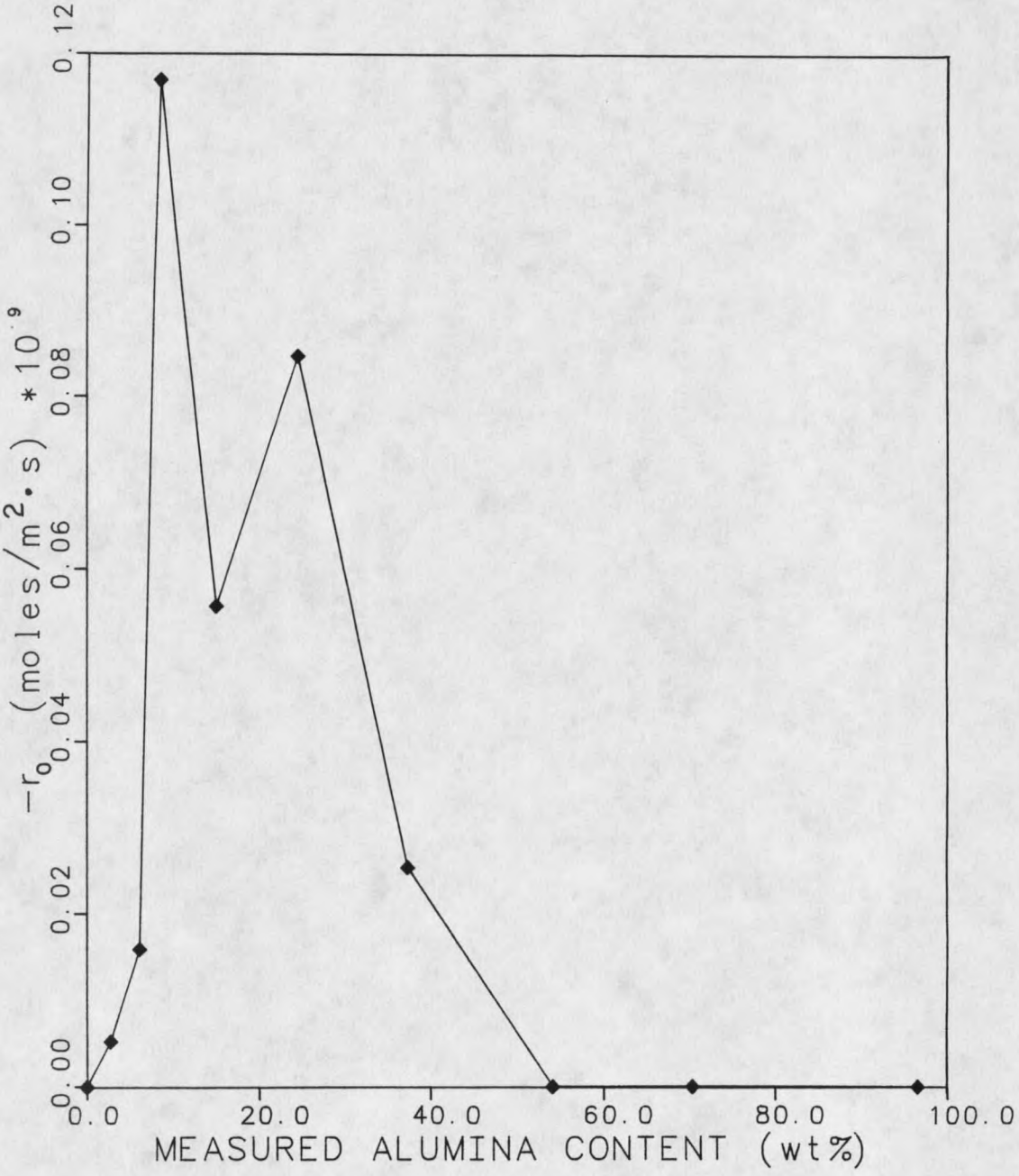

Figure 27. Relationship of the o-xylene isomerization rate at 300°C to the measured alumina contents of the catalysts.

match that of the activity increase. In addition, the two intermediate alumina compositions (samples A-26 and A-44) have more strong acid sites than is reflected by their isomerization activities. It is clear that the acid contents measured for samples A-26 and A-44 include acid sites of the type associated with pure alumina, which are not active for isomerization.

Figures 26 and 27 indicate that the strong surface acidity is not directly proportional to the activity. However, a linear relationship is found to exist between the logarithm of the reaction rate and the surface acidity, as shown in Figure 28. Similar observations have been reported in the literature for o-xylene isomerization on zeolites [31,74,75] and for cumene cracking on amorphous silica-alumina [24]. It is postulated that the exponential effect of surface acidity on reaction rate is due to an interaction of acid sites. Should such an interaction exist, Figure 28 implies that the acid sites are very near each other, perhaps as clusters.

Figure 28 indicates that the exponential relationship is good only for the A-3, A-7, A-10, and A-18 catalysts. If, however, the acidity associated with pure alumina is subtracted from the measured acidities for samples A-26 and A-44 on a weight fraction basis, then these two materials will also fit the exponential relationship. Correction of the A-3, A-7, A-10, and A-18 catalysts for the acidity associated with pure alumina was not necessary. The evidence of Figure 9 indicates that the low alumina content materials do not form an appreciable amount of the alumina phase.

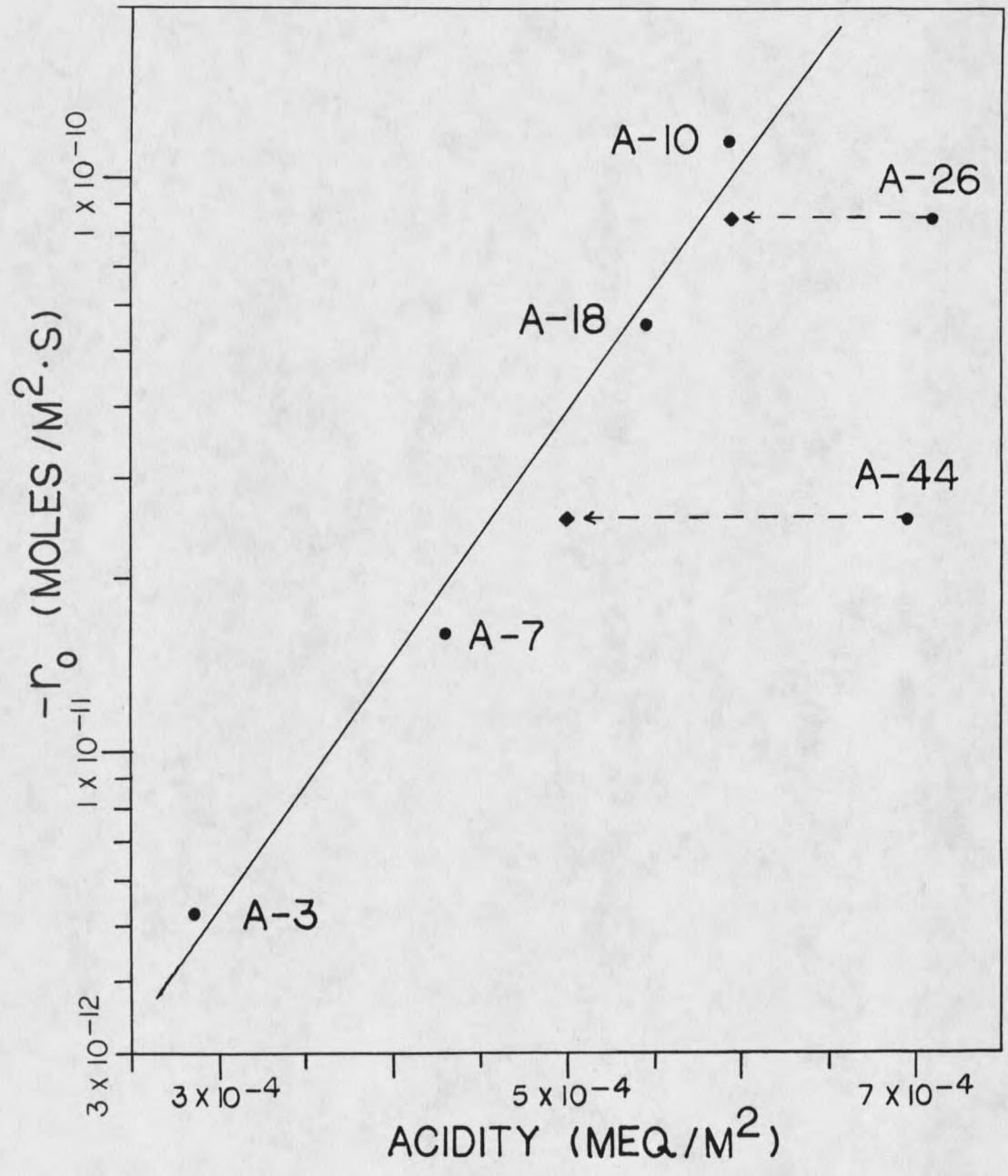

Figure 28. Logarithm of the o-xylene isomerization rate shown as a function of the strong acidity of the catalysts. Catalysts A-26 and A-44 indicate the effect of correcting for the strong acidity associated with pure alumina.

V. CONCLUSIONS

1. A series of silica-alumina xerogels were synthesized ranging in composition from pure silica to pure alumina. The synthesis procedure avoided contamination of the materials by sodium.
2. Qualitative measurement of the base required for neutral gel formation indicated that Al-O-Si bonds were formed in low alumina content materials.
3. Substantial water loss was observed for the high alumina content materials. However, the water loss is irreversible with calcination, indicating substantial restructuring of these materials.
4. Alumina content of the xerogels was lost due to alumina peptization during washing steps in the catalyst synthesis procedure.
5. Surface area determinations on the test materials indicate unexpected losses of surface area at two compositions, one slight surface area loss at 15% alumina and a substantial surface area loss at 50-75% alumina. Density measurements also indicate unusual properties for the 50-75% alumina materials.
6. TEA adsorption isotherms were measured for all test samples gravimetrically using an apparatus constructed as a part of this study.
7. The minimum TEA injection possible with the equipment used was not small enough to obtain the low-coverage portion of the adsorption isotherm associated with very strong adsorption sites.

8. Acid-site strength distributions essentially measured the quantity of strong acid sites on the test catalyst surfaces. The acid amounts are in good agreement with literature reports for both commercial and research silica-aluminas.

9. The pure alumina catalyst was found to have strong surface acidity from adsorption measurements. This observation is corroborated by the heavy coking found on the alumina catalyst after activity testing.

10. o-Xylene isomerization activities were measured for the test catalysts in an apparatus constructed as part of this investigation. Reaction rates were determined free of diffusional effects.

11. Activation energies and reaction rates determined were in excellent agreement with literature results for similar materials.

12. Coking was observed on catalysts as a result of activity testing. Irregularities in the coking indicate bulk heterogeneity of the test catalysts.

13. Reaction rates were generally found to be exponentially related to the concentration of strong acid sites for low alumina content materials. Correction of intermediate alumina content materials for strong acidity associated with pure alumina also yields the exponential activity relationship.

VI. RECOMMENDATIONS FOR FURTHER STUDY

Further investigation into the areas delineated by this study should concentrate on questions where partial evidence has been obtained but where more conclusive proof is desired. There are three questions that need further study. The first concerns the postulate that there are only two predominant strong acid-site types on silica-alumina over the entire composition range. One acid-site type is the Brønsted acid site which is active for o-xylene isomerization. The other acid-site type is the Lewis acid site associated with pure alumina, which is not active for isomerization yet is strong enough to cause coking. In this study, all of the strong acid sites on low alumina content catalysts have been assumed to be of the Brønsted type, with no dehydration to the Lewis type. It would be desirable to further characterize the catalysts using infrared spectroscopy, where differences due to Lewis and Brønsted acidity are more readily observed. A similar characterization might also be performed by making activity measurements using a reaction catalyzed by Lewis acid sites. The isobutane cracking reaction has been correlated to Lewis acid sites [6] and other paraffin cracking reactions might be used.

A second question involves the exponential relationship observed between the catalyzed o-xylene isomerization rate and the surface acidity of the silica-alumina catalysts. Calculations performed by Dr. John Sears at MSU [76] indicate that, with some justifiable assumptions, literature data for zeolite materials fit the exponential

relationship observed in this study. It would be interesting to analyze the zeolite materials more closely for the cause or functionality of the exponential effect since the crystalline zeolites are better characterized structurally.

A final area of the present investigation that needs further study is the anomalous physical property measurements observed for the 50-75% alumina composition materials. It is curious that these materials should be amorphous, have such low surface areas and densities, and be derived from such high water-content xerogels. In addition, proton NMR studies by Dr. Smith at UNM have ruled out the possibility of occluded solvent as a cause of the behavior [77]. Complete x-ray analysis of the materials will be necessary to clarify the cause of trends observed thus far.

REFERENCES CITED

1. Snel,R., "Surface Concentration of Aluminum in Amorphous Silica-Alumina Catalysts", Ind. Eng. Chem. Prod. Res. Dev., 24, 219 (1985).
2. Oblad,A.G., Milliken,T.H., & Mills,G.A., "Chemical Characteristics and Structure of Cracking Catalysts", Adv. Catal. III, 199 (1951).
3. Ryland,L.B., Tamele,M.W., & Wilson,J.N., "Cracking Catalysts" in Emmett,P.H.(Ed.), Catalysis VII, 1 (1960).
4. Tanabe,K., Solid Acids & Bases, Academic Press, NY (1970).
5. Benesi,H.A. & Winquist, Adv. Catal., 27, 97 (1978).
6. Gates,B.C., Katzer,J.R., & Schuit,G.C.A., Chemistry of Catalytic Processes, McGraw-Hill, NY (1979).
7. Satterfield,C.N., Heterogeneous Catalysis in Practice, McGraw-Hill, NY (1980).
8. Johnson,O., "Acidity and Polymerization Activity of Solid Acid Catalysts", J. Phys. Chem., 59, 827 (1955).
9. Thomas,C.L., "Chemistry of Cracking Catalysts", Ind. Eng. Chem., 41, 2564 (1949).
10. Holm, V.C.F. & Clark,A., "The Nature of Silica-Alumina Surfaces II. Cracking of n-Octane, Polymerization of Propylene, o-Xylene Isomerization, Hydrogen Transfer, and H-D Exchange", J. Catal., 2, 16 (1963).
11. Bourne,K.H., Cannings,F.A., & Pitkethly,R.C., "The Structure and Properties of Acid Sites in a Mixed-Oxide System I. Synthesis and Infrared Characterization", J. Phys. Chem., 74, 2197 (1970).
12. Andreau,P., Martin,G., & Noller,H., "On the Mechanism of Contact Eliminations XXX. The Cracking of Butyl-Benzenes over Silica-Alumina Catalysts", J. Phys. Chem., 21, 255 (1971).
13. Bremer,V.H., Steinberg,K.H., & Chuong,T.K., "The Influence of Alkali Contamination of the Surface Chemical Properties of Amorphous Alumina-Silica Catalysts", Z. Anorg. Allg. Chem., 400, 115 (1973).
14. Leonard,A.J., Ratnasamy,P., Declerck,F.D., & Fripiat,J.J., "Structure and Properties of Amorphous Silico-Aluminas Part 5. Nature and Properties of Silico-Alumina Surfaces", Discuss. Faraday Soc., 52, 98 (1971).
15. Rouxhet,P.G., & Sempels,R.E., "Hydrogen Bond Strengths and Acidities of Hydroxyl Groups on Silica-Alumina Surfaces and in Molecules in Solution", J. Chem. Soc. Faraday Trans., 70, 2021 (1974).
16. Tomida, et al., Chem. Lett., p.375 (1973).
17. Schwarz,J.A., "Simultaneous Determination of Lewis and Bronsted Site Densities on Silica Alumina using Infrared Techniques", J. Vac. Sci. Tech., 12, 32 (1975).
18. Gayer,F.H., "The Catalytic Polymerization of Propylene", Ind. Eng. Chem., 25, 1122 (1933).
19. Hammett,L.P. & Deyrup,A.J., "A Series of Simple Basic Indicators. I. The Acidity Functions of Mixtures of Sulfuric and Perchloric Acids with Water", J. Am. Chem. Soc., 54, 2721 (1932).
20. Walling,C., "The Acid Strength of Surfaces", J. Am. Chem. Soc., 72, 1164 (1950).

21. Benesi,H.A., "Acidity of Catalyst Surfaces II. Amine Titration Using Hammett Indicators", J. Phys. Chem., 61, 970 (1957).
22. Tanabe,K., "Solid Acid and Base Catalysts", Catalysis Sci. & Tech., 2, 231 (1981).
23. Take,J., Tsuruya,T., Sato,T., & Yoneda,Y., "Measurements of Acid-Strength Distribution beyond H_o = -8.2 of Silica-Alumina Catalysts by UV-Spectrophotometric n-Butylamine Titration Method", Bull. Chem. Soc. Jpn., 45 (11), 3409 (1972).
24. Mills,G.A, Boedecker,E.R., & Oblad,A.G., "Chemical Characterization of Catalysts I. Poisoning of Cracking Catalysts by Nitrogen Compounds and Potassium Ion", J. Am. Chem. Soc., 72, 1554 (1950).
25. Barth,R.T. & Ballou,E.V., "Determination of Acid Sites on Solid Catalysts by Ammonia Gas Adsorption", Anal. Chem., 33, 1080 (1961).
26. Hsieh,P.Y., "Heats of Adsorption of Ammonia on Silica-Alumina Catalysts and Their Surface Energy Distributions", J. Catal., 2, 211 (1963).
27. Adamson,A.W., & Ling,I., Adv. Chem. Ser., 33,51 (1961).
28. Clark,A., Holm,V.C.F., & Blackburn,D.M., "The Nature of Silica-Alumina Surfaces I. Thermodynamics of Adsorption of Ammonia", J. Catal., 1, 244 (1962).
29. Mapes,J.E. & Eischens,R.P., "The Infrared Spectra of Ammonia Chemisorbed on Cracking Catalysts", J. Phys. Chem., 58, 1059 (1954).
30. Parry,E.P., "An Infrared Study of Pyridine Adsorbed on Acidic Solids. Characterization of Surface Acidity", J. Catal., 2, 371 (1963).
31. Ward,J.W., "The Nature of Active Sites on Zeolites VIII. Rare Earth Y Zeolite", J. Catal., 13, 321 (1969).
32. Mizuno,K., Ikeda,M., Imokawa,T., Take,J., & Yoneda,Y., "Nature of Catalytically Active Sites over Solid Acids. I. Selective Poisoning of Lewis Acid Sites on Silica-Alumina with Pyridine and Its Application to Olefin Polymerization", Bull. Chem. Soc. Jpn., 49, 1788 (1976).
33. Perera,J.M., Hillar,S.A., Vincenzini,J.C., and Figoli,N.S., "Acid Strength of the Active Sites on Silica-Alumina Catalyst for Cracking of Cumene, Dehydration of Methanol and Methylation of Methylaniline Studied by the Poisoning Technique", J. Catal., 21, 70 (1971).
34. Johnson,M.F.L. & Melik,J.S., "Dealkylation of t-Butylbenzene by Cracking Catalysts", J. Phys. Chem., 65, 1146 (1961).
35. Sugioka & Aomura, Bull. Jpn. Petr. Inst., 15, 136 (1973).
36. Gay,I.D. & Liand,S., "Investigation of Surface Acidity by ^{13}C NMR Adsorption of Amines on Silica, Alumina, and Mixed Silica-Alumina", J. Catal., 44, 306 (1976).
37. Morrison,S.R., The Chemical Physics of Surfaces, Plenum Press, NY (1977).
38. Adamson,A.W., Physical Chemistry of Surfaces, 4th Ed., Wiley & Sons, NY (1982).

39. Wagner,C.D., Six,H.A., Jansen,W.T., & Taylor,J.A., "Improving the Accuracy of Determination of Line Energies by ESCA Chemical State Plots for Silico-Aluminum Compounds", App. Surface Sci., 9, 203, (1981).
40. Drain,L.E. & Morrison,J.A., "Thermodynamic Properties of Nitrogen and Oxygen Adsorbed on Rutile", Trans. Faraday Soc., 49, 654 (1953).
41. Froment,G.F. & Bischoff,K.B., Chemical Reactor Analysis & Design, Wiley & Sons, NY (1979).
42. House,W.A. & Jaycock,M.J., "A Numerical Algorithm for the Determination of the Adsorptive Energy Distribution Function from Isotherm Data", Coll. & Poly. Sci., 256, 52 (1978).
43. Ross,S. & Morrison,I.D., "Computed Adsorptive Energy Distribution in the Monolayer (CAEDMON)", Surface Sci., 52, 103 (1975).
44. Sacher,R.S. & Morrison,I.D., "An Improved CAEDMON Program for the Adsorption Isotherms of Heterogeneous Substrates", J. Colloid & Int. Sci., 70, 153 (1979).
45. Wesson,S.P., Vajo,J.J., & Ross,S., "Determination of Specific Surface Areas of Glass Filaments by BET and CAEDMON Methods", J. Colloid & Interface Sci., 94, 552 (1983).
46. Morrison,I.D. & Ross,S., "A Critique of Adamson and Ling's Analysis of Adsorption Isotherms to Obtain the Site-Energy Distribution", Surface Sci., 62, 331 (1977).
47. Dormant,L.M. & Adamson,A.W., "Reply to the Critique of Morrison and Ross and Comments on the Analysis of Physical Adsorption Data", Surface Sci., 62, 337 (1977).
48. Lecloux,J., "Texture of Catalysts", Catalysis Sci. & Tech., 2, 171 (1981).
49. Lowell,S. & Shields,J.E., Powder Surface Area and Porosity, Powder Technology Series, Chapman & Hall, NY (1984).
50. Brunauer,S., Emmett,P.H., & Teller,E.J., "Adsorption of Gases in Multimolecular Layers", J. Am. Chem. Soc., 60, 309 (1938).
51. Iler, R.K., The Colloid Chemistry of Silica and Silicates, Cornell Univ. (1955).
52. Huizenga,D.G., Knudsen Diffusion in Beds of Monodisperse Silica Spheres, M.S. Thesis, Montana State University (1984).
53. Crock,J.G. & Severson,R.C., "Four Reference Soil and Rock Samples for Measuring Element Availability in the Western Energy Regions", U.S. Department of the Interior, Geological Survey Circular 841 (1980).
54. Hendrickson,J.B., Cram,D.J., & Hammond,G.S., Organic Chemistry, p. 326, 3rd Ed., McGraw-Hill, NY (1970).
55. Sax,I.N., Dangerous Properties of Industrial Materials, 4th Ed., Van Nostrand Reinhold Co., NY (1975).
56. Boudeulle,M., Durand,D., & Michel,P., "Use of a Microbalance for the Determination of the Mass of Oxygen Reacting during the Oxidation of Thin Films of Binary Alloys", Vacuum Microbalance Techniques, 7, 1 (1970).
57. Cudenhead,D.A. & Wagner,N.J., "Gravimetric Adsorption Studies of Hydrogen on Granular Metal Surfaces Using a Vacuum Microbalance" Vacuum Microbalance Techniques, 8, 97 (1971).

58. Czanderna,A.W. & Vasofsky,R., "Surface Studies with the Vacuum Microbalance", Progress in Surface Sci., 9, 45 (1981).
59. Morrison,I.D. & Ross,S., "The Second and Third Virial Coefficients of a Two-Dimensional Gas", Surface Sci., 39, 21 (1973).
60. Hirschfelder,J.O., Curtis,C.F., & Bird,R.B. Molecular Theory of Gases & Liquids, Wiley & Sons, NY (1954).
61. Reid,R.C., Prausnitz,J.M., & Sherwood,T.K., The Properties of Gases & Liquids, 3rd Ed., McGraw-Hill, NY (1977).
62. Treybal,R., Mass Transfer Operations, 3rd Ed., McGraw-Hill, NY (1980).
63. McClellan,A.L. & Harnsberger,H.F., "Cross-Sectional Areas of Molecules Adsorbed on Solid Surfaces", J. of Coll. & Int. Sci. 23, 577 (1967).
64. deBoer,J.H. & Visseren,W.J., "Mechanism and Kinetics of Some Reactions on Silica-Alumina Catalysts", Catalysis Reviews, 5(1), 55-56 (1971).
65. Hansford,R.C. & Ward,J.W., "The Nature of Active Sites on Zeolites VII., Relative Activities of Crystalline and Amorphous Alumino-Silicates", J. Catal., 13, 316 (1969).
66. Ward,J.W., Union Oil Company of California, Union Science & Technology Division, Staff Consultant, February 1985, personal communication.
67. Luinstra,L., "Silica-Alumina Reactivity Studies: Design of Experimental Apparatus and Analysis of Data", B.S. Thesis, Montana State University (1985).
68. Berty,J.M., Hambrick,J.O., Malone,T.R., & Ullock,D.S., "Reactor for Vapor-Phase Catalytic Studies", AIChE 64th National Meeting, New Orleans, LA, Preprint 42E (1969).
69. Spencer,S.F., "Rapid Separation of Xylenes and Ethylbenzene by Gas Chromatography Using Packed Columns", Anal. Chem., 35, 592 (1963).
70. Drushel,H.V. & Sommers,A.L., "Catalyst Acidity Distributions Using Visible and Fluorescent Indicators", Anal. Chem., 38, 12, 1723 (1966).
71. Perry,R.H., & Chilton,C.H. (Ed.), Chemical Engineers' Handbook, 5th Ed., McGraw-Hill, NY (1973).
72. Weast,R.C. (Ed.), Handbook of Chemistry and Physics, 53rd Ed. Chemical Rubber Co., Cleveland (1972).
73. Brauer,P. & Jaroniec,M., "Gas Adsorption on Energetically Heterogeneous Solid Surfaces: On the Choice of Local Adsorption Isotherm", J. Colloid & Int. Sci., 108,50 (1985).
74. Ward,J.W., "The Nature of Active Sites on Zeolites X. The Acidity and Catalytic Activity of X Zeolites", J. Catal., 14, 365 (1969).
75. Ward,J.W., "The Nature of Active Sites on Zeolites XI. The Effect of the Silica-to-Alumina Ratio on the Acidity and Catalytic Activity of Synthetic Faujasite-Type Zeolites", J. Catal., 17, 355 (1970).
76. Sears,J.T., Montana State University, Committee Co-chairman, February 1986, personal communication.
77. Smith, D.M., University of New Mexico, Committee Co-chairman, March 1986, personal communication.

APPENDICES

APPENDIX A

Silica-Alumina Surface Structures

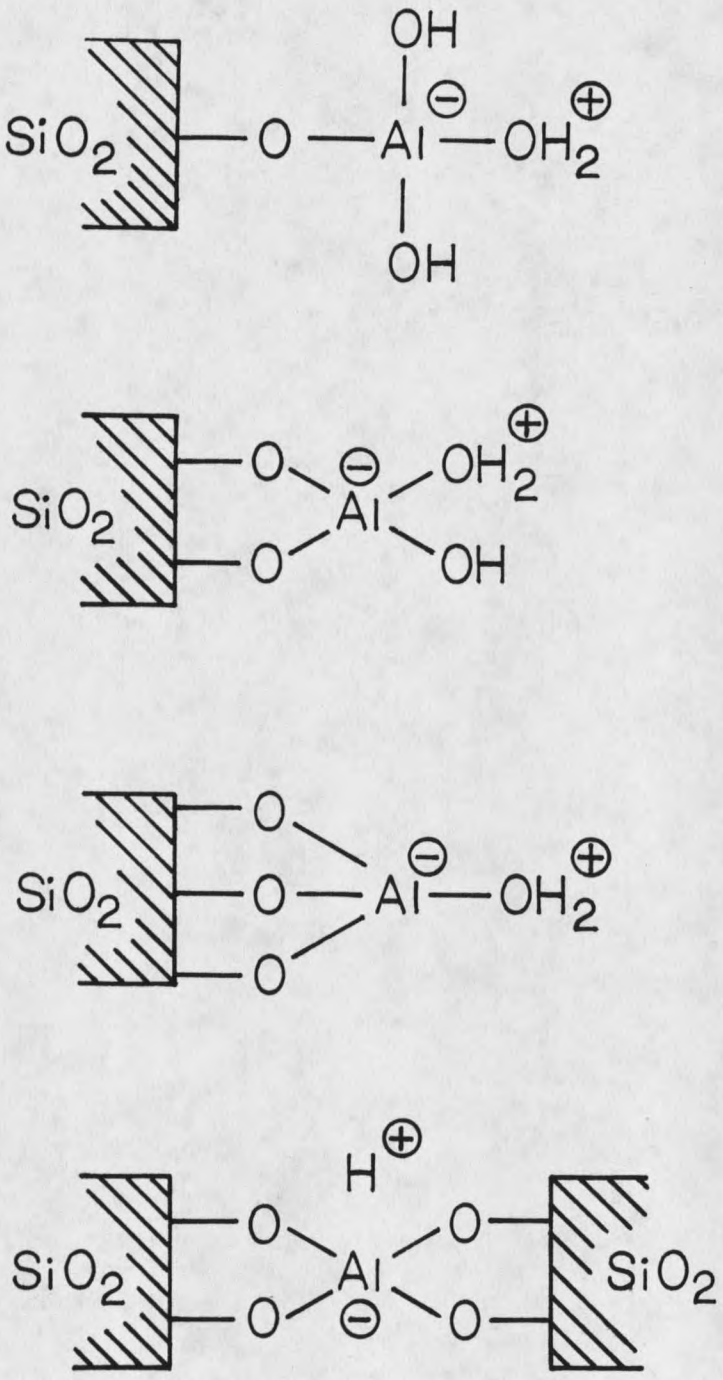

Figure 29. Some proposed silica-alumina surface structures [6, 11, 14, 64].

APPENDIX B

Surface Area Measurement

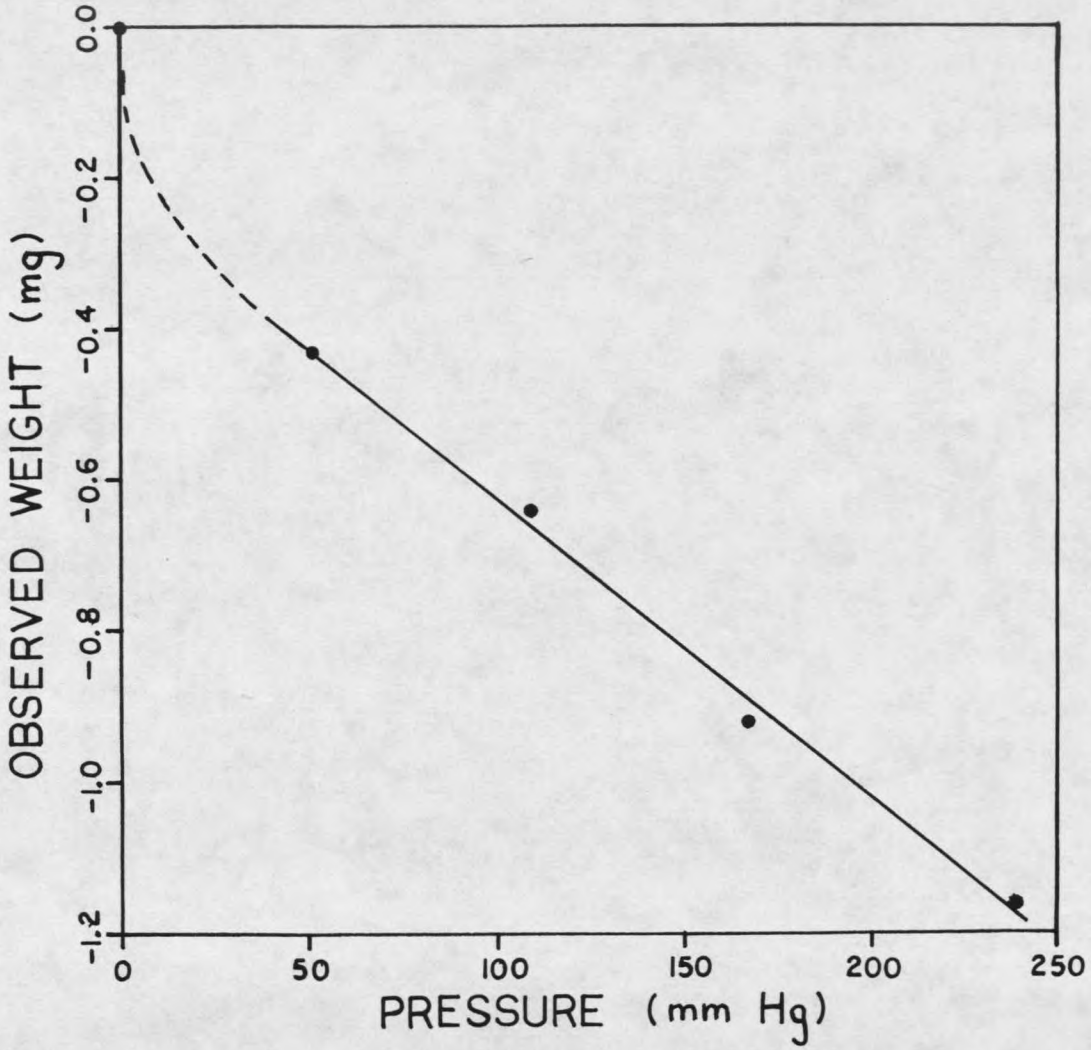

Figure 30. Physisorption apparatus blank response as observed weight loss vs. system pressure.

Figure 31. Program for the calculation of BET surface area.

```
ccccccccccc program BETA
c      user-active surface area computation
c      using the BET method
c      original format by Doug Smith
c      revised by John Golden
       implicit real*8 (a-h,o-z)
       dimension x(100),y(100),p(100),v(100),w(100)
c      nrun is the run number
10     write(6,15)
15     format(' What run is this? 0 to stop ')
       read(5,*) nrun
       if (nrun.eq.0) go to 180
c      den is the gas density(g/cm**3) at STP
c      taken from CRC 53rd ed. for nitrogen
       den=.0012506
c      psat is the saturation pressure(mm Hg) at operating
c      temp.
       write(6,16)
16     format(' What is psat(mm Hg) at operating temp? ')
       read(5,*) psat
c      num is the number of adsorption points with
c      .05<p/psat<.35
       write(6,20)
20     format(' How many data points are there? ')
       read(5,*) num
c      samp is the sample weight(g)
       write(6,25)
25     format(' What is the sample weight in grams? ')
       read(5,*) samp
c      cross is the cross-sectional area of the adsorbent in
c      angstroms
c      for nitrogen from PSA by Lowell and Shields
       cross=16.2
c      p and w are the experimental data, p=pressure(mm Hg),
c      w=weight ad.(g)
       write(6,30)
30     format(' Input experimental pressures in mm Hg ')
       do 35 i=1,num
       read(5,*) p(i)
35     continue
       write(6,40)
40     format(' Input experimental weight ads. in grams ')
       do 45 i=1,num
       read(5,*) w(i)
c      correction for effect of pressure on blank
c      measurement
       w(i)=w(i)+0.0025*p(i)/psat+0.00023
45     continue
```

Figure 31. - Continued

```
      do 50 i=1,num
      v(i)=w(i)/den/samp
      x(i)=p(i)/psat
      y(i)=p(i)/v(i)/(psat-p(i))
50    continue
      call least(num,x,y,a,b)
      c=1.+a/b
      vm=1./(c*b)
      area=vm*6.023*10.**23*cross/(22414*10.**20)
      write(6,60) nrun
60    format(' run number     = ',i3)
      write(6,70) samp
70    format(' sample weight = ',f6.4,' g.')
      write(6,80)
80    format(' adsorbent      = nitrogen')
      write(6,100) vm
100   format('   monolayer capacity = ',1pd10.3,' cm**3/g')
      write(6,110) c
110   format(' interaction constant = ',1pd10.3,
     1' unitless')
      write(6,120) area
120   format('          surface area = ',1pd10.3,' m**2/g')
      write(6,130)
130   format(' p/psat',9x,'p/v/(psat-p) exp',5x,
     1'p/v/(psat-p) bet')
      do 150 i=1,num
      dum=a*x(i)+b
      write(6,140) x(i),y(i),dum
150   continue
140   format(f7.4,8x,1pd12.3,10x,1pd12.3)
      write(6,160)
160   format(' Would you like a data file copy? yes=0 ')
      read (5,*) ans
      if (ans.eq.0) then
      write(1,60) nrun
      write(1,70) samp
      write(1,80)
      write(1,100) vm
      write(1,110) c
      write(1,120) area
      write(1,130)
      do 170 i=1,num
      dum=a*x(i)+b
      write(1,140) x(i),y(i),dum
170   continue
      end if
      go to 10
180   stop
      end
```

Figure 31. - Continued

```
      subroutine least(n,x,y,a,b)
c     this subroutine fits the data set(x,y) to a straight
c     line,y=ax+b
      real*8 x(100),y(100),a,b,z(2,3),dum
      z(1,1)=n
      z(1,2)=0.
      z(1,3)=0.
      z(2,2)=0.
      z(2,3)=0.
      do 100 i=1,n
      z(1,2)=z(1,2)+x(i)
      z(1,3)=z(1,3)+y(i)
      z(2,2)=z(2,2)+x(i)**2
      z(2,3)=z(2,3)+x(i)*y(i)
100   continue
      z(2,1)=z(1,2)
      dum=z(2,1)/z(1,1)
      a=(z(2,3)-dum*z(1,3))/(z(2,2)-dum*z(1,2))
      b=(z(1,3)-a*z(1,2))/z(1,1)
      return
      end
```

APPENDIX C

The CAEDMON Technique

Derivation of the CAEDMON Method

The model used is one in which adsorption is assumed to occur in the form of patches on the heterogeneous solid surface. Each patch is considered to be a separate phase of constant two-dimensional (2D) density, though variations in 2D density occur from patch to patch. The adsorption density of each patch is assumed to be described by a 2D virial expression. The sum of adsorption on all patches is thereby reduced to a function of the system temperature, the system pressure, and the adsorption energies of each patch. In addition, a reasonable range of adsorption energies are known, due to the range of known experimental system pressures. Therefore, a numerical solution to the system can be obtained once the set of adsorption amounts on each patch which yields the best agreement with the total adsorption amounts observed experimentally is found. The most current solution technique used to solve the CAEDMON system of equations and experimental data is a non-negatively constrained linear least squares algorithm.

This description can be made in mathematical terms as follows. The 2D virial equation of state is given by

$$\frac{\Pi A}{RT} = 1 + \frac{B}{A} + \frac{C}{A^2} + \ldots$$

where Π = 2D pressure, A = 2D density, and B and C are the temperature dependent 2D virial coefficients.

Adsorption on each distinct surface phase (patch) is obtained using Gibbs' adsorption theorem at constant temperature, the ideal gas law, and the 2D equation of state.

$$\ln P = \ln \frac{1}{A_j} + \frac{2B}{A_j} + \frac{3C}{2A_j^2} + \ldots + \ln K_j$$

where P = system gas pressure, K_j = integration constant due to the energy difference between the bulk gas and the gas adsorbed on the j^{th} patch, and (consequently) $A_j = f(K_j/P)$.

The number of moles of gas adsorbed on the j^{th} patch is the area of that patch, S_j, divided by the 2D density of the adsorbate on that patch.

$$n_j(P) = S_j/A_j$$

The total number of moles adsorbed on the solid surface is the sum of adsorption on all patches.

$$n(P) = \sum_1^t S_j/A_j = \sum_1^t S_j \cdot f(P/K_j)$$

Data taken at x pressures determines x simultaneous equations.

$$n(P_1) = \sum_j S_j \cdot f(P_1/K_j)$$

$$n(P_2) = \sum_j S_j \cdot f(P_2/K_j)$$

$$\vdots \qquad\qquad \vdots$$

$$n(P_x) = \sum_j S_j \cdot f(P_x/K_j)$$

We know a reasonable range of values for K_j once we know the range of experimental pressures. This knowledge is based on the principle that the only detectable patches are those that appreciable change their 2D density over the range of experimental pressures observed. Hence, by obtaining more data points than the expected number of patches, the system of equations is overdetermined. Numerical solution follows using the non-negatively constrained linear least squares algorithm.

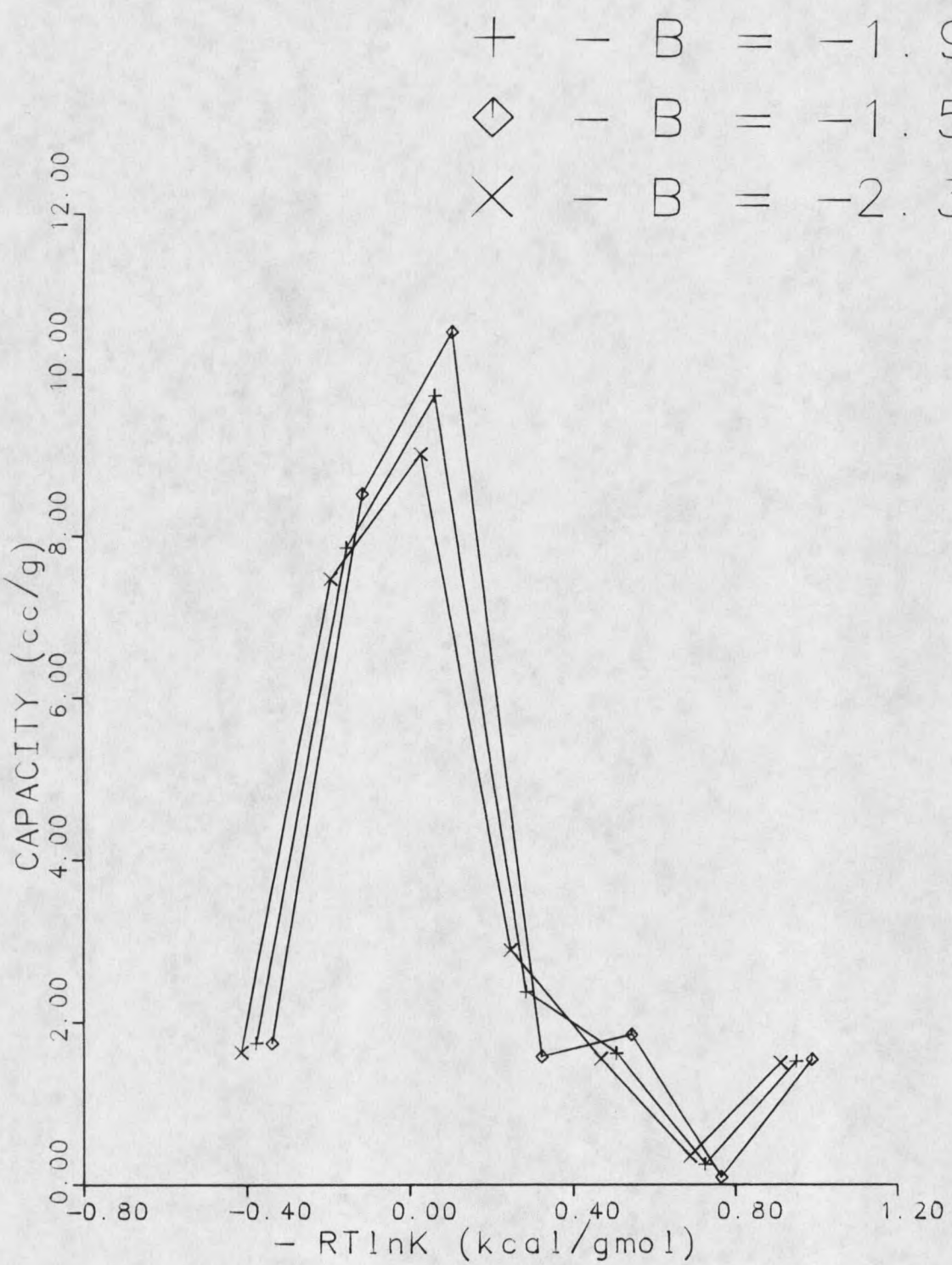

Figure 32. Effect of variation in the second 2D virial coefficient on the calculated adsorption energy distribution using the data of Sacher and Morrison [44].

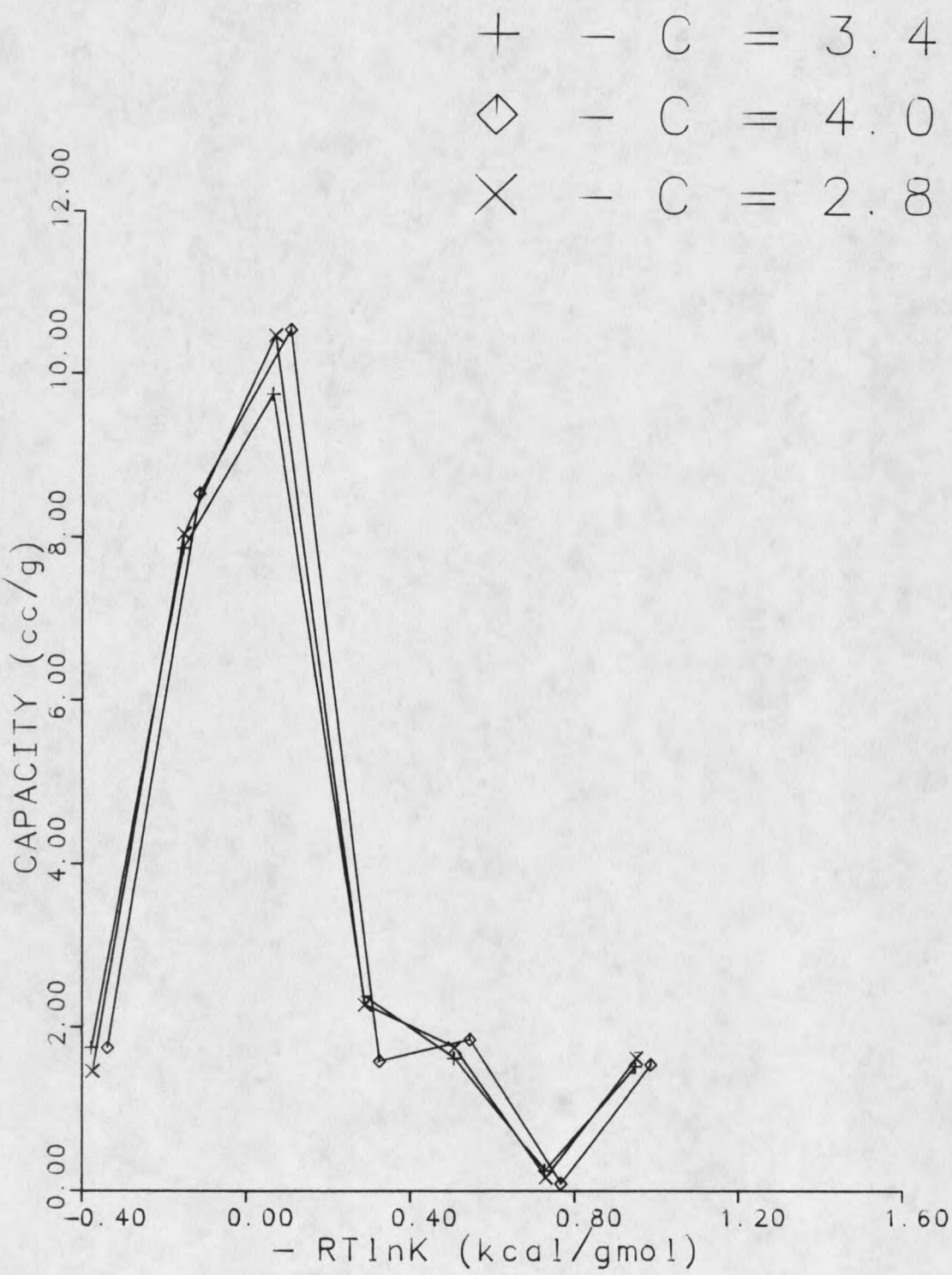

Figure 33. Effect of variation in the third 2D virial coefficient on the calculated adsorption energy distribution using the data of Sacher and Morrison [44].

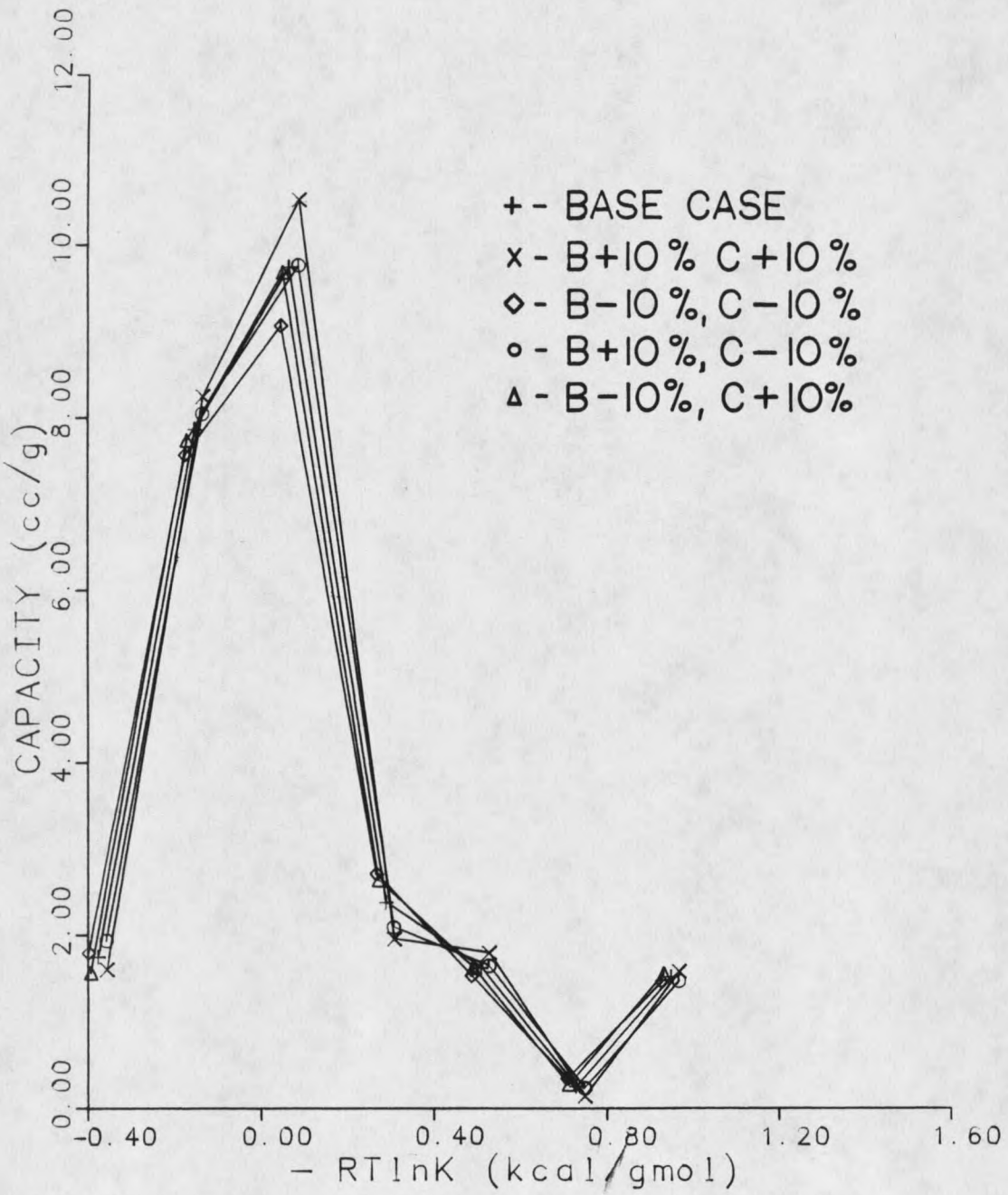

Figure 34. Effect of combined variations in the second and third 2D virial coefficients on the calculated adsorption energy distribution using the data of Sacher and Morrison [44].

Figure 35. Results of testing the CAEDMON program for the effect of variation in the number of surface adsorption patches on the computed adsorption energy distribution using the data of Sacher and Morrison [44].

SACHER SAMPLE DATA TEST FOR VARIATION IN PATCHES

NO. DATA POINTS = 54 NO. OF PATCHES = 7
ISOTHERM TEMP = 77.00 K
B = -0.1900000E+01
C = 0.3400000E+01

ENERGY OF ADSORPTION (Kcal/mol)	CAPACITY OF PATCH (cc/g)
-0.3749772E+00	0.1753727E+01
-0.1543439E+00	0.7867624E+01
0.6628935E-01	0.9754682E+01
0.2869226E+00	0.2381820E+01
0.5075558E+00	0.1627385E+01
0.7281892E+00	0.2553155E+00
0.9488224E+00	0.1523122E+01

THE SUM OF THE CAPACITIES, VM, = 0.2516368E+02

PRESSURE	AMT ADS/GRAM	CALC AMT ADS/GRAM
0.3184000E-03	0.5179061E+00	0.4650165E+00
0.3313000E-03	0.5913848E+00	0.4831854E+00
0.4007000E-03	0.6148453E+00	0.5655615E+00
0.5201999E-03	0.6189498E+00	0.6659700E+00
0.5291000E-03	0.5845490E+00	0.6720909E+00
0.5324000E-03	0.6178818E+00	0.6743231E+00
0.1292600E-02	0.9939498E+00	0.9801250E+00
0.2239800E-02	0.1213608E+01	0.1189375E+01
0.3665500E-02	0.1479752E+01	0.1447317E+01
0.6378700E-02	0.1787964E+01	0.1866627E+01
0.6928100E-02	0.2023193E+01	0.1932209E+01
0.7848599E-02	0.1987930E+01	0.2031681E+01
0.1221190E-01	0.2350159E+01	0.2415258E+01
0.1242160E-01	0.2413177E+01	0.2431993E+01
0.1494610E-01	0.2812835E+01	0.2628955E+01
0.1544570E-01	0.2843200E+01	0.2667203E+01
0.1808880E-01	0.2847717E+01	0.2865149E+01
0.1932880E-01	0.2859009E+01	0.2954566E+01
0.2463790E-01	0.3238861E+01	0.3302482E+01
0.2754400E-01	0.3331238E+01	0.3469506E+01
0.3160140E-01	0.3584869E+01	0.3682390E+01
0.3589530E-01	0.3740784E+01	0.3890604E+01
0.3789660E-01	0.4256164E+01	0.3983809E+01
0.4428050E-01	0.4127197E+01	0.4272313E+01
0.5253740E-01	0.4444946E+01	0.4639404E+01
0.5432220E-01	0.4764709E+01	0.4719088E+01

Figure 35. - Continued

0.5709500E-01	0.5225341E+01	0.4843392E+01
0.6022500E-01	0.4728088E+01	0.4984572E+01
0.6130740E-01	0.5423034E+01	0.5033564E+01
0.7403179E-01	0.6026550E+01	0.5610296E+01
0.7641789E-01	0.5970764E+01	0.5716683E+01
0.9102630E-01	0.6693359E+01	0.6330286E+01
0.1047401E+00	0.6352172E+01	0.6826365E+01
0.1207609E+00	0.7584167E+01	0.7309518E+01
0.1238651E+00	0.7287963E+01	0.7393011E+01
0.1670475E+00	0.8035888E+01	0.8328284E+01
0.1848888E+00	0.8457763E+01	0.8635026E+01
0.1911087E+00	0.8709472E+01	0.8735207E+01
0.2218914E+00	0.9008788E+01	0.9194334E+01
0.2577362E+00	0.9756347E+01	0.9677259E+01
0.3048706E+00	0.1028381E+02	0.1025821E+02
0.3328361E+00	0.1084595E+02	0.1057658E+02
0.3815956E+00	0.1115637E+02	0.1107903E+02
0.3874626E+00	0.1065063E+02	0.1113471E+02
0.4365539E+00	0.1170044E+02	0.1156130E+02
0.5006484E+00	0.1211938E+02	0.1202374E+02
0.5970917E+00	0.1276074E+02	0.1256857E+02
0.7763672E+00	0.1356665E+02	0.1328947E+02
0.7802582E+00	0.1285693E+02	0.1330234E+02
0.1155594E+01	0.1452356E+02	0.1424879E+02
0.1313019E+01	0.1448660E+02	0.1453846E+02
0.1522354E+01	0.1482790E+02	0.1486468E+02
0.1811081E+01	0.1522158E+02	0.1522914E+02
0.1821579E+01	0.1520498E+02	0.1524084E+02

THE PRECEDING SOLUTION IS UNIQUE

NO. DATA POINTS = 54 NO. OF PATCHES = 8
ISOTHERM TEMP = 77.00 K
B = -0.1900000E+01
C = 0.3400000E+01

ENERGY OF ADSORPTION (Kcal/mol)	CAPACITY OF PATCH (cc/g)
-0.3749772E+00	0.6470944E+00
-0.1858629E+00	0.6552708E+01
0.3251285E-02	0.8942466E+01
0.1923655E+00	0.4546173E+01
0.3814797E+00	0.1089263E+01
0.5705940E+00	0.1405296E+01
0.7597082E+00	0.0000000E+00
0.9488224E+00	0.1543996E+01

Figure 35. - Continued

THE SUM OF THE CAPACITIES, VM, = 0.2472699E+02

PRESSURE	AMT ADS/GRAM	CALC AMT ADS/GRAM
0.3184000E-03	0.5179061E+00	0.4668366E+00
0.3313000E-03	0.5913848E+00	0.4850024E+00
0.4007000E-03	0.6148453E+00	0.5671050E+00
0.5201999E-03	0.6189498E+00	0.6660873E+00
0.5291000E-03	0.5845490E+00	0.6720539E+00
0.5324000E-03	0.6178818E+00	0.6742281E+00
0.1292600E-02	0.9939498E+00	0.9598320E+00
0.2239800E-02	0.1213608E+01	0.1186166E+01
0.3665500E-02	0.1479752E+01	0.1490985E+01
0.6378700E-02	0.1787964E+01	0.1867109E+01
0.6928100E-02	0.2023193E+01	0.1926736E+01
0.7848599E-02	0.1987930E+01	0.2021384E+01
0.1221190E-01	0.2350159E+01	0.2413259E+01
0.1242160E-01	0.2413177E+01	0.2429934E+01
0.1494610E-01	0.2812835E+01	0.2618014E+01
0.1544570E-01	0.2843200E+01	0.2652950E+01
0.1808880E-01	0.2847717E+01	0.2829479E+01
0.1932880E-01	0.2859009E+01	0.2909032E+01
0.2463790E-01	0.3238861E+01	0.3240617E+01
0.2754400E-01	0.3331238E+01	0.3420856E+01
0.3160140E-01	0.3584869E+01	0.3671603E+01
0.3589530E-01	0.3740784E+01	0.3929905E+01
0.3789660E-01	0.4256164E+01	0.4045567E+01
0.4428050E-01	0.4127197E+01	0.4387761E+01
0.5253740E-01	0.4444946E+01	0.4771973E+01
0.5432220E-01	0.4764709E+01	0.4847959E+01
0.5709500E-01	0.5225341E+01	0.4962096E+01
0.6022500E-01	0.4728088E+01	0.5085950E+01
0.6130740E-01	0.5423034E+01	0.5127725E+01
0.7403179E-01	0.6026550E+01	0.5590037E+01
0.7641789E-01	0.5970764E+01	0.5672644E+01
0.9102630E-01	0.6693359E+01	0.6163960E+01
0.1047401E+00	0.6352172E+01	0.6610464E+01
0.1207609E+00	0.7584167E+01	0.7108763E+01
0.1238651E+00	0.7287963E+01	0.7201018E+01
0.1670475E+00	0.8035888E+01	0.8292167E+01
0.1848888E+00	0.8457763E+01	0.8645514E+01
0.1911087E+00	0.8709472E+01	0.8758232E+01
0.2218914E+00	0.9008788E+01	0.9254513E+01
0.2577362E+00	0.9756347E+01	0.9740310E+01
0.3048706E+00	0.1028381E+02	0.1028835E+02
0.3328361E+00	0.1084595E+02	0.1058195E+02

Figure 35. - Continued

0.3815956E+00	0.1115637E+02	0.1105259E+02
0.3874626E+00	0.1065063E+02	0.1110597E+02
0.4365539E+00	0.1170044E+02	0.1152566E+02
0.5006484E+00	0.1211938E+02	0.1200084E+02
0.5970917E+00	0.1276074E+02	0.1257587E+02
0.7763672E+00	0.1356665E+02	0.1333398E+02
0.7802582E+00	0.1285693E+02	0.1334731E+02
0.1155594E+01	0.1452356E+02	0.1429477E+02
0.1313019E+01	0.1448660E+02	0.1456887E+02
0.1522354E+01	0.1482790E+02	0.1486962E+02
0.1811081E+01	0.1522158E+02	0.1520002E+02
0.1821579E+01	0.1520498E+02	0.1521059E+02

THE PRECEDING SOLUTION IS UNIQUE

NO. DATA POINTS = 54 NO. OF PATCHES = 9
ISOTHERM TEMP = 77.00 K
B = -0.1900000E+01
C = 0.3400000E+01

ENERGY OF ADSORPTION (Kcal/mol)	CAPACITY OF PATCH (cc/g)
-0.3749772E+00	0.0000000E+00
-0.2095022E+00	0.6534887E+01
-0.4402727E-01	0.5874215E+01
0.1214477E+00	0.7647892E+01
0.2869226E+00	0.7057726E+00
0.4523976E+00	0.1659235E+01
0.6178725E+00	0.7228816E+00
0.7833475E+00	0.0000000E+00
0.9488224E+00	0.1539453E+01

THE SUM OF THE CAPACITIES, VM, = 0.2468434E+02

PRESSURE	AMT ADS/GRAM	CALC AMT ADS/GRAM
0.3184000E-03	0.5179061E+00	0.4662333E+00
0.3313000E-03	0.5913848E+00	0.4844132E+00
0.4007000E-03	0.6148453E+00	0.5664866E+00
0.5201999E-03	0.6189498E+00	0.6656258E+00
0.5291000E-03	0.5845490E+00	0.6716205E+00
0.5324000E-03	0.6178818E+00	0.6738039E+00
0.1292600E-02	0.9939498E+00	0.9638432E+00
0.2239800E-02	0.1213608E+01	0.1195541E+01
0.3665500E-02	0.1479752E+01	0.1463150E+01
0.6378700E-02	0.1787964E+01	0.1861533E+01

Figure 35. - Continued

0.6928100E-02	0.2023193E+01	0.1933497E+01
0.7848599E-02	0.1987930E+01	0.2044837E+01
0.1221190E-01	0.2350159E+01	0.2446136E+01
0.1242160E-01	0.2413177E+01	0.2462073E+01
0.1494610E-01	0.2812835E+01	0.2641580E+01
0.1544570E-01	0.2843200E+01	0.2675010E+01
0.1808880E-01	0.2847717E+01	0.2844019E+01
0.1932880E-01	0.2859009E+01	0.2919533E+01
0.2463790E-01	0.3238861E+01	0.3222924E+01
0.2754400E-01	0.3331238E+01	0.3379776E+01
0.3160140E-01	0.3584869E+01	0.3594096E+01
0.3589530E-01	0.3740784E+01	0.3820083E+01
0.3789660E-01	0.4256164E+01	0.3926170E+01
0.4428050E-01	0.4127197E+01	0.4269420E+01
0.5253740E-01	0.4444946E+01	0.4717074E+01
0.5432220E-01	0.4764709E+01	0.4812243E+01
0.5709500E-01	0.5225341E+01	0.4957566E+01
0.6022500E-01	0.4728088E+01	0.5116911E+01
0.6130740E-01	0.5423034E+01	0.5170696E+01
0.7403179E-01	0.6026550E+01	0.5744969E+01
0.7641789E-01	0.5970764E+01	0.5841002E+01
0.9102630E-01	0.6693359E+01	0.6363860E+01
0.1047401E+00	0.6352172E+01	0.6780327E+01
0.1207609E+00	0.7584167E+01	0.7210758E+01
0.1238651E+00	0.7287963E+01	0.7289191E+01
0.1670475E+00	0.8035888E+01	0.8264410E+01
0.1848888E+00	0.8457763E+01	0.8609492E+01
0.1911087E+00	0.8709472E+01	0.8721931E+01
0.2218914E+00	0.9008788E+01	0.9223348E+01
0.2577362E+00	0.9756347E+01	0.9712542E+01
0.3048706E+00	0.1028381E+02	0.1025132E+02
0.3328361E+00	0.1084595E+02	0.1053383E+02
0.3815956E+00	0.1115637E+02	0.1098277E+02
0.3874626E+00	0.1065063E+02	0.1103381E+02
0.4365539E+00	0.1170044E+02	0.1143972E+02
0.5006484E+00	0.1211938E+02	0.1191611E+02
0.5970917E+00	0.1276074E+02	0.1251917E+02
0.7763672E+00	0.1356665E+02	0.1333364E+02
0.7802582E+00	0.1285693E+02	0.1334792E+02
0.1155594E+01	0.1452356E+02	0.1434144E+02
0.1313019E+01	0.1448660E+02	0.1461773E+02
0.1522354E+01	0.1482790E+02	0.1491494E+02
0.1811081E+01	0.1522158E+02	0.1523684E+02
0.1821579E+01	0.1520498E+02	0.1524709E+02

THE PRECEDING SOLUTION IS UNIQUE

Figure 35. - Continued

NO. DATA POINTS = 54 NO. OF PATCHES = 10
ISOTHERM TEMP = 77.00 K
B = -0.1900000E+01
C = 0.3400000E+01

ENERGY OF ADSORPTION (Kcal/mol)	CAPACITY OF PATCH (cc/g)
-0.3749772E+00	0.0000000E+00
-0.2278883E+00	0.5722264E+01
-0.8079948E-01	0.4435745E+01
0.6628937E-01	0.8025954E+01
0.2133782E+00	0.2315883E+01
0.3604671E+00	0.1105130E+01
0.5075560E+00	0.1145216E+01
0.6546448E+00	0.4950224E+00
0.8017336E+00	0.0000000E+00
0.9488224E+00	0.1530334E+01

THE SUM OF THE CAPACITIES, VM, = 0.2477555E+02

PRESSURE	AMT ADS/GRAM	CALC AMT ADS/GRAM
0.3184000E-03	0.5179061E+00	0.4652581E+00
0.3313000E-03	0.5913848E+00	0.4834016E+00
0.4007000E-03	0.6148453E+00	0.5654832E+00
0.5201999E-03	0.6189498E+00	0.6649526E+00
0.5291000E-03	0.5845490E+00	0.6709997E+00
0.5324000E-03	0.6178818E+00	0.6731814E+00
0.1292600E-02	0.9939498E+00	0.9712269E+00
0.2239800E-02	0.1213608E+01	0.1204915E+01
0.3665500E-02	0.1479752E+01	0.1468094E+01
0.6378700E-02	0.1787964E+01	0.1860669E+01
0.6928100E-02	0.2023193E+01	0.1924240E+01
0.7848599E-02	0.1987930E+01	0.2023046E+01
0.1221190E-01	0.2350159E+01	0.2422545E+01
0.1242160E-01	0.2413177E+01	0.2439766E+01
0.1494610E-01	0.2812835E+01	0.2634414E+01
0.1544570E-01	0.2843200E+01	0.2670451E+01
0.1808880E-01	0.2847717E+01	0.2850913E+01
0.1932880E-01	0.2859009E+01	0.2931074E+01
0.2463790E-01	0.3238861E+01	0.3256673E+01
0.2754400E-01	0.3331238E+01	0.3427510E+01
0.3160140E-01	0.3584869E+01	0.3657952E+01
0.3589530E-01	0.3740784E+01	0.3889484E+01
0.3789660E-01	0.4256164E+01	0.3992859E+01
0.4428050E-01	0.4127197E+01	0.4306478E+01
0.5253740E-01	0.4444946E+01	0.4688362E+01

Figure 35. - Continued

0.5432220E-01	0.4764709E+01	0.4768989E+01
0.5709500E-01	0.5225341E+01	0.4893416E+01
0.6022500E-01	0.4728088E+01	0.5033004E+01
0.6130740E-01	0.5423034E+01	0.5081083E+01
0.7403179E-01	0.6026550E+01	0.5636858E+01
0.7641789E-01	0.5970764E+01	0.5738051E+01
0.9102630E-01	0.6693359E+01	0.6320035E+01
0.1047401E+00	0.6352172E+01	0.6794226E+01
0.1207609E+00	0.7584167E+01	0.7265513E+01
0.1238651E+00	0.7287963E+01	0.7348322E+01
0.1670475E+00	0.8035888E+01	0.8313623E+01
0.1848888E+00	0.8457763E+01	0.8645103E+01
0.1911087E+00	0.8709472E+01	0.8754131E+01
0.2218914E+00	0.9008788E+01	0.9249997E+01
0.2577362E+00	0.9756347E+01	0.9745242E+01
0.3048706E+00	0.1028381E+02	0.1028872E+02
0.3328361E+00	0.1084595E+02	0.1056819E+02
0.3815956E+00	0.1115637E+02	0.1100242E+02
0.3874626E+00	0.1065063E+02	0.1105109E+02
0.4365539E+00	0.1170044E+02	0.1143525E+02
0.5006484E+00	0.1211938E+02	0.1188604E+02
0.5970917E+00	0.1276074E+02	0.1247187E+02
0.7763672E+00	0.1356665E+02	0.1329538E+02
0.7802582E+00	0.1285693E+02	0.1331002E+02
0.1155594E+01	0.1452356E+02	0.1433163E+02
0.1313019E+01	0.1448660E+02	0.1461519E+02
0.1522354E+01	0.1482790E+02	0.1491960E+02
0.1811081E+01	0.1522158E+02	0.1524854E+02
0.1821579E+01	0.1520498E+02	0.1525902E+02

THE PRECEDING SOLUTION MIGHT NOT BE UNIQUE

NO. DATA POINTS = 54 NO. OF PATCHES = 11
ISOTHERM TEMP = 77.00 K
B = -0.1900000E+01
C = 0.3400000E+01

ENERGY OF ADSORPTION (Kcal/mol)	CAPACITY OF PATCH (cc/g)
-0.3749772E+00	0.0000000E+00
-0.2425972E+00	0.3839871E+01
-0.1102172E+00	0.5876078E+01
0.2216271E-01	0.4974743E+01
0.1545427E+00	0.5762769E+01
0.2869226E+00	0.0000000E+00

Figure 35. - Continued

0.4193026E+00	0.1604508E+01
0.5516826E+00	0.7266857E+00
0.6840626E+00	0.3300238E+00
0.8164425E+00	0.0000000E+00
0.9488224E+00	0.1528032E+01

THE SUM OF THE CAPACITIES, VM, = 0.2464271E+02

PRESSURE	AMT ADS/GRAM	CALC AMT ADS/GRAM
0.3184000E-03	0.5179061E+00	0.4651064E+00
0.3313000E-03	0.5913848E+00	0.4832551E+00
0.4007000E-03	0.6148453E+00	0.5653878E+00
0.5201999E-03	0.6189498E+00	0.6650856E+00
0.5291000E-03	0.5845490E+00	0.6711527E+00
0.5324000E-03	0.6178818E+00	0.6733577E+00
0.1292600E-02	0.9939498E+00	0.9746876E+00
0.2239800E-02	0.1213608E+01	0.1201096E+01
0.3665500E-02	0.1479752E+01	0.1464508E+01
0.6378700E-02	0.1787964E+01	0.1850443E+01
0.6928100E-02	0.2023193E+01	0.1919211E+01
0.7848599E-02	0.1987930E+01	0.2029453E+01
0.1221190E-01	0.2350159E+01	0.2448821E+01
0.1242160E-01	0.2413177E+01	0.2465225E+01
0.1494610E-01	0.2812835E+01	0.2646220E+01
0.1544570E-01	0.2843200E+01	0.2679207E+01
0.1808880E-01	0.2847717E+01	0.2843588E+01
0.1932880E-01	0.2859009E+01	0.2916526E+01
0.2463790E-01	0.3238861E+01	0.3214635E+01
0.2754400E-01	0.3331238E+01	0.3374615E+01
0.3160140E-01	0.3584869E+01	0.3599697E+01
0.3589530E-01	0.3740784E+01	0.3841888E+01
0.3789660E-01	0.4256164E+01	0.3955824E+01
0.4428050E-01	0.4127197E+01	0.4317031E+01
0.5253740E-01	0.4444946E+01	0.4756840E+01
0.5432220E-01	0.4764709E+01	0.4845743E+01
0.5709500E-01	0.5225341E+01	0.4979245E+01
0.6022500E-01	0.4728088E+01	0.5123454E+01
0.6130740E-01	0.5423034E+01	0.5171809E+01
0.7403179E-01	0.6026550E+01	0.5692160E+01
0.7641789E-01	0.5970764E+01	0.5781771E+01
0.9102630E-01	0.6693359E+01	0.6293009E+01
0.1047401E+00	0.6352172E+01	0.6726461E+01
0.1207609E+00	0.7584167E+01	0.7181451E+01
0.1238651E+00	0.7287963E+01	0.7263365E+01
0.1670475E+00	0.8035888E+01	0.8232002E+01
0.1848888E+00	0.8457763E+01	0.8565535E+01

Figure 35. - Continued

0.1911087E+00	0.8709472E+01	0.8675702E+01
0.2218914E+00	0.9008788E+01	0.9184500E+01
0.2577362E+00	0.9756347E+01	0.9712372E+01
0.3048706E+00	0.1028381E+02	0.1030863E+02
0.3328361E+00	0.1084595E+02	0.1061422E+02
0.3815956E+00	0.1115637E+02	0.1107726E+02
0.3874626E+00	0.1065063E+02	0.1112798E+02
0.4365539E+00	0.1170044E+02	0.1151916E+02
0.5006484E+00	0.1211938E+02	0.1196000E+02
0.5970917E+00	0.1276074E+02	0.1251749E+02
0.7763672E+00	0.1356665E+02	0.1330437E+02
0.7802582E+00	0.1285693E+02	0.1331850E+02
0.1155594E+01	0.1452356E+02	0.1431208E+02
0.1313019E+01	0.1448660E+02	0.1458947E+02
0.1522354E+01	0.1482790E+02	0.1488768E+02
0.1811081E+01	0.1522158E+02	0.1521037E+02
0.1821579E+01	0.1520498E+02	0.1522065E+02

THE PRECEDING SOLUTION MIGHT NOT BE UNIQUE

NO. DATA POINTS = 54 NO. OF PATCHES = 12
ISOTHERM TEMP = 77.00 K
B = -0.1900000E+01
C = 0.3400000E+01

ENERGY OF ADSORPTION (Kcal/mol)	CAPACITY OF PATCH (cc/g)
-0.3749772E+00	0.1363356E+01
-0.2546318E+00	0.3852071E+00
-0.1342863E+00	0.9285048E+01
-0.1394091E-01	0.1610901E+00
0.1064045E+00	0.9084221E+01
0.2267499E+00	0.0000000E+00
0.3470953E+00	0.1484956E+01
0.4674408E+00	0.6724796E+00
0.5877862E+00	0.9496484E+00
0.7081316E+00	0.6276350E-01
0.8284771E+00	0.0000000E+00
0.9488226E+00	0.1537106E+01

THE SUM OF THE CAPACITIES, VM, = 0.2498588E+02

PRESSURE	AMT ADS/GRAM	CALC AMT ADS/GRAM
0.3184000E-03	0.5179061E+00	0.4660439E+00
0.3313000E-03	0.5913848E+00	0.4842284E+00

Figure 35. - Continued

0.4007000E-03	0.6148453E+00	0.5663126E+00
0.5201999E-03	0.6189498E+00	0.6655960E+00
0.5291000E-03	0.5845490E+00	0.6715931E+00
0.5324000E-03	0.6178818E+00	0.6737971E+00
0.1292600E-02	0.9939498E+00	0.9655173E+00
0.2239800E-02	0.1213608E+01	0.1194318E+01
0.3665500E-02	0.1479752E+01	0.1478547E+01
0.6378700E-02	0.1787964E+01	0.1857883E+01
0.6928100E-02	0.2023193E+01	0.1921599E+01
0.7848599E-02	0.1987930E+01	0.2021604E+01
0.1221190E-01	0.2350159E+01	0.2429550E+01
0.1242160E-01	0.2413177E+01	0.2447301E+01
0.1494610E-01	0.2812835E+01	0.2647738E+01
0.1544570E-01	0.2843200E+01	0.2684495E+01
0.1808880E-01	0.2847717E+01	0.2864853E+01
0.1932880E-01	0.2859009E+01	0.2942597E+01
0.2463790E-01	0.3238861E+01	0.3243951E+01
0.2754400E-01	0.3331238E+01	0.3396335E+01
0.3160140E-01	0.3584869E+01	0.3603013E+01
0.3589530E-01	0.3740784E+01	0.3819945E+01
0.3789660E-01	0.4256164E+01	0.3921655E+01
0.4428050E-01	0.4127197E+01	0.4251958E+01
0.5253740E-01	0.4444946E+01	0.4691949E+01
0.5432220E-01	0.4764709E+01	0.4787735E+01
0.5709500E-01	0.5225341E+01	0.4935838E+01
0.6022500E-01	0.4728088E+01	0.5100818E+01
0.6130740E-01	0.5423034E+01	0.5157072E+01
0.7403179E-01	0.6026550E+01	0.5770681E+01
0.7641789E-01	0.5970764E+01	0.5874185E+01
0.9102630E-01	0.6693359E+01	0.6429938E+01
0.1047401E+00	0.6352172E+01	0.6852884E+01
0.1207609E+00	0.7584167E+01	0.7264826E+01
0.1238651E+00	0.7287963E+01	0.7337113E+01
0.1670475E+00	0.8035888E+01	0.8189590E+01
0.1848888E+00	0.8457763E+01	0.8491149E+01
0.1911087E+00	0.8709472E+01	0.8592310E+01
0.2218914E+00	0.9008788E+01	0.9072273E+01
0.2577362E+00	0.9756347E+01	0.9599730E+01
0.3048706E+00	0.1028381E+02	0.1024050E+02
0.3328361E+00	0.1084595E+02	0.1058377E+02
0.3815956E+00	0.1115637E+02	0.1110811E+02
0.3874626E+00	0.1065063E+02	0.1116503E+02
0.4365539E+00	0.1170044E+02	0.1159547E+02
0.5006484E+00	0.1211938E+02	0.1205564E+02
0.5970917E+00	0.1276074E+02	0.1259663E+02
0.7763672E+00	0.1356665E+02	0.1331578E+02

Figure 35. - Continued

```
0.7802582E+00      0.1285693E+02      0.1332861E+02
0.1155594E+01      0.1452356E+02      0.1426617E+02
0.1313019E+01      0.1448660E+02      0.1454855E+02
0.1522354E+01      0.1482790E+02      0.1486405E+02
0.1811081E+01      0.1522158E+02      0.1521481E+02
0.1821579E+01      0.1520498E+02      0.1522607E+02

THE PRECEDING SOLUTION MIGHT NOT BE UNIQUE
```

Estimation of Two-Dimensional Virial Coefficients

The first step is to estimate intermolecular force constants. This is most simply accomplished using Treybal [62] p.32 {original reference is Wilke & Lee, Ind. Eng. Chem., 47, 1253 (1955)}.

$$\varepsilon/k = 1.21T_b(K)$$

For TEA, T_b = 362.7 K [61]

$$\varepsilon/k = \underline{439\ K}$$

The 2-D virial coefficients are tabulated in terms of reduced temperature,

$$T^* = kT/\varepsilon$$

@ T = 300°C, T^* = 1.305

@ T = 200°C, T^* = 1.077

From a linear interpolation of Table 2 in [59], the second (B) and third (C) 2-D virial coefficients are found.

$T^* = 1.305, \quad B^* = -0.3447$

$C^* = 1.6602$

$T^* = 1.077, \quad B^* = -0.8399$

$C^* = 2.1442$

The parameter, σ, is estimated by [62]

$$\sigma = 1.18 V_b^{0.333}$$

For TEA, V_b = 149.8 cm^3/mol (Estimated from critical properties [61], using Eq.3-25 from Perry's [71])

$$\sigma = \underline{6.3\ A}$$

Another technique to estimate the potential parameters is described in Reid, et al. [61] {original reference is Brokaw, Ind. Eng. Chem. Process Des. Dev., 8, 240 (1969)}.

For TEA, μ_p = 0.9 debyes [61] .

V_b = 149.8 cm^3/mol

T_b = 362.7 K

$$\delta = 1940\mu_p^2/(V_b \cdot T_b)$$

$$\delta = 0.0289$$

$$\varepsilon/k = 1.18(1+1.3\delta^2)T_b = \underline{428\ K}$$

$$\sigma = (1.585V_b/(1+1.3\delta^2))^{0.333} = \underline{6.2\ A}$$

Molecular cross-sectional area of an adsorbate can be estimated using two techniques shown in McClellan and Harnsberger [63]. The first method (originally by Emmett & Brunauer) assumes that molecules are spherical and that they form a hexagonal closest packing arrangement.

$$\sigma^2 = 1.091(M/N\rho)^{0.667}$$

Assuming that the adsorbate density is taken at 20°C,

$$\sigma^2 = 41.0\ A^2$$

The second molecular cross-sectional area technique, (originally by Hill) assumes that the adsorbate can be described with a 2-D van der Waals constant.

$$\sigma^2 = 6.354(T_c/P_c)^{0.667} = 43.4\ A^2$$

The reason for all this estimation is that no force constants are available for TEA or other large polar molecules. The closest analogy is ammonia. I will test the most current estimation technique, that shown in Reid, et al. [61], and compare the results to tabled values for ammonia.

From [61] Appendix C; ε/k = 558.3 K, σ = 2.9 A
From [61] Table 9-2; ε/k = 358 K, 3.15 A

For ammonia, μ_p = 1.5 debyes [61]
T_b = 239.7 K [61]
V_b = 25.4 cm^3/mol [61]

δ = 0.72

ε/k = 472 K, almost the average of the two tabled values listed in [61].

σ = 2.9 A, this value checks with the value in Appendix C [61].

Expected error in 2-D virial coefficients will come from the estimate of the intermolecular energy parameter, ε/k. This error will be first projected on the reduced temperature, T^*.

@ T = 300°C = 573 K

T^* = 1.3388, using the more current estimation method.

From comparison to ammonia, the estimate of ε/k is most likely low.

If T = 300°C,

ε/k	T^*	B^*	C^*
439	1.3388	-0.289	1.615
450	1.2733	-0.392	1.709
475	1.2063	-0.539	1.826
500	1.1460	-0.662	1.956
525	1.0914	-0.804	2.100
550	1.0418	-0.941	2.256

It appears that changes in the energy interaction parameter result in 2-D virial coefficient changes which are equal in magnitude but opposite in sign.

APPENDIX D

Mercury Porosimetry Data and Calculations

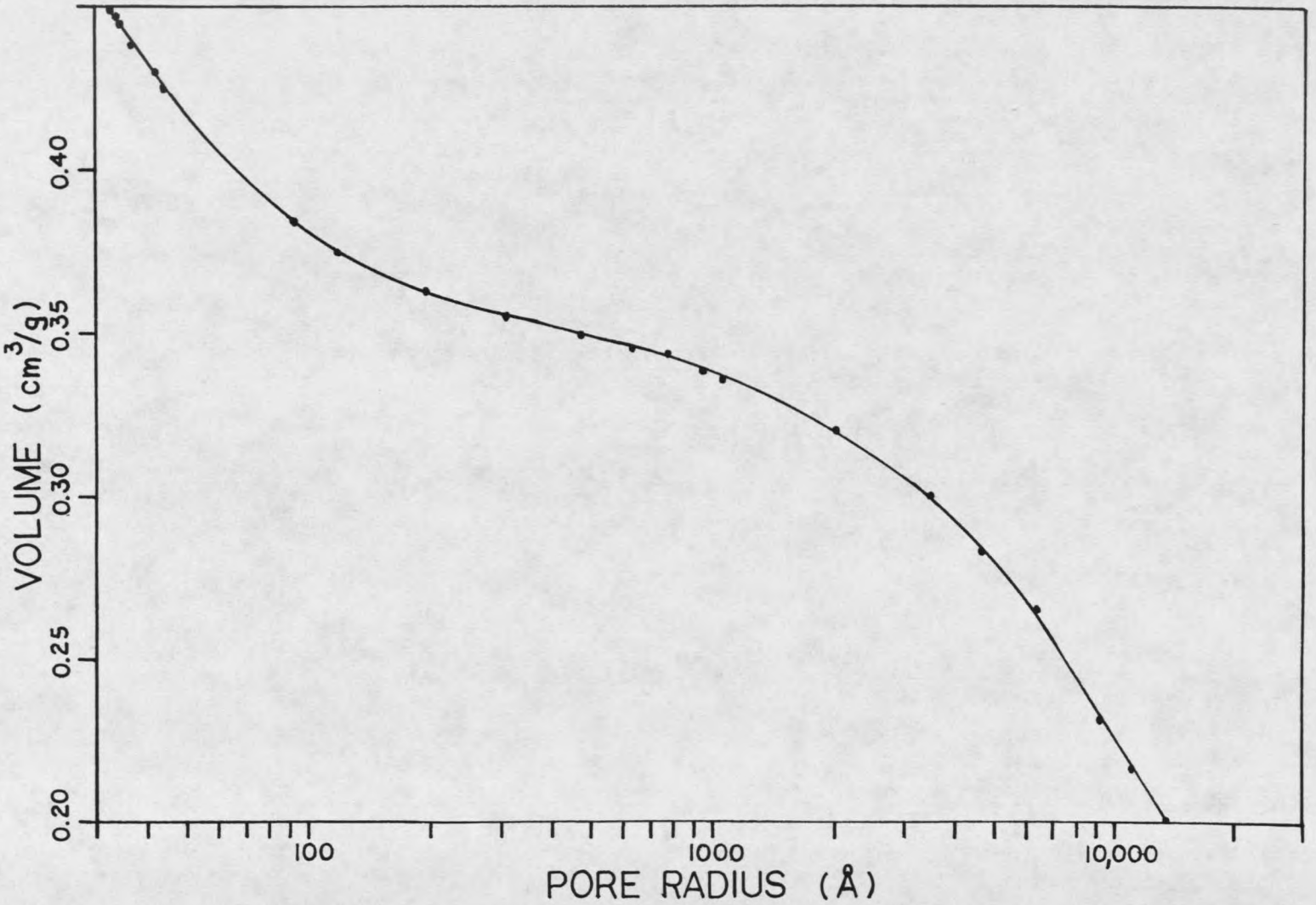

Figure 36. Mercury penetration volume vs. pore radius for sample A-0.

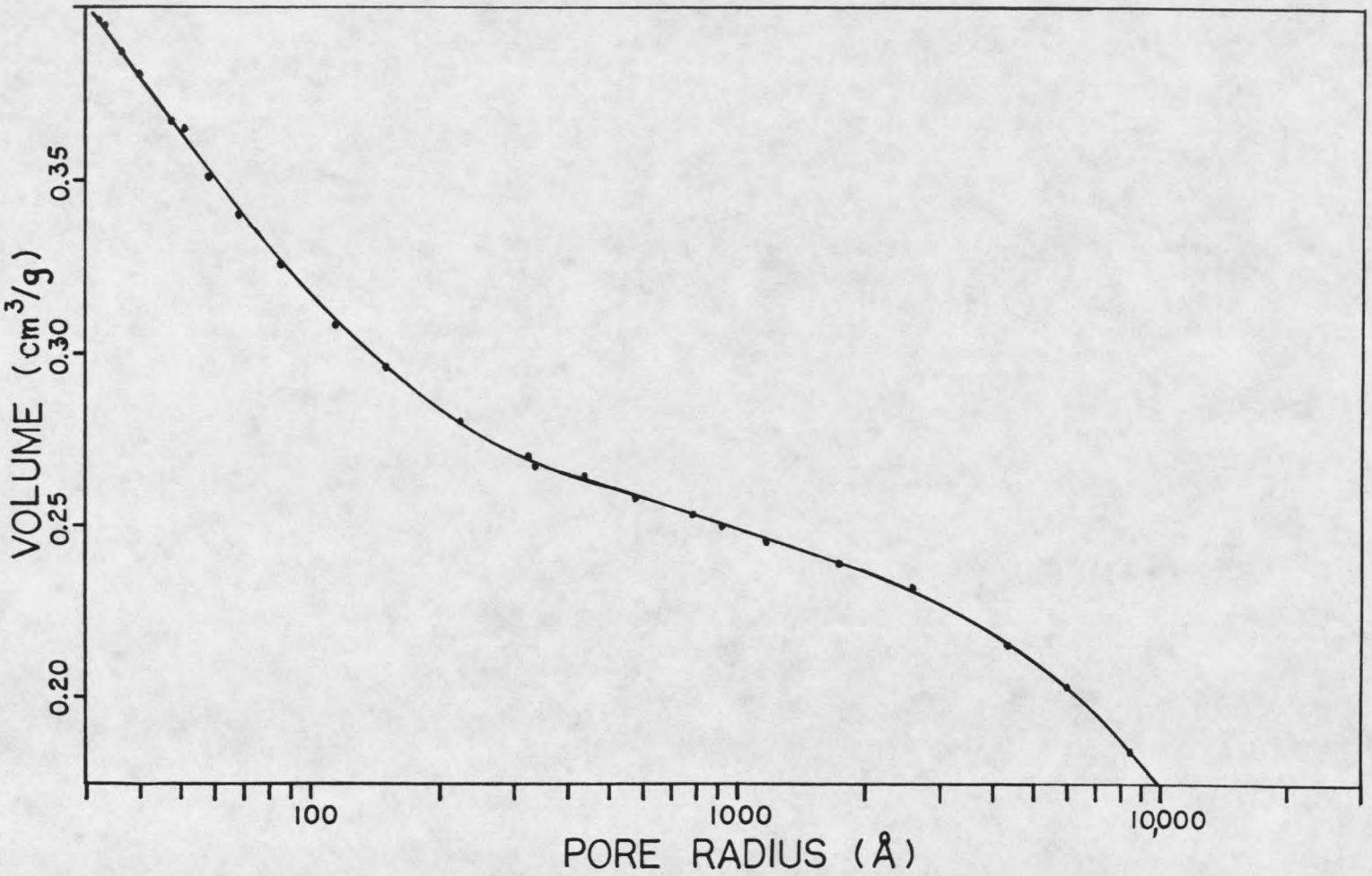

Figure 37. Mercury penetration volume vs. pore radius for sample A-3.

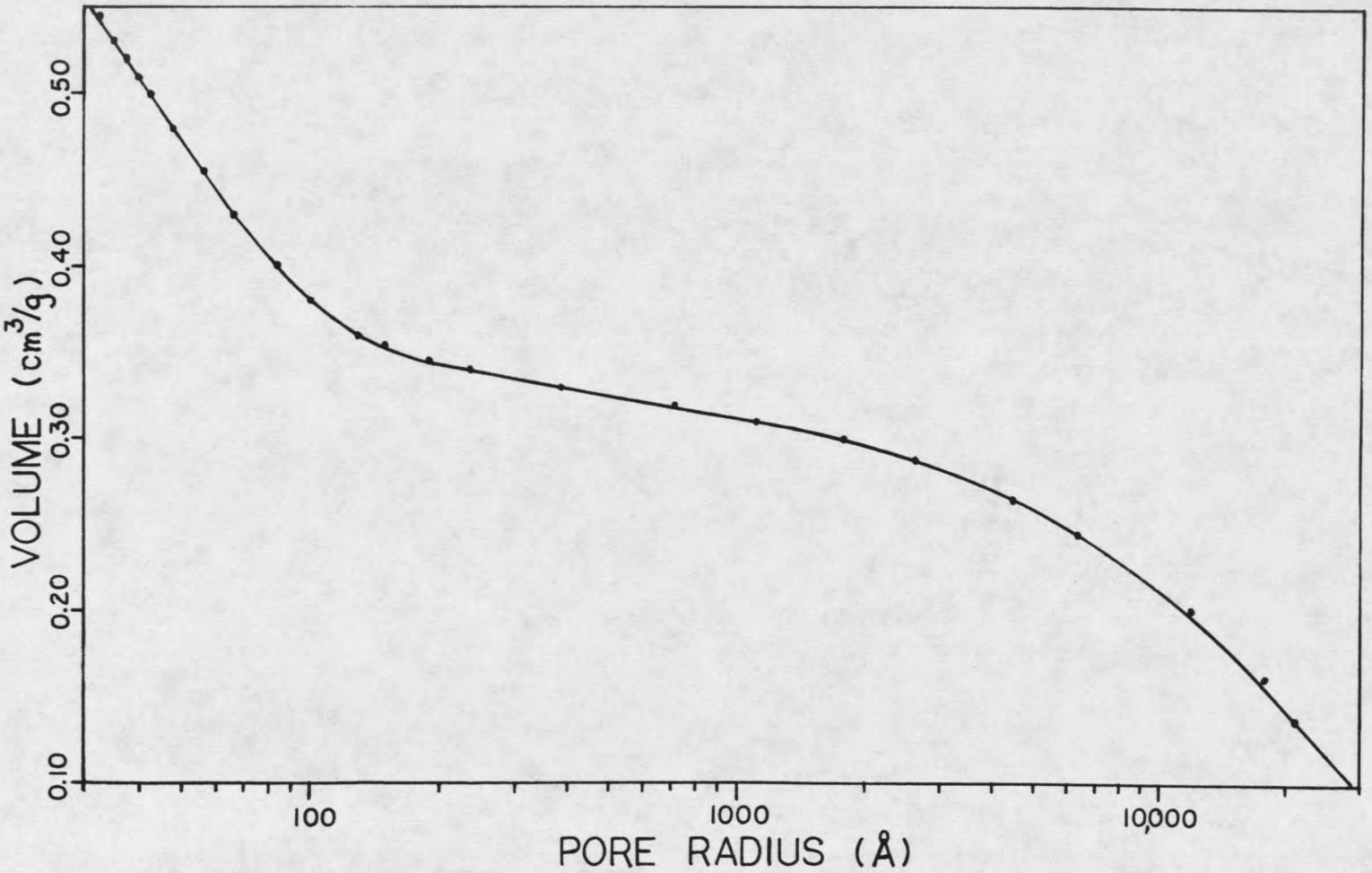

Figure 38. Mercury penetration volume vs. pore radius for sample A-7.

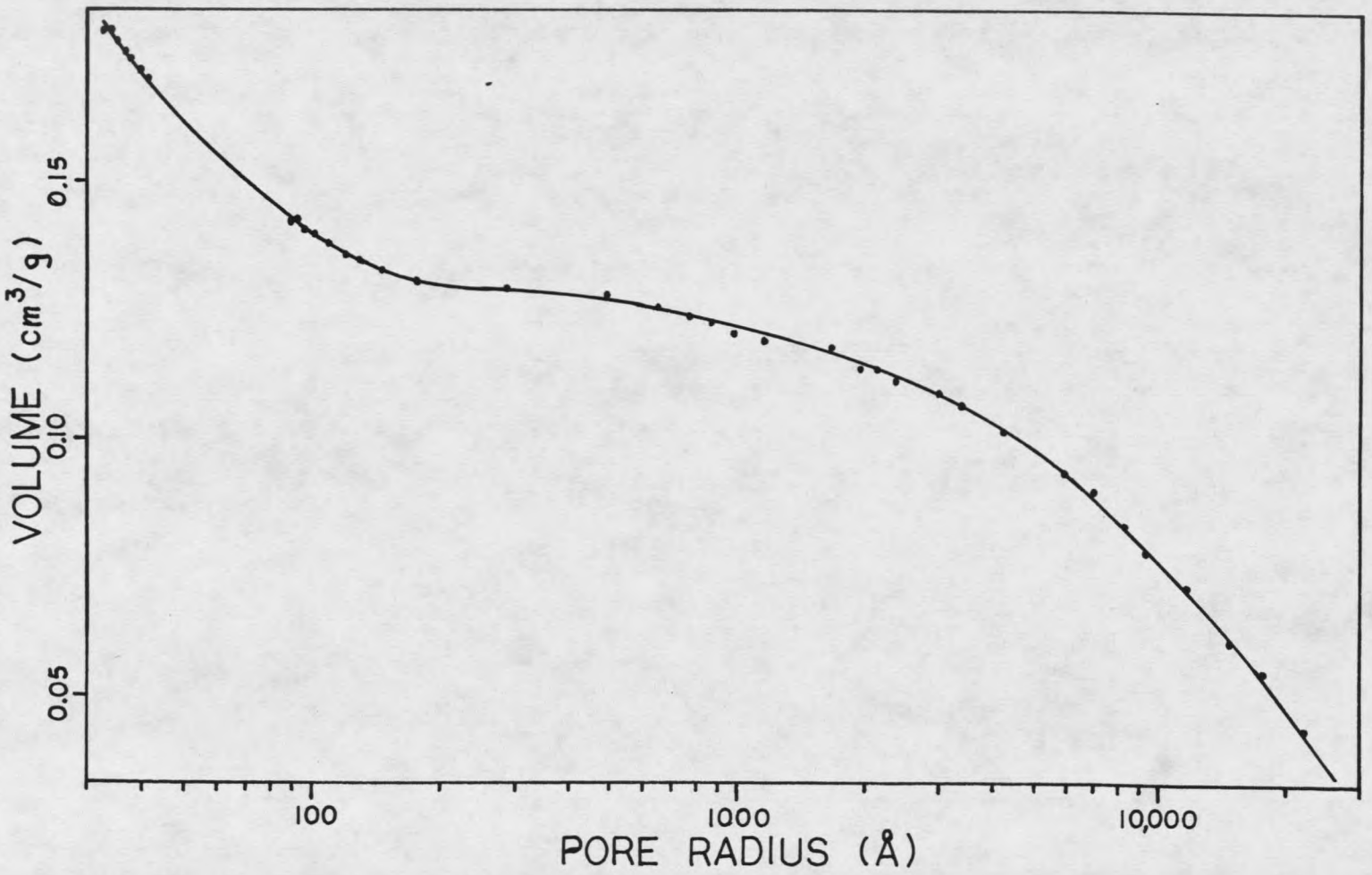

Figure 39. Mercury penetration volume vs. pore radius for sample A-10.

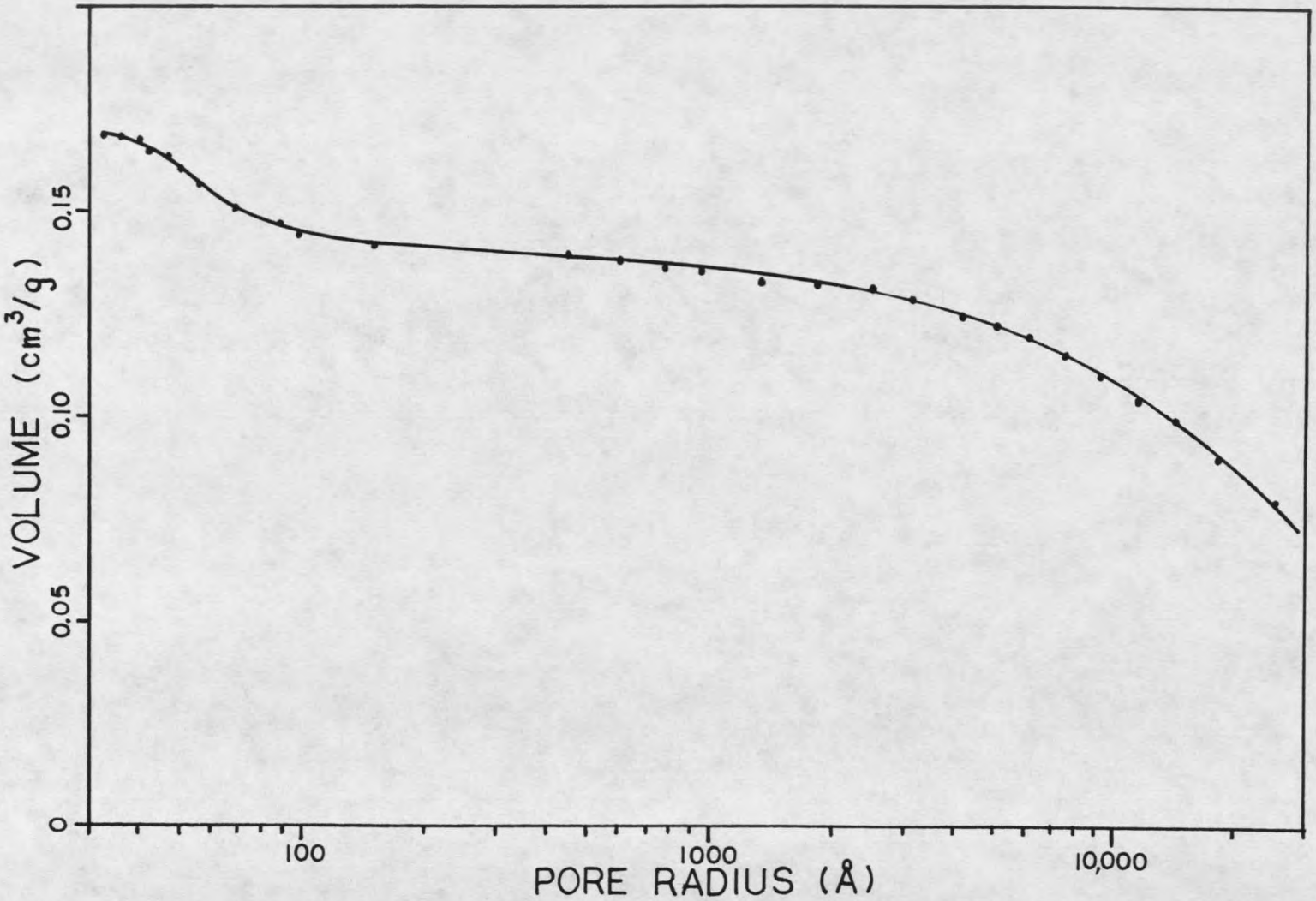

Figure 40. Mercury penetration volume vs. pore radius for sample A-18.

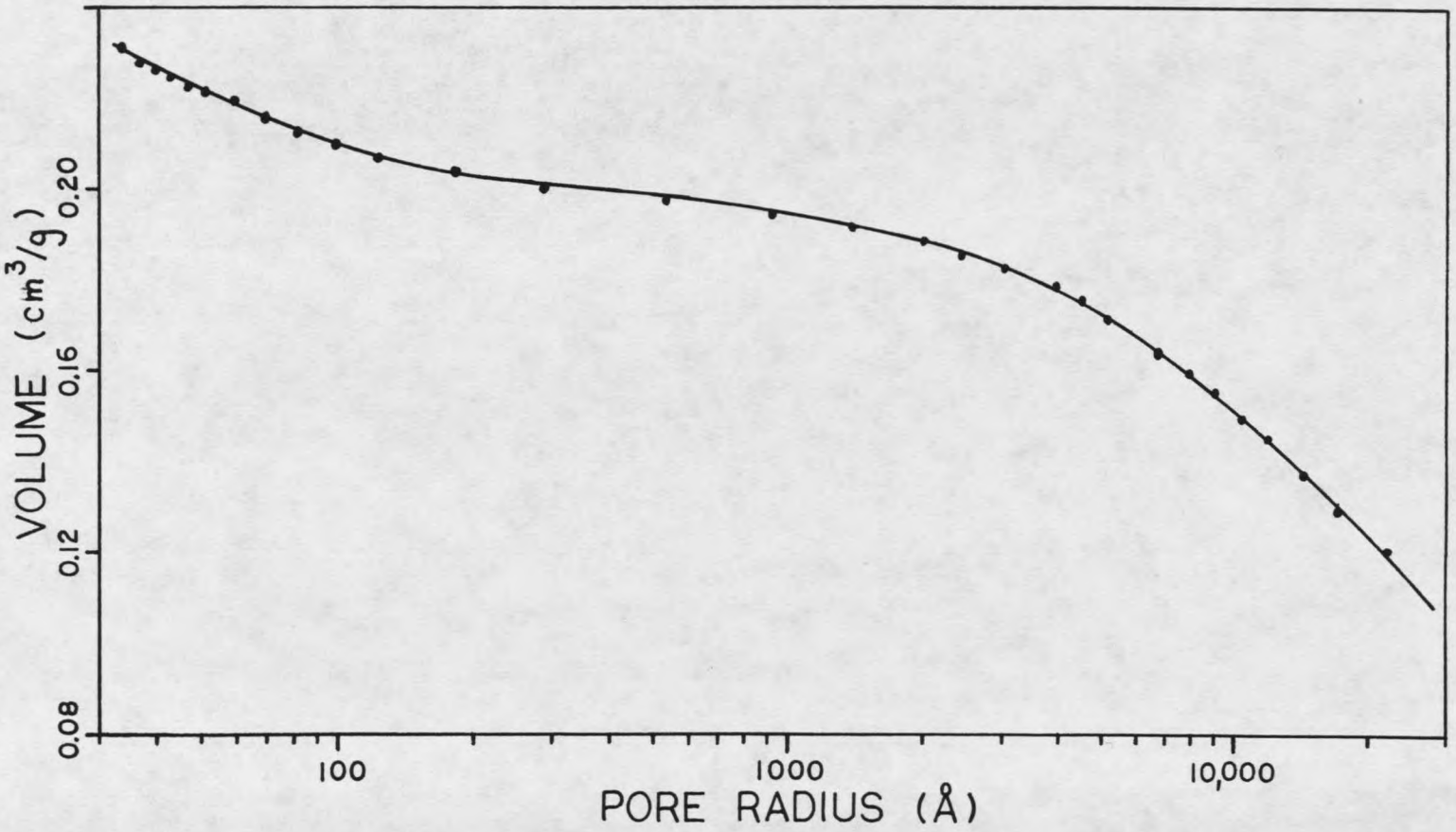

Figure 41. Mercury penetration volume vs. pore radius for sample A-26.

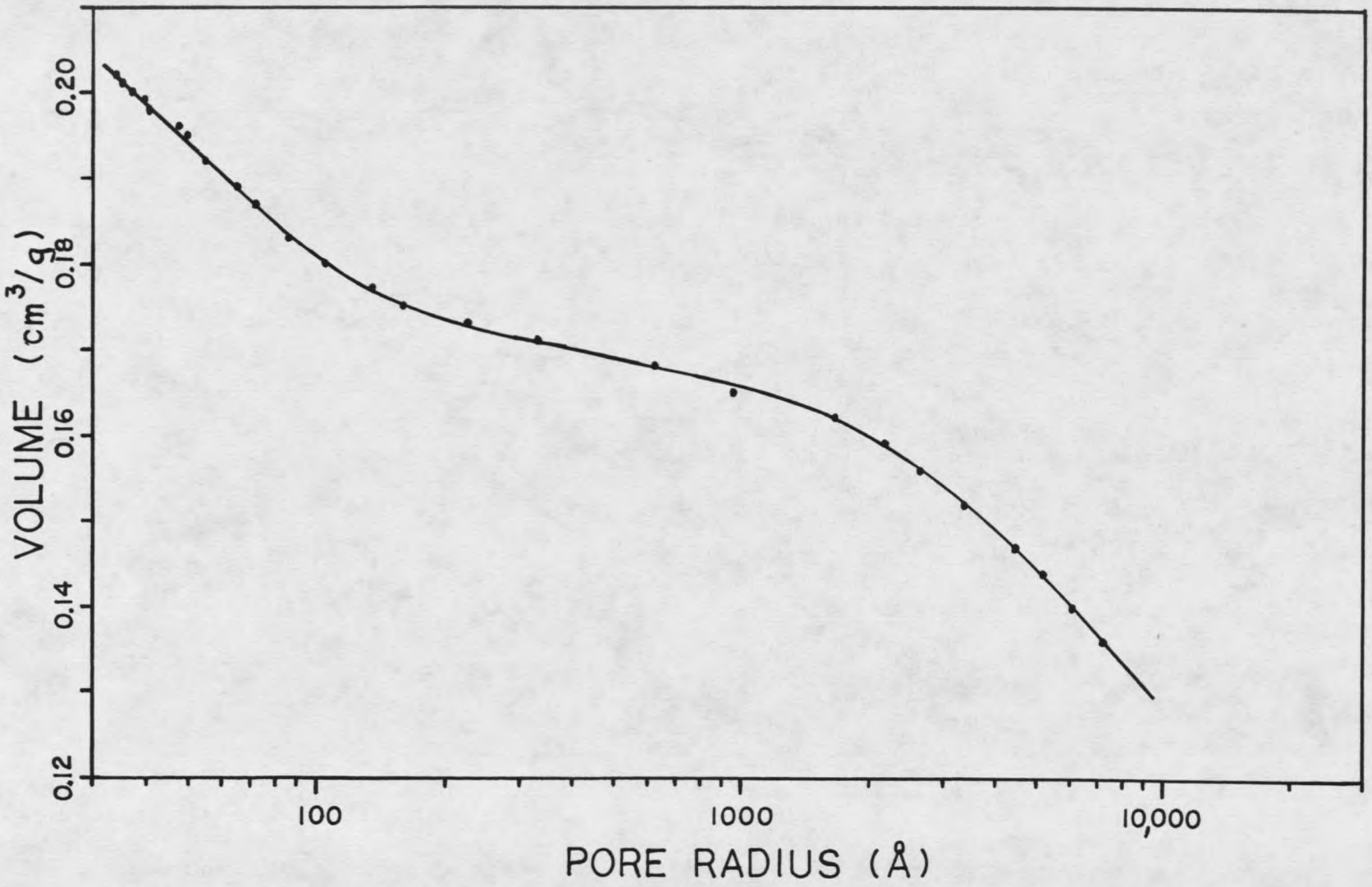

Figure 42. Mercury penetration volume vs. pore radius for sample A-44.

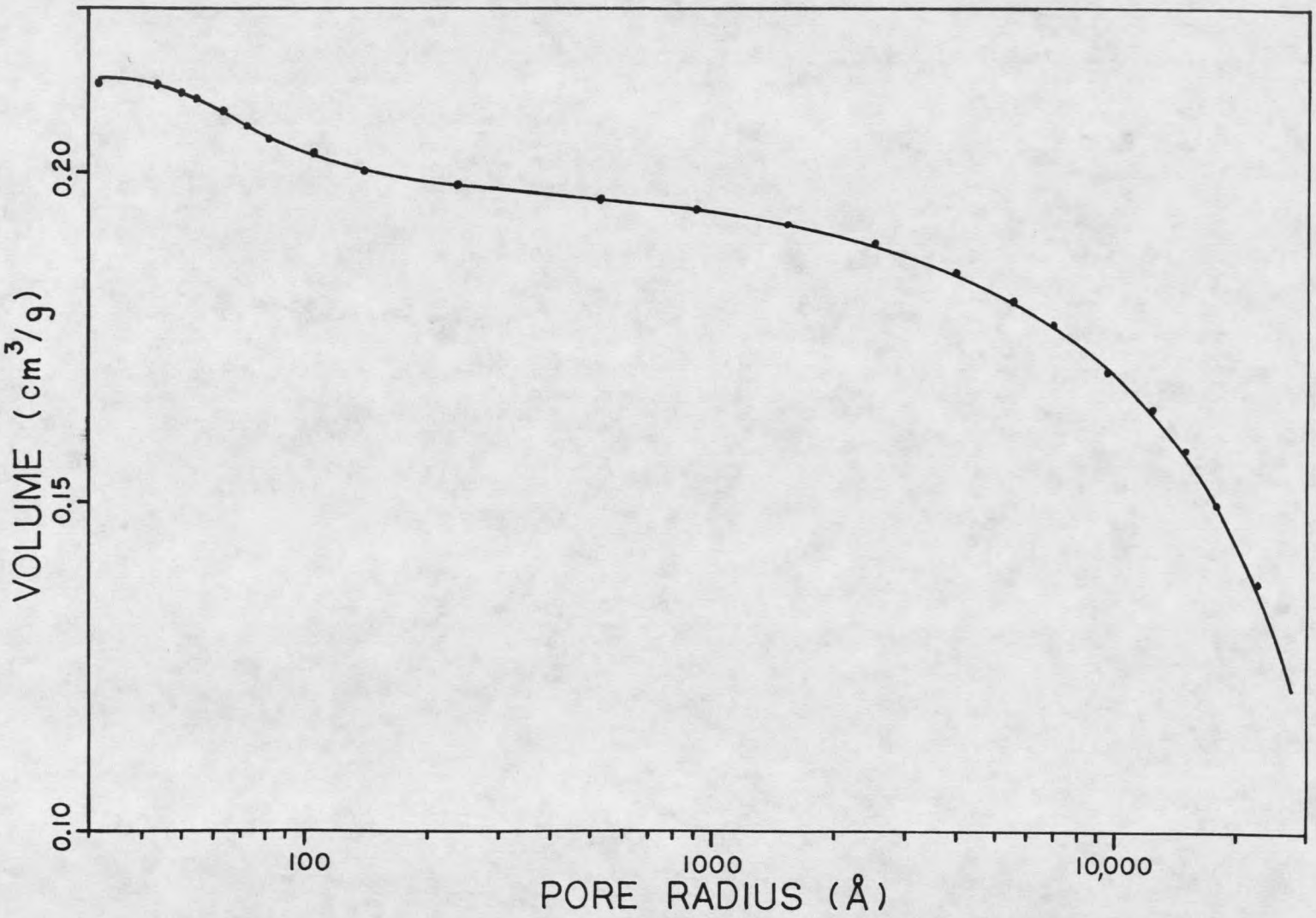

Figure 43. Mercury penetration volume vs. pore radius for sample A-65.

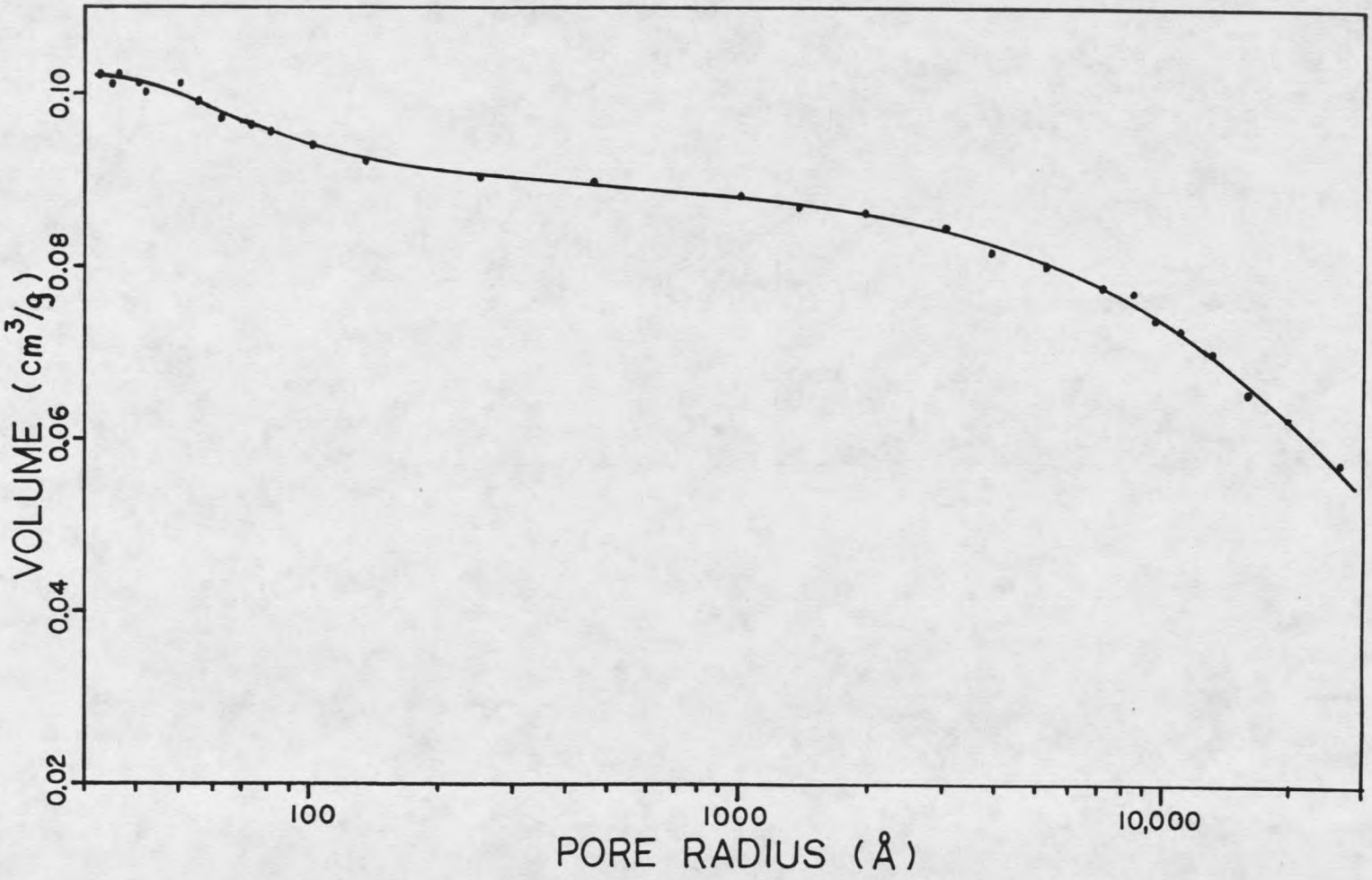

Figure 44. Mercury penetration volume vs. pore radius for sample A-88.

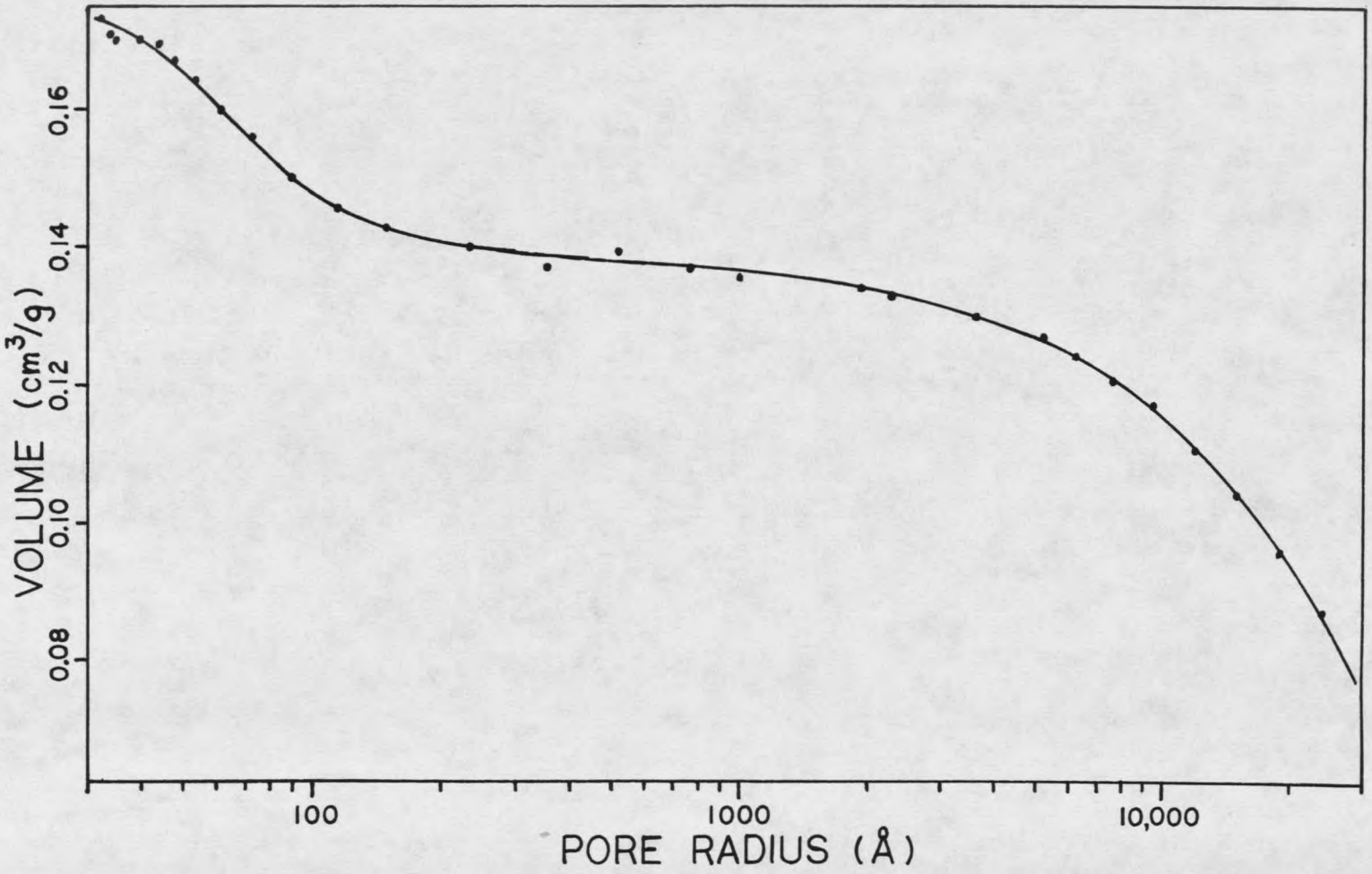

Figure 45. Mercury penetration volume vs. pore radius for sample A-100.

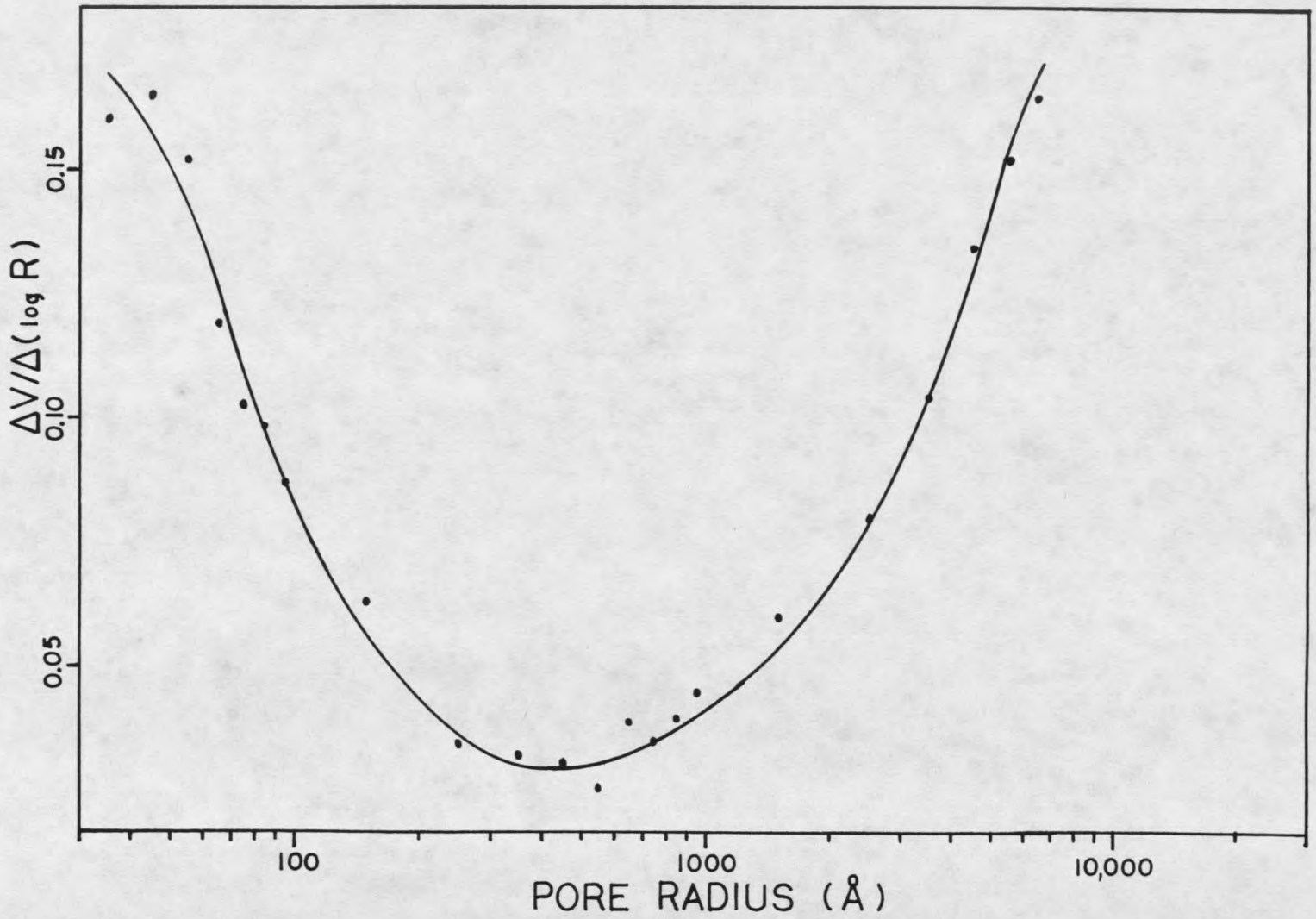

Figure 46. Pore size distribution for sample A-0, calculated from the porosimetry data shown on Figure 36.

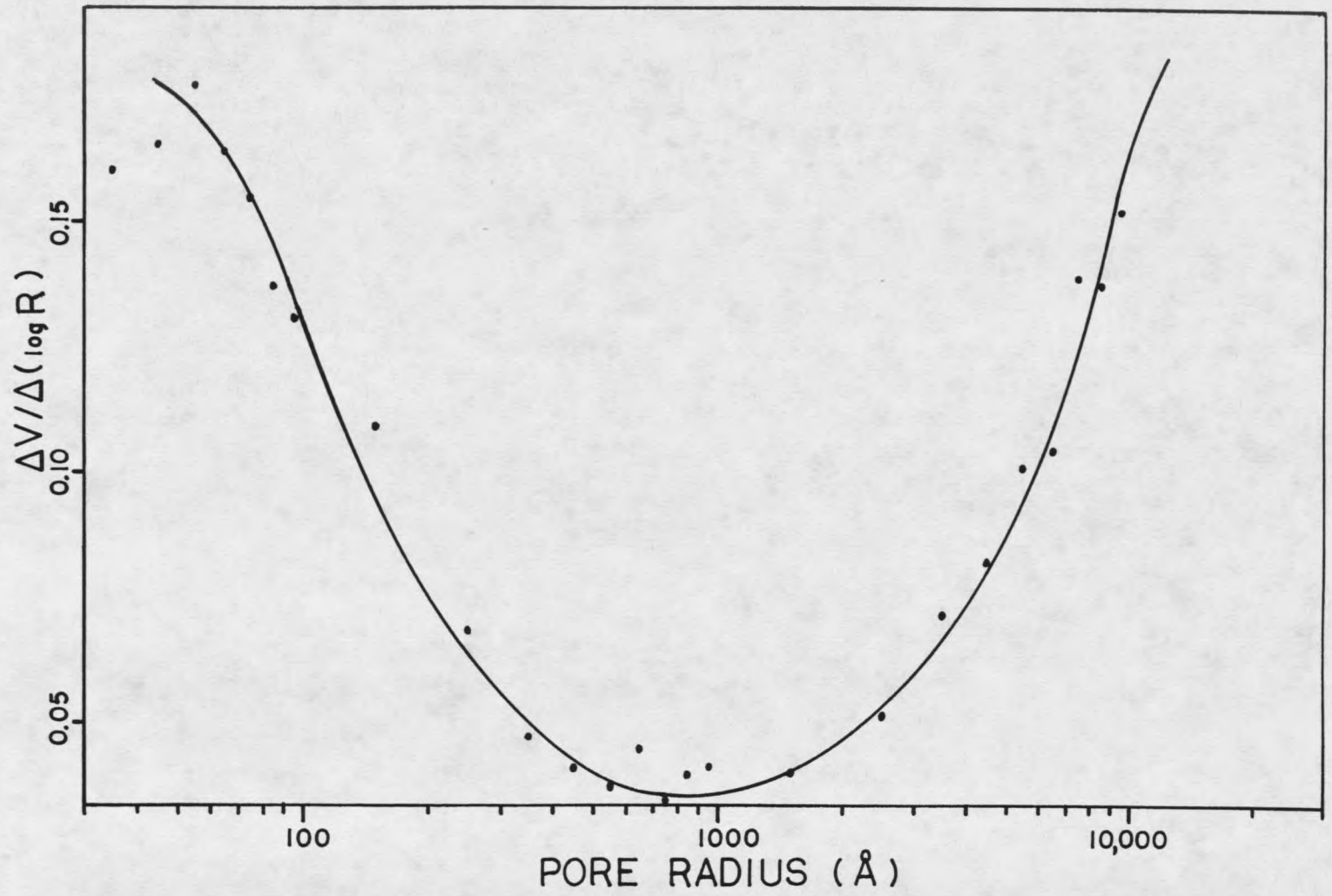

Figure 47. Pore size distribution for sample A-3, calculated from the porosimetry data shown on Figure 37.

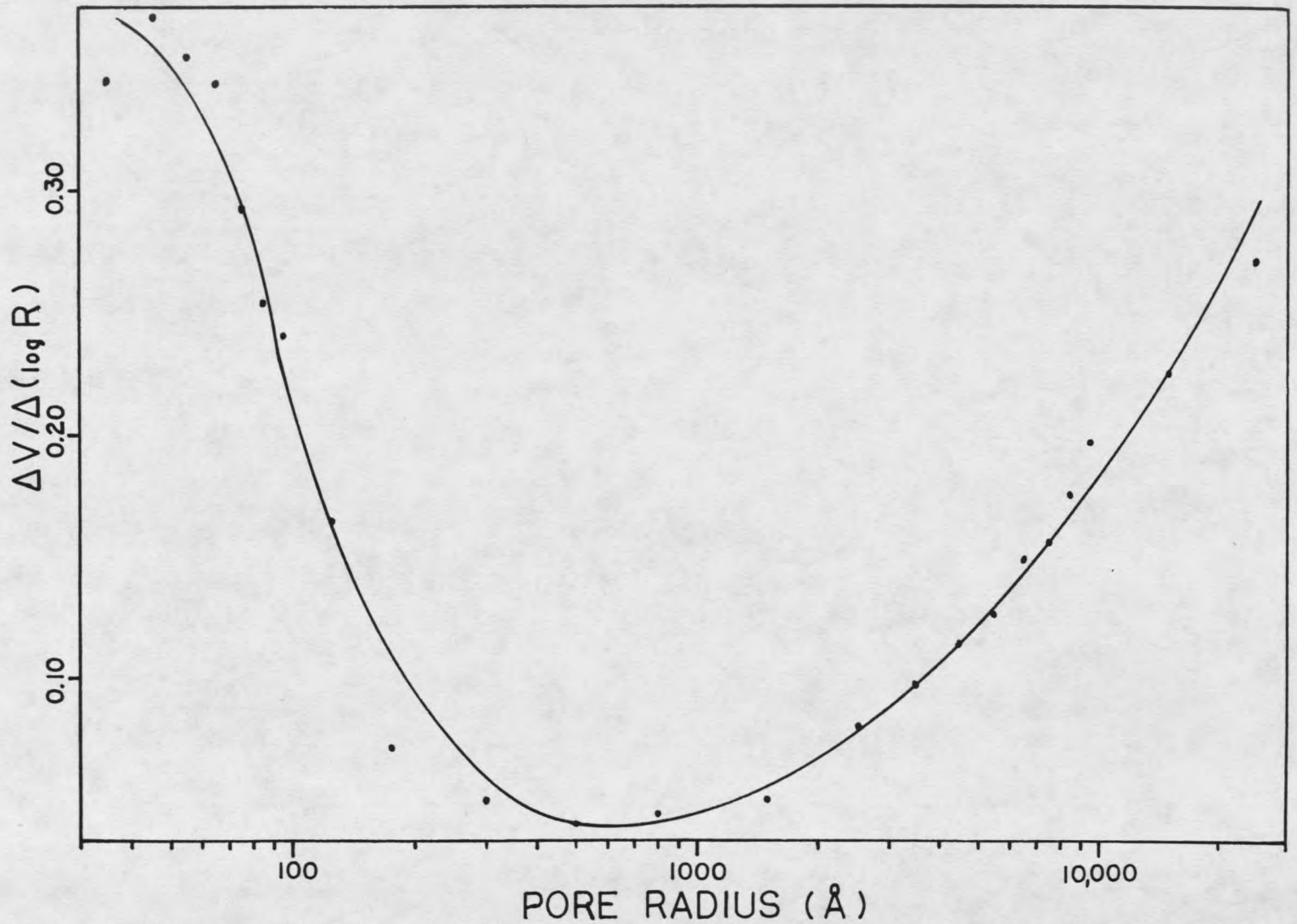

Figure 48. Pore size distribution for sample A-7, calculated from the porosimetry data shown on Figure 38.

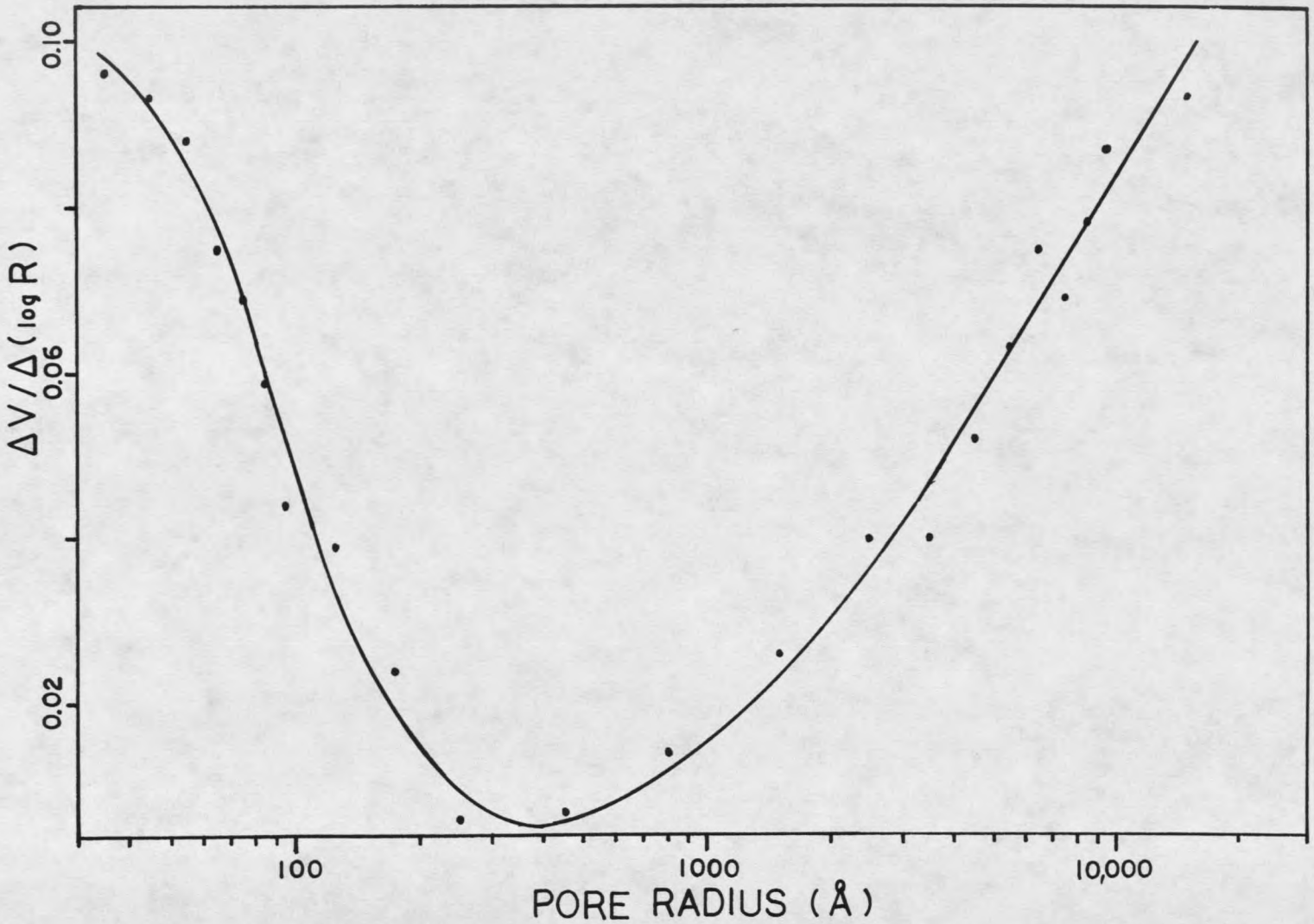

Figure 49. Pore size distribution for sample A-10, calculated from the porosimetry data shown on Figure 39.

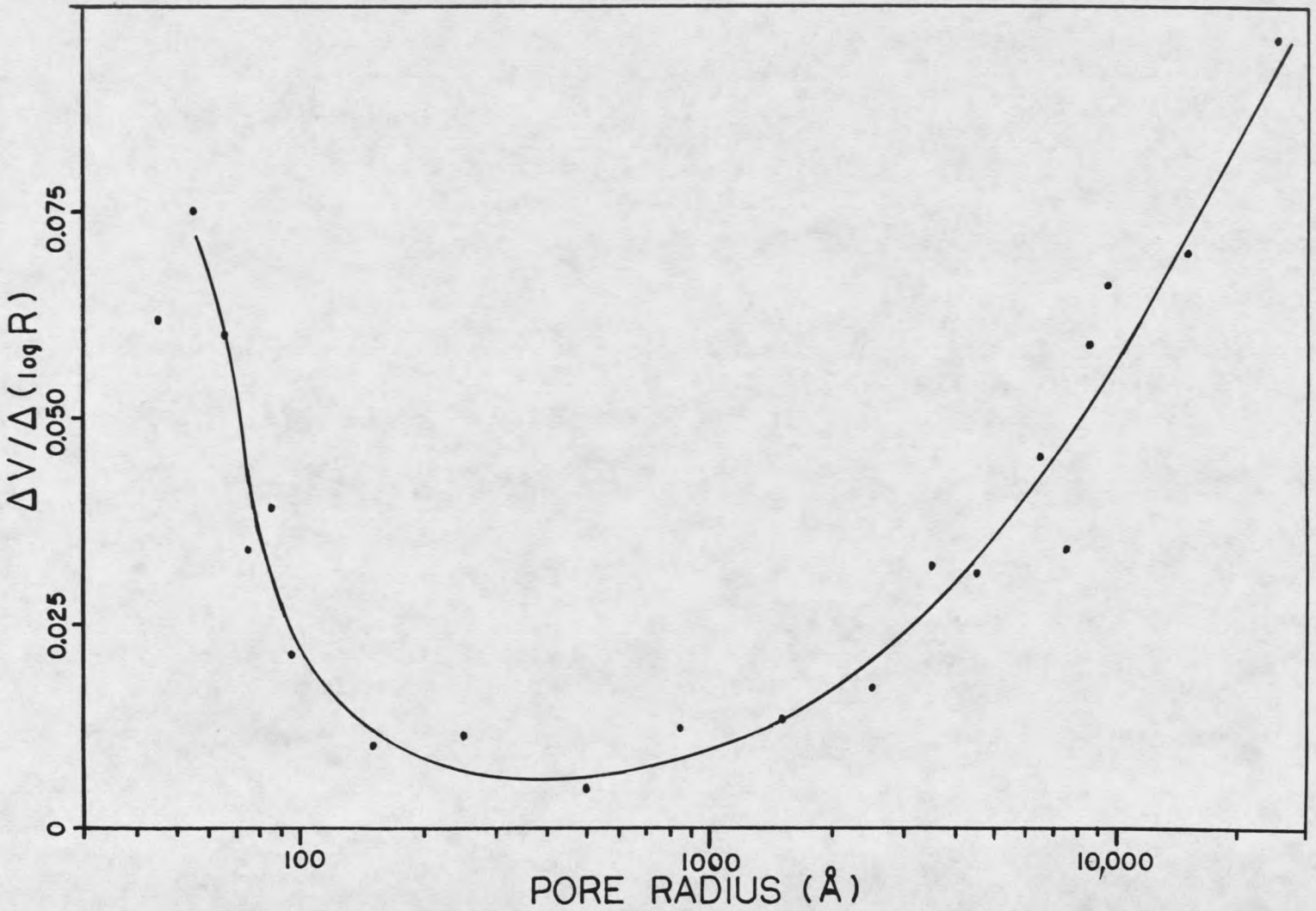

Figure 50. Pore size distribution for sample A-18, calculated from the porosimetry data shown on Figure 40.

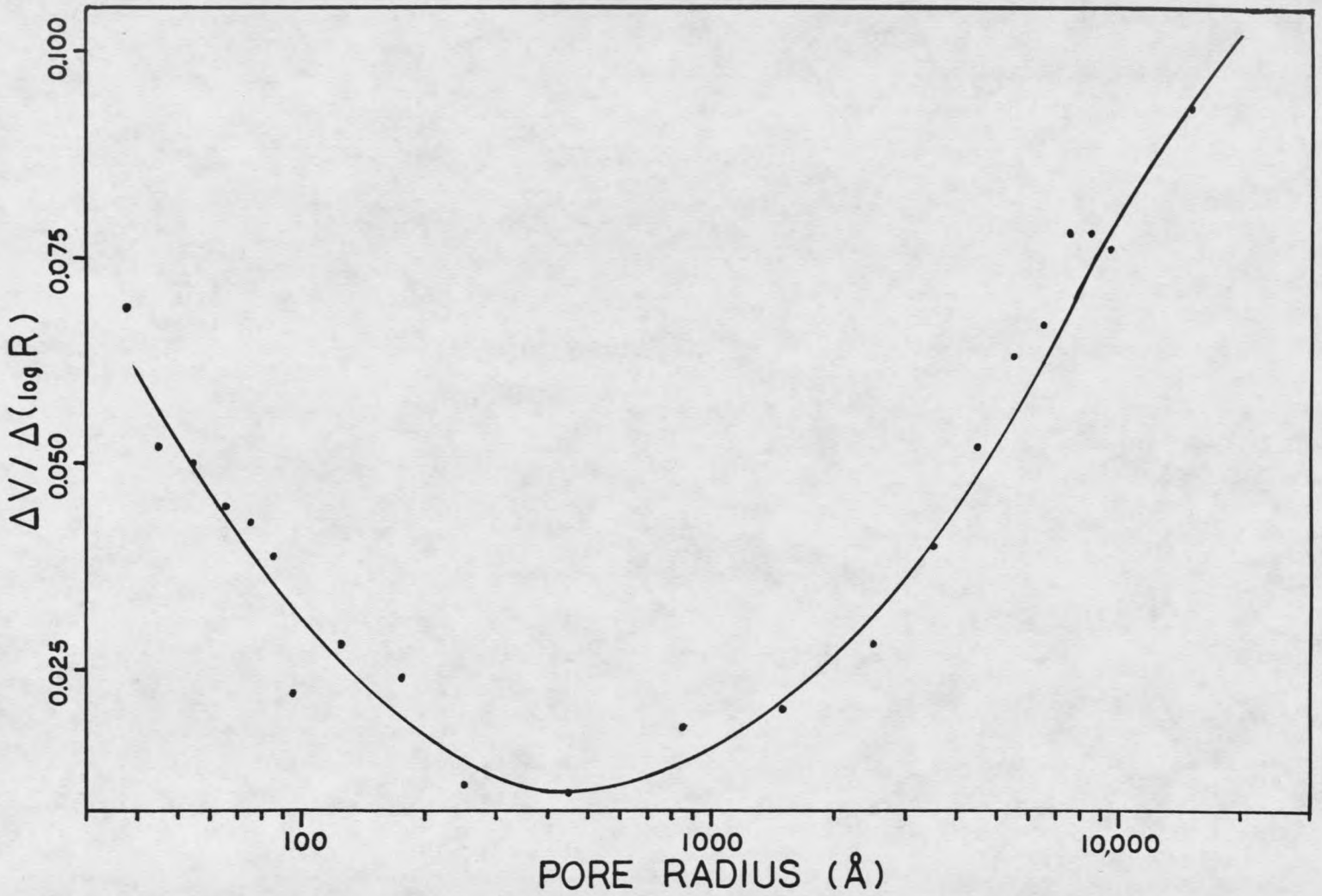

Figure 51. Pore size distribution for sample A-26, calculated from the porosimetry data shown on Figure 41.

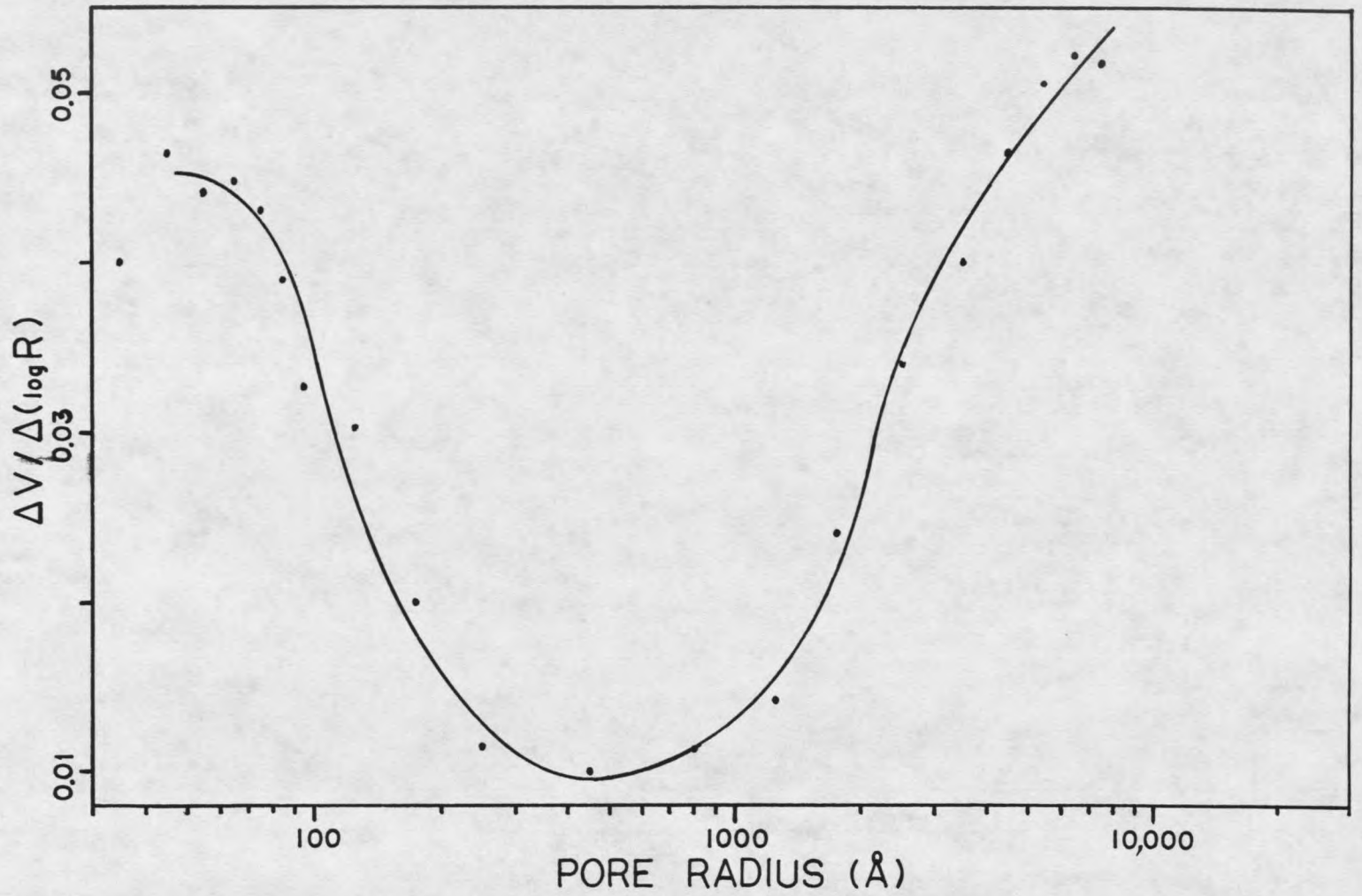

Figure 52. Pore size distribution for sample A-44, calculated from the porosimetry data shown on Figure 42.

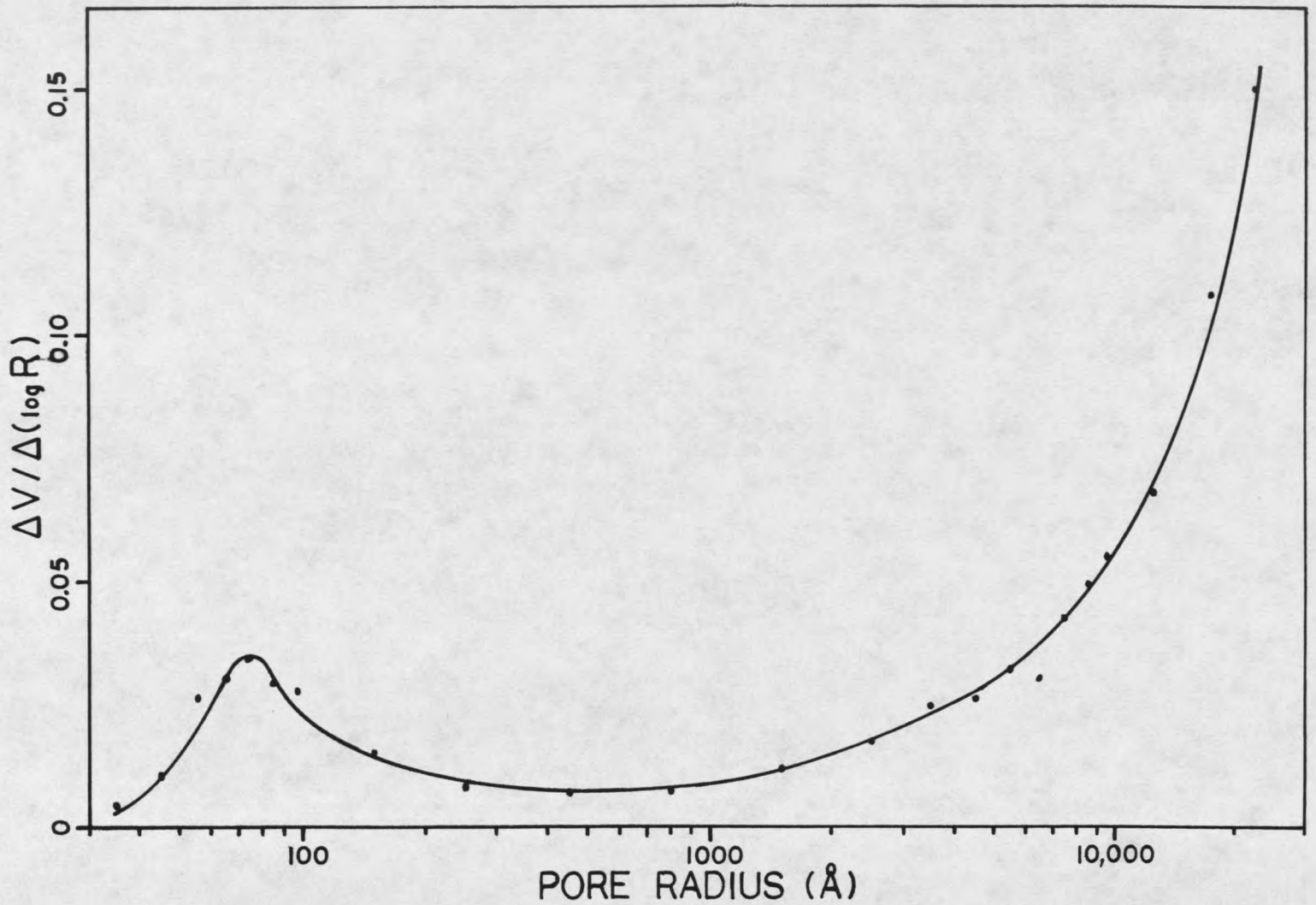

Figure 53. Pore size distribution for sample A-65, calculated from the porosimetry data shown on Figure 43.

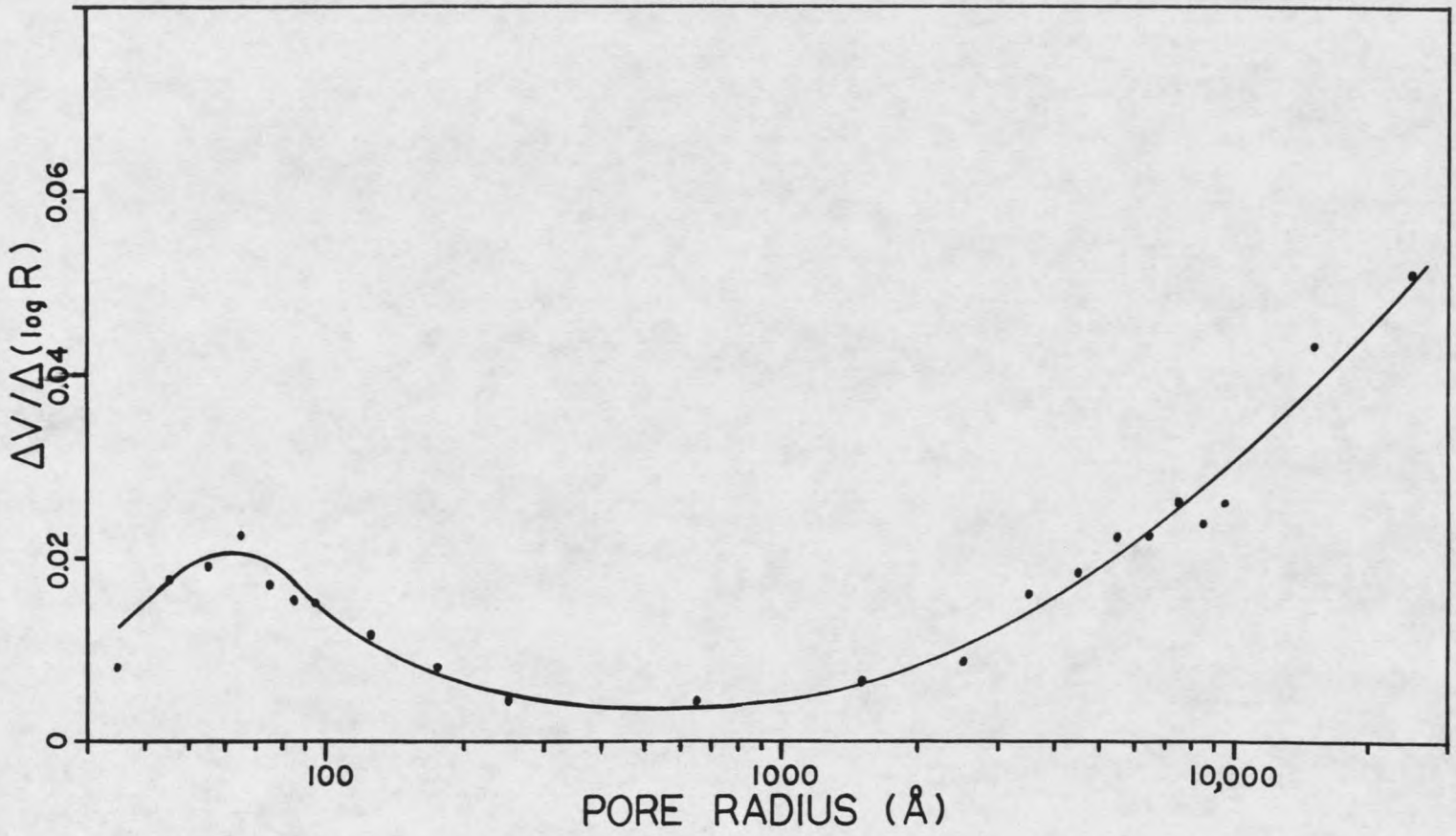

Figure 54. Pore size distribution for sample A-88, calculated from the porosimetry data shown on Figure 44.

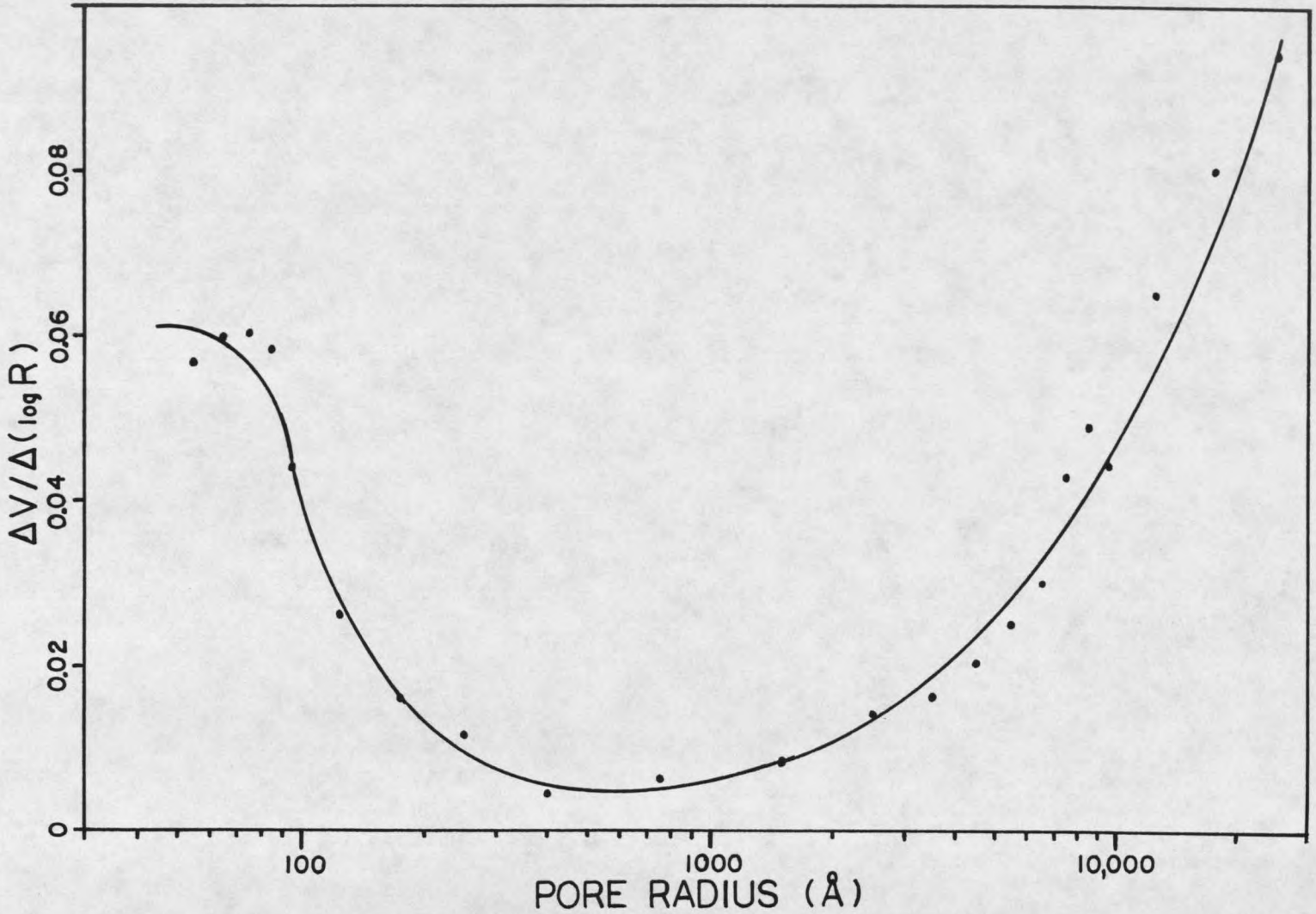

Figure 55. Pore size distribution for sample A-100, calculated from the porosimetry data shown on Figure 45.

Example Porosimetry Calculations Using the Data of Sample A-0

From geometric considerations using a spherical particle assumption, the radius of the particles is a function of surface area and particle density.

$$r_p = 3/S\rho \quad ; \; S = 513 \; m^2/g, \; \rho = 2.23 \; g/cm^3$$

$$r_p = 26.6 \; A$$

Using the parallel-pore model, the average pore radius can be calculated from the total pore volume and surface area.

$$R = 2V_p/S = 17.5 \; A$$

To calculate surface area from mercury penetration data, we use the expression from Lowell & Shields [49].

$$S = 2\int dV/r \quad ; \text{ evaluated from } V_3 \text{ to } V_1 = 2I$$

The integral will be determined using Simpson's Rule.

$V_1 = 0.449\ cm^3/g,\ 1/r_1 = 0.0308$

$V_3 = 0.350\ cm^3/g,\ 1/r_3 = 0.0021$

$V_2 = (0.449 - 0.350)/2 + 0.350 = 0.400$ and $1/r_2 = 0.0156$

$I = (.449 - 0.35)(.0308 + 4(.0156) + .0021)/6 = 15.7\ m^2/g$

$S = 2I = 31.4\ m^2/g$; this value is far short of the 513 m^2/g measured by the BET method.

Table 8. Pore volume distribution calculations for sample A-0

Radius (Å)	ΔR (Å)	Δ(log R)	ΔV (cm^3/g)	ΔV/Δ(log R)
35,000	10,000	0.12494	0.023	0.184
25,000	10,000	0.17609	0.035	0.199
15,000	10,000	0.30103	0.058	0.193
9,500	1,000	0.04576	0.009	0.197
8,500	1,000	0.05115	0.010	0.196
7,500	1,000	0.05799	0.012	0.207
6,500	1,000	0.06695	0.011	0.164
5,500	1,000	0.07918	0.012	0.152
4,500	1,000	0.09691	0.013	0.134
3,500	1,000	0.12494	0.013	0.104
2,500	1,000	0.17609	0.014	0.080
1,500	1,000	0.30103	0.018	0.060
950	100	0.04576	0.002	0.044
850	100	0.05115	0.002	0.039
750	100	0.05799	0.002	0.034
650	100	0.06695	0.0025	0.038
550	100	0.07918	0.002	0.025
450	100	0.09691	0.003	0.031
350	100	0.12494	0.004	0.032
250	100	0.17609	0.006	0.034
150	100	0.30103	0.019	0.063
95	10	0.04576	0.004	0.087
85	10	0.05115	0.005	0.098
75	10	0.05799	0.006	0.103
65	10	0.06695	0.008	0.119
55	10	0.07918	0.012	0.152
45	10	0.09691	0.016	0.165

Table 9. Mercury porosimetry results

Sample	Surface Area by BET (m^2/g)	Surface Area by Hg (m^2/g)	ρ (g/cm^3)	r_p (Å)	R (Å)
A-0	513	31	2.23	27	18
A-3	426	36	2.26	31	19
A-7	338	34	2.23	40	32
A-10	285	17	2.37	44	13
A-18	138	10	2.36	92	24
A-26	174	10	2.39	72	27
A-44	198	10	2.55	59	20
A-65	7	5	2.23	1900	610
A-88	68	4	2.44	180	30
A-100	202	10	3.13	47	17

APPENDIX E

Calculation of TEA Diffusivity

I would like to calculate the pellet diffusivity knowing the time required for equilibrium after a TEA injection. Assume that the pellet is essentially spherical. The absorbed phase is sufficiently large to require inclusion in the mass balance equation. Assume that the diffusivity is a constant and that adsorption equilibrium is instantaneous. Thus,

$$-\frac{1}{r^2}\frac{\partial\left(r^2 N_{Ar}\right)}{\partial r} = \varepsilon_s \frac{\partial C_A}{\partial t} + \rho_s \frac{\partial C_A}{\partial t}$$

$$N_{Ar} = -D_e \frac{\partial C_A}{\partial r}$$

$$\frac{1}{r^2}\frac{\partial\left(r^2 D_e \frac{\partial C_A}{\partial r}\right)}{\partial r} = \left(\varepsilon_s + \rho_s \frac{\partial C_{A1}}{\partial C_A}\right)\frac{\partial C_A}{\partial t}$$

IC) $C_A(r,0) = P_o/RT = C_o$ initial pressure

BC 1) $C_A(R,t) = P_1/RT = C_1$ final pressure

BC 2) $\frac{\partial C_A}{\partial r}(0,t) = 0$

$$\hat{\theta} = \frac{C_{A1}}{C_T} = K_A C_A \longrightarrow C_{A1} = C_T K_A C_A$$

$$\frac{\partial C_{A1}}{\partial C_A} = C_T K_A$$

$$\frac{1}{r^2}\frac{\partial(r^2\,\partial C_A/\partial r)}{\partial r} = \left(\frac{\varepsilon_s + \rho_s C_T K_A}{D_e}\right)\frac{\partial C_A}{\partial t} \qquad D = \left[\frac{D_e}{\varepsilon_s + \rho_s C_T K_A}\right]$$

$$\frac{D}{r^2}\frac{\partial}{\partial r}\left(r^2 \frac{\partial C_A}{\partial r}\right) = \frac{\partial C_A}{\partial t}$$

Dimensionless variables

$$\eta = \frac{r}{R}\ ,\ \phi = \frac{C-C_o}{C_1-C_o},\quad \tau = \frac{Dt}{R^2}$$

$$\frac{1}{\eta^2}\ \frac{\partial}{\partial \eta}\ \eta^2\ \frac{\partial \phi}{\partial \eta} = \frac{\partial \phi}{\partial \tau}$$

IC) $\phi\ (\eta, 0) = 0$

BC 1) $\phi\ (1, \tau) = 1$

BC 2) $\frac{\partial \phi}{\partial \eta}\ (0, \tau) = 0$

Transform

$$\theta = \eta\phi$$

$$\frac{\partial^2 \theta}{\partial \eta^2} = \frac{\partial \theta}{\partial \tau}$$

IC) $\theta\ (\eta, 0) = 0$

BC 1) $\theta\ (1, \tau) = 1$

BC 2) $\theta\ (0, \tau) = 0$

Laplace Transform

$$\frac{d^2\bar{\theta}}{d\eta^2} = S\bar{\theta}$$

BC 1) $\bar{\theta}\ (1) = \frac{1}{S}$

BC 2) $\bar{\theta}\ (0) = 0$

$$\bar{\theta} = C_1 \sinh\ (\sqrt{s}\,\eta) + C_2 \cosh\ (\sqrt{s}\,\eta)$$

BC 2)

$$\bar{\theta}(0) = 0 = C_1 \sinh\ (0) + C_2 \cosh\ (0)$$

$$0 = 0 + C_2$$

$$\therefore\ C_2 = 0$$

$$\bar{\theta} = C_1 \sinh\ (\sqrt{s}\,\eta)$$

BC 1)

$$\bar{\theta}\ (1) = \frac{1}{S} = C_1 \sinh\ (\sqrt{s})$$

$$\therefore\ C_1 = 1/s \cdot \sinh\ (\sqrt{s})$$

$$\bar{\theta} = \sinh\ (\sqrt{s}\,\eta)\ /\ s \cdot \sinh(\sqrt{s})$$

Back Transform

$$\theta = \eta + \frac{2}{\pi} \sum_{N=1}^{\infty} \frac{(-1)^N}{N} e^{-N^2\pi^2\tau} \sin(N\pi\eta) = \eta\,\phi$$

$$\phi = 1 + \frac{2}{\eta\pi} \sum_{N=1}^{\infty} \frac{(-1)^N}{N} e^{-N^2\pi^2\tau} \sin(N\pi\eta)$$

$$\frac{C - C_o}{C_1 - C_o} = 1 + \frac{2R}{\pi r} \sum_{N=1}^{\infty} \frac{(-1)^N}{N} e^{-N^2\pi^2\, Dt/R^2} \sin\left(\frac{N\pi r}{R}\right)$$

in the limit as $r \to 0$

$$\frac{C - C_o}{C_1 - C_o} = 1 + 2 \sum_{N=1}^{\infty} (-1)^N e^{-N^2\pi^2 Dt/R^2}$$

and

$$\frac{M_t}{M_\infty} = 1 - \frac{6}{\pi^2} \sum_{N=1}^{\infty} \frac{1}{N^2} e^{-N^2\pi^2 Dt/R^2}$$

For our purpose, let $\frac{M_t}{M_\infty} = 0.9$ (90% approach to equilibrium)

and R = 0.2 cm

$$0.1645 = \left[e^{-247\ Dt} + \frac{1}{4} e^{-987\ Dt} + \frac{1}{9} e^{-2221\ Dt} + \ldots \right]$$

Only the first term is significant

$$0.1645 = e^{-247Dt}$$

$$\ln(0.1645) = -247\ Dt$$

$$0.00731\ cm^2 = Dt = \left[D_e/\varepsilon_s + \rho_s C_T K_A \right] t$$

$$D_e = 0.0073\ cm^2(\varepsilon_s + \rho_s C_T K_A)/t\ sec$$

We need some values to substitute.

For sample A-18

$\rho_{pellet} = 1.038\ g/cm^3$; $\rho_s = 2.36\ g/cm^3$

$$\varepsilon_s = 1 - \frac{\rho_p}{\rho_s} = \underline{0.56}$$

$$C_T = \frac{138\ m^2/g\ \ (10^{20}\ \mathring{A}^2/m^2)}{43\ \mathring{A}^2/\text{TEA molecule}\ (6.023 \times 10^{23}\ \text{molecules/mole})}$$

$\underline{C_T = 5.33 \times 10^{-4}\ \text{moles/g}}$; assuming the entire surface is available.

$$K_A = C_A\ \hat{\theta} = \frac{RT\hat{\theta}}{P_A} = 62365.6\ \frac{\text{mmHg} \cdot \text{cm}^3}{\text{mol K}}\ (568\text{K})\ \frac{\hat{\theta}}{P_A\ \text{mm Hg}}$$

$$\hat{\theta} = \frac{(V_A\ \text{cm}^3/\text{g})\ (6.023 \times 10^{23}\ \text{molecules/mole})(43\ \mathring{A}^2/\text{molecule})}{(22414\ \text{cm}^3/\text{mole})\ \ (10^{20}\ \mathring{A}^2/\text{m}^2)\ (138\ \text{m}^2/\text{g})}$$

$$\hat{\theta} = 0.0837\ V_A$$

$$K_A = \frac{62365.6\ (568)\ (0.0837)\ V_A}{P_A} = 2.97 \times 10^6\ \frac{V_A}{P_A}$$

@ $P_A = 0.443$ mm Hg, $V_A = 2.11\ \text{cm}^3/\text{g}$

$$K_A = \frac{62365.6\ \frac{\text{mm Hg-cm}^3}{\text{mol K}}\ (568\ \text{K})\ (.0837)(2.11)}{(0.443\ \text{mm Hg})}$$

$\underline{K_A = 1.41 \times 10^7\ \text{cm}^3/\text{mol}}$

Substitute

$$D_e = 0.00731 \text{ cm}^2 \left[0.56 + 1.77 \times 10^4\right] / \text{ t sec}$$

$$D_e = 130 \text{ cm}^2/\text{t sec}$$

If 90% of equilibrium requires 20 hours

t = 72,000 sec

$D_e = 130 \text{ cm}^2/72{,}000 \text{ sec} = 1.8 \times 10^{-3} \text{ cm}^2/\text{s}$

If 90% of equilibrium requires 10 hours

$D_e = 130 \text{ cm}^2/36{,}000 \text{ sec} = 3.6 \times 10^{-3} \text{ cm}^2/\text{s}$

Assuming random pore model

$$D_e = \varepsilon_s^2 D \qquad D = \frac{D_e}{\varepsilon^2} = \frac{3.6 \times 10^{-3} \text{cm}^2/\text{s}}{(0.56)^2} = \frac{1.1 \times 10^{-2} \text{ cm}^2/\text{s}}{}$$

Diffusivity is in the Knudsen regime, as expected for a material with pores of less than 100 Å radius.

APPENDIX F

Data for TEA Adsorption Isotherms

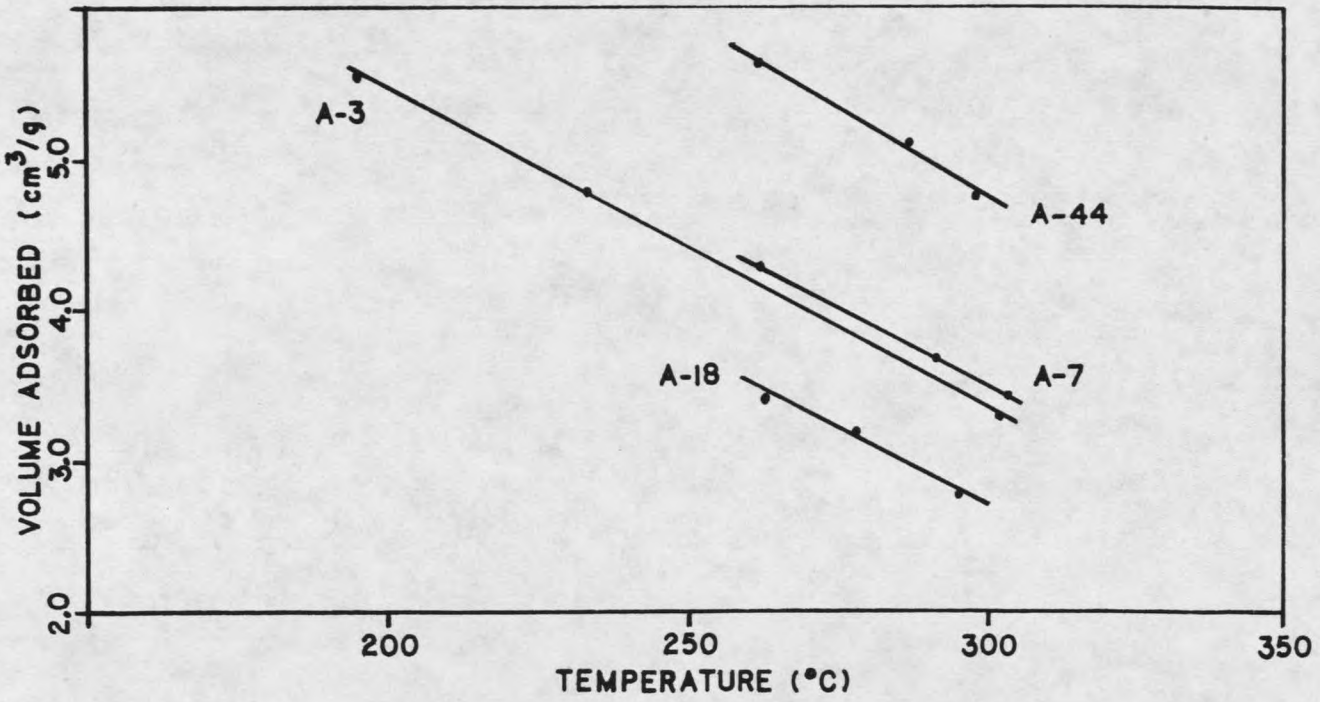

Figure 56. TEA adsorption isobars measured for samples A-3, A-7, A-18, and A-44.

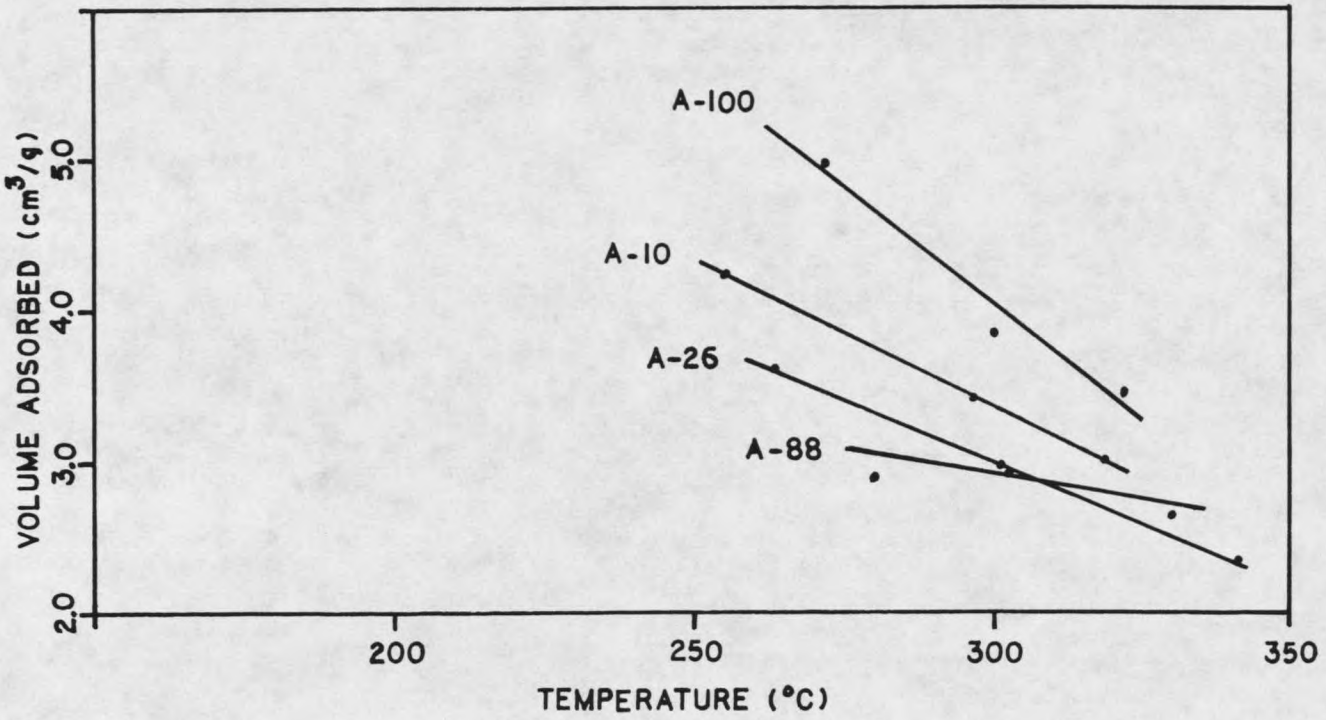

Figure 57. TEA adsorption isobars measured for samples A-10, A-26, A-88, and A-100.

Table 10. Blank experimental TEA adsorption data.

Data	Δm (mg)	T (°C)	V_{ads} (cm^3 @ STP/g)	Σm_i (mg)	P (μm Hg)
1	0.009	15	-	-	p
2	-.018	160	-	-	p
3	-.002	295	-	-	p
4	0	305	-	-	∿.01
5	0.013	305	0.029	0.548	19.6
6	0.007	305	0.016	1.097	39.9
7	0.003	-	0.007	1.645	60.1
8	-.002	-	-.004	2.194	80.4
9	-.004	-	-.009	3.290	121.
10	-.008	304	-.018	4.387	161.
11	-.008	304	-.018	5.484	201.
12	-.004	-	-.009	9.229	338.

p - pumping

Table 11. TEA adsorption data for sample A-0 at ~300°C.

Data	Δm (mg)	T (°C)	V_{ads} (cm^3 @ STP/g)	Σm_i (mg)	P (μm Hg)
1	0	301	-	-	∿.01
2	0.015	302	0.034	0.607	21.8
3	0.011	300	0.025	1.822	66.8
4	-.002	301	-.004	3.643	134.4
5	-.003	302	-.007	6.679	246.
6	0.000	301	0.000	9.716	358.
7	0.018	300	0.040	13.86	510.
8	0.025	302	0.056	18.01	663.

W = 0.0984 g

T = 301 °C = 574 K

Table 12. TEA adsorption data for sample A-3 at ~200°C.

Data	Δm (mg)	T (°C)	V_{ads} (cm^3 @ STP/g)	Σm_i (mg)	P (μm Hg)
1	0	187	-	-	∿.01
2	0.410	196	2.18	1.021	22.6
3	0.446	197	2.39	2.042	59.0
4	0.474	-	2.54	3.063	95.8
5	0.497	199	2.71	4.084	133.
6	0.522	199	2.84	5.105	170.
7	0.565	198	3.05	7.147	244.
8	0.660	198	3.56	9.189	316.
9	0.689	200	3.76	11.23	390.
10	0.743	201	4.07	13.27	464.
11	0.856	199	4.63	15.32	535.
12	0.902	201	4.92	17.36	609.
13	1.036	195	5.51	19.40	680.

W = 0.0413 g

T = 197 °C = 470 K

Table 13. TEA adsorption data for sample A-3 at ~300°C.

Data	Δm (mg)	T (°C)	V_{ads} (cm^3 @ STP/g)	Σm_i (mg)	P (μm Hg)
1	0	303	-	-	∿.01
2	0.395	303	1.18	0.866	18.0
3	0.500	-	1.49	1.772	46.6
4	0.569	303	1.69	2.658	76.5
5	0.614	304	1.84	3.544	107.3
6	0.643	301	1.87	4.431	139.
7	0.719	302	2.11	6.203	201.
8	0.780	303	2.31	7.975	264.
9	0.828	304	2.48	9.747	327.
10	0.881	303	2.61	11.52	390.
11	1.008	303	2.98	15.06	515.
12	1.062	304	3.16	18.61	643.
13	1.118	305	3.35	20.38	706.
14	1.392	301	4.07	23.04	793.

W = 0.0754 g

T = 302 °C = 575 K

Table 14. TEA adsorption data for sample A-7 at ~300°C.

Data	Δm (mg)	T (°C)	V_{ads} (cm^3 @ STP/g)	Σm_i (mg)	P (μm Hg)
1	0	300	-	-	∿.01
2	0.344	300	1.65	0.573	8.4
3	0.375	300	1.80	1.147	28.4
4	0.397	301	1.93	1.720	48.6
5	0.421	300	2.02	2.294	68.8
6	0.440	300	2.11	2.867	89.2
7	0.463	300	2.22	3.440	109.4
8	0.479	302	2.35	4.014	130.
9	0.514	302	2.51	5.161	171.
10	0.545	303	2.68	6.308	212.
11	0.572	303	2.81	7.455	253.
12	0.630	298	2.98	8.601	293.
13	0.635	303	3.11	9.748	335.
14	0.663	303	3.25	11.47	397.
15	0.712	303	3.48	13.19	459.

W = 0.0461 g

T = 300 °C = 573 K

Table 15. TEA adsorption data for sample A-10 at ~300°C.

Data	Δm (mg)	T (°C)	V_{ads} (cm^3 @ STP/g)	Σm_i (mg)	P (μm Hg)
1	0	298	-	-	∿.01
2	0.447	296	1.81	0.665	8.1
3	0.492	298	2.04	1.330	31.1
4	0.516	298	2.14	1.996	54.9
5	0.534	299	2.21	2.661	79.0
6	0.564	299	2.34	3.326	102.5
7	0.574	299	2.38	3.992	127.
8	0.599	298	2.48	5.322	175.
9	0.634	298	2.62	6.653	223.
10	0.657	298	2.72	7.983	272.
11	0.699	297	2.89	9.979	344.
12	0.738	297	3.06	11.97	417.
13	0.752	298	3.11	13.97	491.
14	0.781	297	3.21	15.97	564.
15	0.827	297	3.40	19.29	685.

W = 0.0535 g

T = 298 °C = 571 K

Table 16. TEA adsorption data for sample A-18 at ~300°C.

Data	Δm (mg)	T (°C)	V_{ads} (cm^3 @ STP/g)	Σm_i (mg)	P (μm Hg)
1	0	294	-	-	∿.01
2	0.198	295	0.76	0.778	26.6
3	0.239	296	0.94	1.556	49.0
4	0.274	296	1.08	2.334	76.7
5	0.302	298	1.22	3.112	104.7
6	0.333	295	1.28	3.890	132.
7	0.359	294	1.36	4.668	160.
8	0.381	294	1.45	5.446	189.
9	0.396	295	1.53	6.224	217.
10	0.412	295	1.59	7.002	245.
11	0.471	293	1.78	8.558	301.
12	0.490	294	1.87	10.11	358.
13	0.498	294	1.90	10.89	387.
14	0.547	295	2.11	12.45	443.
15	0.558	297	2.19	14.00	501.
16	0.612	294	2.35	15.56	557.
17	0.623	294	2.38	16.34	585.
18	0.667	294	2.55	17.12	613.
19	0.721	295	2.78	19.45	698.

W = 0.0574 g

T = 295 °C = 568 K

Table 17. Duplicate TEA adsorption data for sample A-18 @ ~300°C

Data	Δm (mg)	T (°C)	V_{ads} (cm^3 @ STP/g)	Σm_i (mg)	P (μm Hg)
1	0	302	-	-	∿.01
2	0.288	304	0.59	0.548	9.5
3	0.453	300	0.93	1.096	23.6
4	0.491	302	1.00	2.192	62.3

W = 0.1083 g

T = 302 °C = 575 K

Table 18. TEA adsorption data for sample A-26 at ~300°C.

Data	Δm (mg)	T (°C)	V_{ads} (cm^3 @ STP/g)	Σm_i (mg)	P (μm Hg)
1	0	302	-	-	∿.01
2	0.316	303	1.13	0.548	8.5
3	0.423	302	1.50	1.097	24.7
4	0.466	302	1.65	1.645	43.2
5	0.492	303	1.76	2.194	62.3
6	0.516	302	1.82	2.742	81.5
7	0.537	303	1.92	3.839	121.
8	0.576	303	2.05	4.936	160.
9	0.601	303	2.14	6.032	199.
10	0.624	303	2.22	7.129	238.
11	0.650	303	2.32	8.774	298.
12	0.674	303	2.40	10.42	357.
13	0.696	303	2.48	12.06	416.
14	0.748	303	2.66	15.36	535.
15	0.839	302	2.97	19.10	669.

W = 0.0626 g

T = 302 °C = 575 K

Table 19. TEA adsorption data for sample A-44 at ~300°C.

Data	Δm (mg)	T (°C)	V_{ads} (cm^3 @ STP/g)	Σm_i (mg)	P (μm Hg)
1	0	299	-	-	∿.01
2	0.382	300	1.38	0.548	6.1
3	0.511	301	1.86	1.097	21.5
4	0.577	301	2.10	1.645	39.1
5	0.648	301	2.36	2.194	56.6
6	0.639	300	2.30	2.742	77.0
7	0.719	302	2.64	3.290	94.2
8	0.777	302	2.84	3.839	112.2
9	0.816	301	2.96	4.387	131.
10	0.840	299	3.00	4.936	150.
11	0.893	300	3.22	5.484	168.
12	0.927	300	3.34	6.032	187.
13	0.994	299	3.56	7.129	225.
14	1.060	298	3.77	8.226	262.
15	1.117	299	4.00	9.323	301.
16	1.224	299	4.38	10.97	357.
17	1.322	298	4.72	12.61	413.

W = 0.0615 g

T = 300 °C = 573 K

Table 20. TEA adsorption data for sample A-65 at ~300°C.

Data	Δm (mg)	T (°C)	V_{ads} (cm^3 @ STP/g)	Σm_i (mg)	P (μm Hg)
1	0.796	156	-	-	p
2	0	303	-	-	∿.01
3	-.097	303	-.16	0.607	26.0
6	-.107	303	-.17	1.822	71.1
7	-.133	302	-.22	5.969	225.

p - pumping
W = 0.1357 g
T = 303 °C = 576 K

Table 21. TEA adsorption data for sample A-88 at ~300°C.

Data	Δm (mg)	T (°C)	V_{ads} (cm^3 @ STP/g)	Σm_i (mg)	P (μm Hg)
1	1.737	20	-	-	p
2	0.737	141	-	-	p
3	0	299	-	-	∿.01
4	0.159	301	0.35	0.573	15.2
5	0.341	301	0.75	1.147	29.6
6	0.863	305	1.90	2.294	52.6
7	1.369	301	3.01	4.014	97.3
8	1.616	301	3.55	5.734	152.

p - pumping
W = 0.1008 g
T = 299 °C = 572 K

Table 22. TEA adsorption data for sample A-100 at ~300°C.

Data	Δm (mg)	T (°C)	V_{ads} (cm^3 @ STP/g)	Σm_i (mg)	P (μm Hg)
1	0	301	-	-	∿.01
2	0.278	302	0.918	0.548	9.9
3	0.392	302	1.28	1.097	25.8
4	0.550	302	1.79	2.194	60.2
5	0.699	298	2.15	3.291	94.9
6	0.837	300	2.64	4.936	150.
7	1.022	297	3.14	7.130	224.
8	1.211	300	3.83	9.872	317.

W = 0.0694 g

T = 301 °C = 574 K

APPENDIX G

CAEDMON Results of Adsorption Energy Distributions

Figure 58. CAEDMON results for sample A-3.

TEA ADSORPTION ON CATALYST A-3 AT 302C
NO. DATA POINTS = 8 NO. OF PATCHES = 6
ISOTHERM TEMP = 575.00 K
B = -0.2830000E+00
C = 0.1610000E+01

ENERGY OF ADSORPTION (Kcal/mol)	CAPACITY OF PATCH (cc/g)
0.6545090E+00	0.1397665E+01
0.1317113E+01	0.0000000E+00
0.1979717E+01	0.0000000E+00
0.2642320E+01	0.0000000E+00
0.3304924E+01	0.0000000E+00
0.3967528E+01	0.2721749E+01

THE SUM OF THE CAPACITIES, VM, = 0.4119414E+01

PRESSURE	AMT ADS/GRAM	CALCULATED AMT ADS/GRAM
0.1800000E-01	0.1180000E+01	0.1104206E+01
0.4660000E-01	0.1490000E+01	0.1519166E+01
0.7650000E-01	0.1690000E+01	0.1723482E+01
0.1073000E+00	0.1840000E+01	0.1869048E+01
0.1390000E+00	0.1870000E+01	0.1983474E+01
0.2010000E+00	0.2110000E+01	0.2144381E+01
0.2640000E+00	0.2310000E+01	0.2256055E+01
0.3270000E+00	0.2480000E+01	0.2337361E+01

THE PRECEDING SOLUTION IS UNIQUE

Figure 59. CAEDMON results for sample A-7.

TEA ADSORPTION ON CATALYST A-7 AT 300C
NO. DATA POINTS = 11 NO. OF PATCHES = 6
ISOTHERM TEMP = 573.00 K
B = -0.2890000E+00
C = 0.1610000E+01

ENERGY OF ADSORPTION (Kcal/mol)	CAPACITY OF PATCH (cc/g)
0.7710204E+00	0.1221219E+01
0.1579874E+01	0.0000000E+00
0.2388728E+01	0.0000000E+00
0.3197582E+01	0.0000000E+00
0.4006436E+01	0.0000000E+00
0.4815290E+01	0.3257299E+01

THE SUM OF THE CAPACITIES, VM, = 0.4478518E+01

PRESSURE	AMT ADS/GRAM	CALCULATED AMT ADS/GRAM
0.8400000E-02	0.1650000E+01	0.1287202E+01
0.2840000E-01	0.1800000E+01	0.1833243E+01
0.4860000E-01	0.1930000E+01	0.2032754E+01
0.6880000E-01	0.2020000E+01	0.2163218E+01
0.8920000E-01	0.2110000E+01	0.2264333E+01
0.1094000E+00	0.2220000E+01	0.2345969E+01
0.1300000E+00	0.2350000E+01	0.2415626E+01
0.1710000E+00	0.2510000E+01	0.2524945E+01
0.2120000E+00	0.2680000E+01	0.2607155E+01
0.2530000E+00	0.2810000E+01	0.2671357E+01
0.2930000E+00	0.2980000E+01	0.2721984E+01

THE PRECEDING SOLUTION IS UNIQUE

Figure 60. CAEDMON results for sample A-10.

TEA ADSORPTION ON CATALYST A-10 AT 298C
NO. DATA POINTS = 9 NO. OF PATCHES = 6
ISOTHERM TEMP = 571.00 K
B = -0.2980000E+00
C = 0.1620000E+01

ENERGY OF ADSORPTION (Kcal/mol)	CAPACITY OF PATCH (cc/g)
0.8408580E+00	0.0000000E+00
0.1638265E+01	0.0000000E+00
0.2435672E+01	0.0000000E+00
0.3233078E+01	0.0000000E+00
0.4030485E+01	0.0000000E+00
0.4827892E+01	0.3779433E+01

THE SUM OF THE CAPACITIES, VM, = 0.3779433E+01

PRESSURE	AMT ADS/GRAM	CALCULATED AMT ADS/GRAM
0.8100000E-02	0.1810000E+01	0.1466407E+01
0.3110000E-01	0.2040000E+01	0.2088553E+01
0.5490000E-01	0.2140000E+01	0.2261910E+01
0.7900000E-01	0.2230000E+01	0.2355117E+01
0.1025000E+00	0.2350000E+01	0.2414969E+01
0.1270000E+00	0.2400000E+01	0.2460529E+01
0.1750000E+00	0.2480000E+01	0.2523197E+01
0.2230000E+00	0.2620000E+01	0.2566723E+01
0.2720000E+00	0.2720000E+01	0.2600189E+01

THE PRECEDING SOLUTION IS UNIQUE

Figure 61. CAEDMON results for sample A-18.

TEA ADSORPTION ON CATALYST A-18 AT 295C
NO. DATA POINTS = 11 NO. OF PATCHES = 6
ISOTHERM TEMP = 568.00 K
B = -0.3090000E+00
C = 0.1630000E+01

ENERGY OF ADSORPTION (Kcal/mol)	CAPACITY OF PATCH (cc/g)
0.5125945E+00	0.1768363E+01
0.1099419E+01	0.0000000E+00
0.1686244E+01	0.0000000E+00
0.2273068E+01	0.0000000E+00
0.2859892E+01	0.0000000E+00
0.3446717E+01	0.1674496E+01

THE SUM OF THE CAPACITIES, VM, = 0.3442858E+01

PRESSURE	AMT ADS/GRAM	CALCULATED AMT ADS/GRAM
0.2660000E-01	0.7600000E+00	0.7237960E+00
0.4900000E-01	0.9400000E+00	0.9351271E+00
0.7670000E-01	0.1080000E+01	0.1099419E+01
0.1047000E+00	0.1220000E+01	0.1225651E+01
0.1320000E+00	0.1280000E+01	0.1326693E+01
0.1600000E+00	0.1360000E+01	0.1413611E+01
0.1890000E+00	0.1450000E+01	0.1489390E+01
0.2170000E+00	0.1530000E+01	0.1551463E+01
0.2450000E+00	0.1590000E+01	0.1604757E+01
0.3010000E+00	0.1780000E+01	0.1691371E+01
0.3580000E+00	0.1870000E+01	0.1759926E+01

THE PRECEDING SOLUTION IS UNIQUE

Figure 62. CAEDMON results for sample A-26.

TEA ADSORPTION ON CATALYST A-26 AT 302C
NO. DATA POINTS = 10 NO. OF PATCHES = 6
ISOTHERM TEMP = 575.00 K
B = -0.2830000E+00
C = 0.1610000E+01

ENERGY OF ADSORPTION (Kcal/mol)	CAPACITY OF PATCH (cc/g)
0.7606167E+00	0.8942096E+00
0.1573456E+01	0.0000000E+00
0.2386296E+01	0.0000000E+00
0.3199136E+01	0.0000000E+00
0.4011975E+01	0.0000000E+00
0.4824814E+01	0.2755796E+01

THE SUM OF THE CAPACITIES, VM, = 0.3650005E+01

PRESSURE	AMT ADS/GRAM	CALCULATED AMT ADS/GRAM
0.8500000E-02	0.1130000E+01	0.1087053E+01
0.2470000E-01	0.1500000E+01	0.1494655E+01
0.4320000E-01	0.1650000E+01	0.1666906E+01
0.6230000E-01	0.1760000E+01	0.1776651E+01
0.8150000E-01	0.1820000E+01	0.1858752E+01
0.1210000E+00	0.1920000E+01	0.1982811E+01
0.1600000E+00	0.2050000E+01	0.2070406E+01
0.1990000E+00	0.2140000E+01	0.2136459E+01
0.2380000E+00	0.2220000E+01	0.2188142E+01
0.2980000E+00	0.2320000E+01	0.2249227E+01

THE PRECEDING SOLUTION IS UNIQUE

Figure 63. CAEDMON results for sample A-44.

TEA ADSORPTION ON CATALYST A-44 AT 300C
NO. DATA POINTS = 14 NO. OF PATCHES = 6
ISOTHERM TEMP = 573.00 K
B = -0.2890000E+00
C = 0.1610000E+01

ENERGY OF ADSORPTION (Kcal/mol)	CAPACITY OF PATCH (cc/g)
0.7403491E+00	0.3959854E+01
0.1628195E+01	0.0000000E+00
0.2516041E+01	0.0000000E+00
0.3403888E+01	0.0000000E+00
0.4291734E+01	0.0000000E+00
0.5179580E+01	0.3077456E+01

THE SUM OF THE CAPACITIES, VM, = 0.7037310E+01

PRESSURE	AMT ADS/GRAM	CALCULATED AMT ADS/GRAM
0.6100000E-02	0.1380000E+01	0.1243468E+01
0.2150000E-01	0.1860000E+01	0.1844325E+01
0.3910000E-01	0.2100000E+01	0.2135724E+01
0.5660000E-01	0.2360000E+01	0.2351426E+01
0.7700000E-01	0.2300000E+01	0.2563669E+01
0.9420000E-01	0.2640000E+01	0.2720521E+01
0.1122000E+00	0.2840000E+01	0.2866588E+01
0.1310000E+00	0.2960000E+01	0.3001502E+01
0.1500000E+00	0.3000000E+01	0.3121571E+01
0.1680000E+00	0.3220000E+01	0.3222116E+01
0.1870000E+00	0.3340000E+01	0.3316224E+01
0.2250000E+00	0.3560000E+01	0.3474351E+01
0.2620000E+00	0.3770000E+01	0.3598705E+01
0.3010000E+00	0.4000000E+01	0.3706648E+01

THE PRECEDING SOLUTION IS UNIQUE

Figure 64. CAEDMON results for sample A-88.

TEA ADSORPTION ON CATALYST A-88 AT 299C
NO. DATA POINTS = 5 NO. OF PATCHES = 6
ISOTHERM TEMP = 572.00 K
B = -0.2940000E+00
C = 0.1620000E+01

ENERGY OF ADSORPTION (Kcal/mol)	CAPACITY OF PATCH (cc/g)
0.1507880E+01	0.7493650E+01
0.2031313E+01	0.0000000E+00
0.2554746E+01	0.0000000E+00
0.3078180E+01	0.0000000E+00
0.3601613E+01	0.0000000E+00
0.4125046E+01	0.0000000E+00

THE SUM OF THE CAPACITIES, VM, = 0.7493650E+01

PRESSURE	AMT ADS/GRAM	CALCULATED AMT ADS/GRAM
0.1520000E-01	0.3500000E+00	0.4403467E+00
0.2960000E-01	0.7500000E+00	0.8620010E+00
0.5260000E-01	0.1900000E+01	0.1478754E+01
0.9730000E-01	0.3010000E+01	0.2325282E+01
0.1520000E+00	0.3550000E+01	0.2908144E+01

THE PRECEDING SOLUTION IS UNIQUE

Figure 65. CAEDMON results for sample A-100.

TEA ADSORPTION ON CATALYST A-100 AT 301C
NO. DATA POINTS = 7 NO. OF PATCHES = 6
ISOTHERM TEMP = 574.00 K
B = -0.2860000E+00
C = 0.1610000E+01

ENERGY OF ADSORPTION (Kcal/mol)	CAPACITY OF PATCH (cc/g)
0.6856818E+00	0.5575531E+01
0.1476426E+01	0.0000000E+00
0.2267171E+01	0.0000000E+00
0.3057915E+01	0.0000000E+00
0.3848660E+01	0.0000000E+00
0.4639405E+01	0.2003161E+01

THE SUM OF THE CAPACITIES, VM, = 0.7578692E+01

PRESSURE	AMT ADS/GRAM	CALCULATED AMT ADS/GRAM
0.9900000E-02	0.9180000E+00	0.8808565E+00
0.2580000E-01	0.1286000E+01	0.1300209E+01
0.6020000E-01	0.1790000E+01	0.1813993E+01
0.9490000E-01	0.2150000E+01	0.2220295E+01
0.1500000E+00	0.2640000E+01	0.2722200E+01
0.2240000E+00	0.3140000E+01	0.3179166E+01
0.3170000E+00	0.3830000E+01	0.3543108E+01

THE PRECEDING SOLUTION IS UNIQUE

Figure 66. CAEDMON results for the ammonia adsorption data of Hsieh [26].

AMMONIA ADSORPTION ON HSIEH DATA AT 0C
NO. DATA POINTS = 27 NO. OF PATCHES = 15
ISOTHERM TEMP = 273.20 K
B = -0.2253000E+01
C = 0.3798000E+01

ENERGY OF ADSORPTION (Kcal/mol)	CAPACITY OF PATCH (cc/g)
-0.3556524E+01	0.2018525E+02
-0.3012684E+01	0.5395489E+01
-0.2468844E+01	0.7707394E+01
-0.1925004E+01	0.1270086E+01
-0.1381165E+01	0.1037106E+02
-0.8373247E+00	0.3987766E+01
-0.2934849E+00	0.6549043E+01
0.2503550E+00	0.3585176E+01
0.7941948E+00	0.0000000E+00
0.1338035E+01	0.0000000E+00
0.1881875E+01	0.0000000E+00
0.2425714E+01	0.0000000E+00
0.2969554E+01	0.0000000E+00
0.3513394E+01	0.7348640E+01
0.4057234E+01	0.7468419E+00

THE SUM OF THE CAPACITIES, VM, = 0.6714674E+02

Figure 66. - Continued

PRESSURE	AMT ADS/GRAM	CALCULATED AMT ADS/GRAM
0.7300000E-04	0.6800000E+00	0.6457576E+00
0.1180000E-03	0.9070000E+00	0.1176111E+01
0.1310000E-03	0.1814000E+01	0.1351318E+01
0.1560000E-03	0.2384000E+01	0.1715910E+01
0.3040000E-03	0.3407000E+01	0.3186216E+01
0.3370000E-03	0.3634000E+01	0.3350500E+01
0.5510000E-03	0.4314000E+01	0.3969456E+01
0.9320000E-03	0.4995000E+01	0.4444802E+01
0.1220000E-02	0.3634000E+01	0.4643231E+01
0.1260000E-02	0.5675000E+01	0.4665476E+01
0.1620000E-02	0.5454000E+01	0.4829115E+01
0.5710000E-02	0.4768000E+01	0.5482771E+01
0.2000000E-01	0.5454000E+01	0.6076533E+01
0.2140000E-01	0.6105000E+01	0.6114834E+01
0.3150000E-01	0.6338000E+01	0.6368879E+01
0.6340000E-01	0.7036000E+01	0.7189816E+01
0.6570000E-01	0.8199000E+01	0.7253917E+01
0.1140000E+00	0.8199000E+01	0.8377140E+01
0.1730000E+00	0.9304000E+01	0.9470100E+01
0.2930000E+00	0.1134000E+02	0.1116697E+02
0.1310000E+01	0.1657000E+02	0.1657880E+02
0.2930000E+01	0.2024000E+02	0.2022814E+02
0.8100000E+01	0.2407000E+02	0.2402057E+02
0.1510000E+02	0.2681000E+02	0.2701873E+02
0.2730000E+02	0.3024000E+02	0.2991739E+02
0.4960000E+02	0.3314000E+02	0.3332870E+02
0.9000000E+02	0.3814000E+02	0.3810154E+02

THE PRECEDING SOLUTION IS UNIQUE

APPENDIX H

Reactor Tracer Experiment

A pulse of natural gas was admitted to the Berty reactor. The reactor contained 0.5 g of catalyst A-7 and was operating at room temperature and 1500 RPM with a 100 ml/min He flow rate. The tracer elution curve was measured by periodic GC sampling. The elution curve, shown in Figure 67, is plotted in a semi-log fashion to verify the legitimacy of the mixed-flow reactor model. Ideal mixed-flow behavior is indicated by the linear section of Figure 67, which holds for the 13 minutes following tracer injection (4 to 5 times the mean residence time).

The area under the elution curve, obtained by integration, is proportional to the amount of tracer being removed from the reactor.

Area under the ideal behavior line (up to 15 minutes)

$$A_i = \frac{1790000}{-0.331}\left[e^{-0.331(15)} - 1\right] = 5370120.$$

Area under the deviation from ideality (between 15 and 25 minutes)

$$A_d = \frac{230000}{-0.1906}\left[e^{-0.1906(25)} - e^{-0.1906(15)}\right] = 58890.$$

Area under the ideal behavior line (15 and 25 minutes)

$$A_c = \frac{1790000}{-0.331}\left[e^{-0.331(25)} - e^{-0.331(15)}\right] = 36360.$$

The ideal behavior area fraction per total area is

$$A_i + A_c \Big/ A_i + A_d = \frac{5370120 + 36360}{5370120 + 58890} = 0.996$$

Integration of the amount of tracer from the ideal mixed-flow behavior line compared to the total amount of tracer from integration under the elution curve indicates that ~99% of the methane tracer moves through the reactor in an ideal mixed-flow pattern.

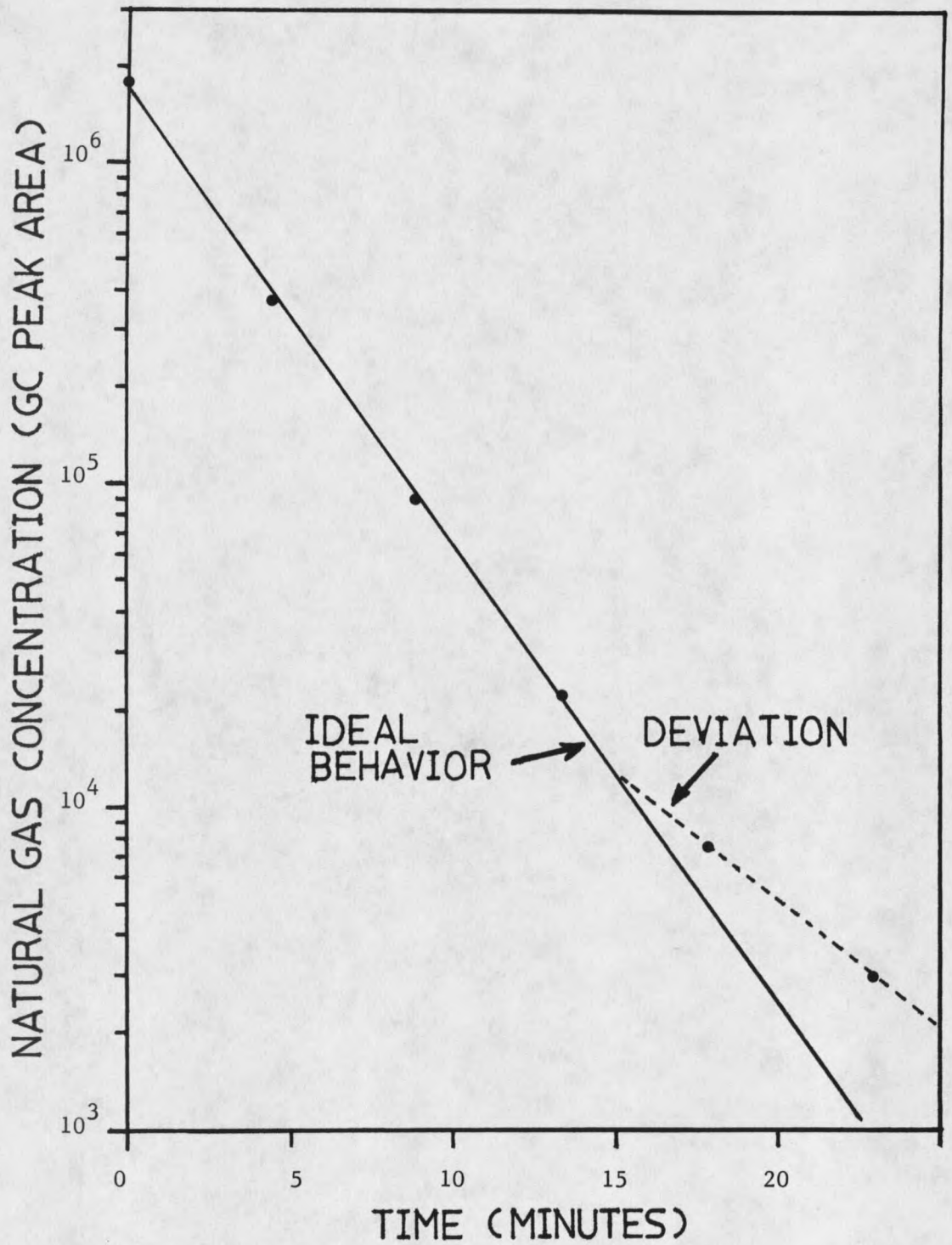

Figure 67. Natural gas (methane) tracer response of the Berty reactor, indicated by the logarithm of the natural gas concentration (GC peak area) versus time after tracer injection.

APPENDIX I

Intraparticle Diffusion Criterion

Criterion for the Importance of Pore Diffusion Limitation

$$\Phi = \frac{(r_v)_{obs} L^2}{D_e C_o^s} \ll 1 \qquad \text{Weisz-Prater criterion}$$

All of the criterion variables must be calculated from known properties, using sample A-18 information.

At 318°C, $-r_o = 3.36 \times 10^{-10}$ mol/m^2·s

with $\rho_p = 1.038$ g/cm^3 and $S = 138$ m^2/g

then, $(r_v)_{obs} = 4.8 \times 10^{-8}$ mol/cm^3·s

$L = R/3$ where R is the pellet radius

$$L = \frac{0.442 \text{ cm}/2}{3} = 0.074 \text{ cm}$$

The diffusivity will be estimated from the assumption that Knudsen diffusion is controlling.

$D_K = 9.7 \times 10^3 \, r_p (T/M)^{0.5}$

$r_p = 18$ Å, from porosimetry data, $T = 318°C = 591$ K, and $M = 106.17$ g/mol yields

$D_K = 4.1 \times 10^{-3}$ cm^2/s

Assume that the catalyst pellet pore structure can be described using the random pore model.

$D_e = \epsilon^2 D_K = (0.56)^2(4.1 \times 10^{-3}) = 1.3 \times 10^{-3}$ cm^2/s

$$C_o^s = \frac{5 \text{ mm Hg}}{640 \text{ mm Hg}} \cdot \frac{1 \text{ mol}}{22414 \text{ cm}^3} = 3.5 \times 10^{-7} \text{ mol/cm}^3$$

Substitute

$$\Phi = \frac{4.8 \times 10^{-8}(.074)^2}{I.3 \times 10^{-3}(3.5 \times 10^{-7})} = 0.58$$

the absence of pore diffusion is not certain

Use catalyst powder that has been seived to ensure all particles pass 80 mesh ($d \leq 0.177$ mm).

If all other parameters remain the same,

$$L = \frac{0.018/2}{3} = 0.003 \text{ cm}$$

and

$$\Phi = \frac{4.8 \times 10^{-8} \text{ mol/cm}^3 \cdot \text{s}(0.003 \text{ cm})^2}{1.3 \times 10^{-3} \text{ cm}^2/\text{s}(3.5 \times 10^{-7} \text{ mol/cm}^3)} = 0.00095$$

Such a low value for the Weisz-Prater criterion theoretically indicates the absence of significant pore diffusion.

APPENDIX J

o-Xylene Isomerization

Equilibrium Limitations

Figure 68. Conversion limits for xylene isomerization reactions calculated from thermodynamic equilibrium.

2 o-xylene = m-xylene + p-xylene

ΔG° = 28.405 + 28.952 - 2(29.177) = -0.977 kcal/mole
ΔH° = 4.120 + 4.290 - 2(4.540) = -0.670 kcal/mole

T (°C)	T (K)	ΔG° (kcal/mol)	K	lnK	ε	y_o
25	298	-0.997	5.38	1.684	0.41	0.18
300	573	-1.30	3.13	1.141	0.39	0.22
350	623	-1.35	2.98	1.093	0.39	0.22
400	673	-1.41	2.87	1.053	0.39	0.22
450	723	-1.46	2.77	1.019	0.38	0.24

o-xylene = m-xylene

T (°C)	T (K)	ΔG° (kcal/mol)	K	lnK	y_o
25	298	-0.772	3.68	1.304	0.214
300	573	-1.10	2.62	0.963	0.276
350	623	-1.16	2.54	0.934	0.282
400	673	-1.21	2.48	0.908	0.287
450	723	-1.27	2.43	0.887	0.292

m-xylene = p-xylene

T (°C)	T (K)	ΔG° (kcal/mol)	K	lnK	y_o
25	298	0.547	0.397	-0.924	0.72
300	573	0.895	0.456	-0.786	0.69
350	623	0.958	0.461	-0.774	0.68
400	673	1.021	0.466	-0.764	0.68
450	723	1.085	0.470	-0.755	0.68

APPENDIX K

Catalyst o-Xylene Isomerization Activity Data

Table 23. o-Xylene isomerization activity data for sample A-0.

Data	m (g o-xyl/s) x 10^5	T (°C)	ΔX_o	$-r_o$ (mol o-xyl/m^2·s) x 10^{12}	k (1/s) x 10^7
1	5.91	327	-.0002	-	-
2	5.90	326	-.0025	-	-
3	6.02	326	-.0070	-	-
4	6.14	411	0.0007	-	-
5	6.18	426	-.0016	-	-
6	6.12	433	-.0039	-	-
7	6.21	435	-.0060	-	-

W = 0.8578 g

S = 513 m^2/g

Table 24. o-Xylene isomerization activity data for sample A-3.

Data	m (g o-xyl/s) x 10^5	T (°C)	ΔX_o	$-r_o$ (mol o-xyl/m^2·s) x 10^{12}	k (1/s) x 10^7
1	5.45	305	0.0048	6.21	2.82
2	5.29	348	0.0176	22.1	10.2
3	5.16	370	0.0301	36.9	17.2
4	5.18	376	0.0350	43.1	20.2
5	5.07	378	0.0394	47.5	22.3
6	5.00	379	0.0417	49.5	23.4
7	4.94	404	0.0716	83.9	40.9
8	4.93	418	0.1046	122.	61.8
9	4.89	419	0.1047	122.	61.4

W = 0.9311 g

S = 426 m^2/g

Table 25. o-Xylene isomerization activity data for sample A-7.

Data	m (g o-xyl/s) x 10^5	T (°C)	ΔX_o	$-r_o$ (mol o-xyl/m^2·s) x 10^{12}	k (1/s) x 10^7
1	3.57	306	0.0143	21.1	7.68
2	5.38	307	0.0089	19.8	7.16
3	5.24	334	0.0173	37.5	13.7
4	5.15	341	0.0235	50.0	18.4
5	5.10	360	0.0365	76.9	28.6
6	4.95	375	0.0603	123.	47.1
7	4.74	379	0.0660	129.	49.7
8	4.67	381	0.0692	134.	51.5
9	4.69	398	0.1066	207.	83.0
10	6.08	398	0.0868	218.	85.7

W = 0.6744 g

S = 338 m^2/g

Table 26. o-Xylene isomerization activity data for sample A-10.

Data	m (g o-xyl/s) x 10^5	T (°C)	ΔX_o	$-r_o$ (mol o-xyl/m^2·s) x 10^{12}	k (1/s) x 10^7
1	3.91	411	0.4930	694.	410.
2	3.82	412	0.5062	697.	423.
3	3.73	355	0.3591	482.	226.
4	3.65	330	0.2094	276.	104.
5	3.56	330	0.2102	270.	102.
6	3.47	331	0.2145	268.	102.
7 *	3.36	330	0.2117	257.	97.4
8 *	3.36	330	0.2011	244.	91.3
9 **	3.41	331	0.2098	258.	97.7
10 **	3.22	333	0.2480	288.	115.

* - 1750 RPM

** - 1250 RPM

W = 0.9265 g

S = 285 m^2/g

Table 27. o-Xylene isomerization activity data for sample A-18.

Data	m (g o-xyl/s) x 10^5	T (°C)	ΔX_o	$-r_o$ (mol o-xyl/m^2·s) x 10^{12}	k (1/s) x 10^7
1	4.61	321	0.0259	92.5	13.9
2	4.79	318	0.0256	95.0	14.3
3	4.54	317	0.0260	91.6	13.8
4	4.39	316	0.0294	100.	15.1
5	4.25	331	0.0371	122.	18.6
6	4.13	340	0.0647	207.	32.4
7	3.89	341	0.0718	216.	34.2
8	4.72	341	0.0534	196.	30.2
9	4.59	349	0.0651	231.	36.3
10	4.55	369	0.1018	359.	58.6
11	4.49	373	0.1257	438.	73.3
12	4.44	374	0.1302	449.	75.5

W = 0.8804 g

S = 138 m^2/g

Table 28. o-Xylene isomerization activity data for sample A-26.

Data	m (g o-xyl/s) x 10^5	T (C)	ΔX_o	$-r_o$ (mol o-xyl/m^2 s) x 10^{12}	k (1/s) x 10^7
1	6.19	307	0.0219	94.8	17.9
2	6.14	306	0.0247	106.	20.1
3	6.13	305	0.0220	94.3	17.8
4	6.11	327	0.0375	160.	30.8
5	6.29	331	0.0465	204.	39.6
6	6.28	343	0.0531	234.	45.5
7	6.40	360	0.0702	314.	62.5
8	6.42	363	0.0798	358.	72.0
9	6.73	363	0.0887	418.	84.7
10	6.49	363	0.0806	366.	73.5
11	6.62	363	0.0880	407.	82.6

W = 0.7736 g

S = 174 m^2/g

Table 29. o-Xylene isomerization activity data for sample A-44.

Data	m (g o-xyl/s) x 10^5	T (°C)	ΔX_o	$-r_o$ (mol o-xyl/m^2·s) x 10^{12}	k (1/s) x 10^7
1	4.68	304	0.0097	25.2	5.36
2	4.65	304	0.0121	31.3	6.66
3	4.65	305	0.0111	28.7	6.10
4	4.60	348	0.0335	85.6	18.7
5	4.60	352	0.0389	99.4	21.8
6	4.60	351	0.0429	110.	24.1
7	4.64	351	0.0375	96.7	21.1
8	4.61	373	0.0566	147.	32.3
9	4.61	377	0.0647	166.	37.2
10	4.66	377	0.0712	184.	41.7
11	4.70	378	0.0643	168.	37.7
12	2.50	379	0.1304	181.	35.0
13	2.59	381	0.1359	196.	47.6

W = 0.8557 g

S = 198 m^2/g

Table 30. o-Xylene isomerization activity data for sample A-65.

Data	m (g o-xyl/s) x 10^5	T (°C)	ΔX_o	$-r_o$ (mol o-xyl/m^2·s) x 10^{12}	k (1/s) x 10^7
1	5.42	309	-.0008	-	-
2	5.13	308	-.0011	-	-
3	5.11	338	-.0011	-	-
4	5.02	372	0.0015	-	-
5	5.04	417	-.0010	-	-
6	5.06	423	0.0015	-	-
7	4.97	427	-.0005	-	-

W = 0.8441 g

S = 7.0 m^2/g

Table 31. o-Xylene isomerization activity data for sample A-88.

Data	m (g o-xyl/s) x 10^5	T (°C)	ΔX_o	$-r_o$ (mol o-xyl/m^2·s) x 10^{12}	k (1/s) x 10^7
1	3.24	300	-.0061	-	-
2	5.04	300	-.0021	-	-
3	4.77	324	-.0009	-	-
4	4.43	368	0.0000	-	-
5	4.35	408	0.0012	-	-
6	4.32	421	0.0003	-	-
7	4.29	428	0.0009	-	-

W = 0.8525 g

S = 68.5 m^2/g

Table 32. o-Xylene isomerization activity data for sample A-100.

Data	m (g o-xyl/s) x 10^5	T (°C)	ΔX_o	$-r_o$ (mol o-xyl/m^2·s) x 10^{12}	k (1/s) x 10^7
1	5.17	307	-.0072	-	-
2	5.30	306	-.0007	-	-
3	5.11	305	-.0025	-	-
4	5.04	366	-	-	-
5	4.95	384	-.0027	-	-
6	4.84	403	-	-	-
7	4.69	409	-.0020	-	-
8	4.66	419	0.0004	-	-
9	4.48	433	0.0061	-	-

W = 0.6143 g

S = 202 m^2/g